DISSERTATION

ON THE MAGNITUDE AND FREQUENCY OF SEDIMENT TRANSPORT IN RIVERS

Submitted by

Joel Stephen Sholtes

Department of Civil and Environmental Engineering

In partial fulfillment of the requirements

For the Degree of Doctor of Philosophy

Colorado State University

Fort Collins, Colorado

Fall 2015

Doctoral Committee:

Advisor: Brian Bledsoe

Ellen Wohl
Peter Nelson
Mazdak Arabi

ABSTRACT

ON THE MAGNITUDE AND FREQUENCY OF SEDIMENT TRANSPORT IN RIVERS

What flow or range of flows is most responsible for transporting sediment and maintaining sediment continuity in a river over human time scales? This question has inspired scores of studies analyzing the magnitude and frequency of sediment transport (MFA) in rivers and has been a part of the ongoing debate regarding process vs. form-based approaches to stable channel design. MFA in rivers is of general scientific and management interest as it influences channel form, water quality, aquatic habitat, and channel restoration design considerations.

The research presented in this dissertation asks the following overarching question: What influences how much and how often sediment is transported in a river? In this dissertation, I consider relationships between the drivers of sediment transport at a point in a river (flow regime, sediment size, and channel form) and metrics describing sediment yield, which integrate the relationship between flow regime and transport over time. To study this question, I use theoretical and empirical approaches in a spectrum of stream types from fine bed streams dominated by suspended load transport to gravel and cobble streams dominated by bed load transport. I find that, for example, the

frequency of the most effective discharge decreases and the range of flows most responsible for sediment yield increases with increasing flow regime variability. As river bed material becomes coarser, a more narrow range of less frequent flows becomes most effective in sediment transport.

The river management and restoration community has given much effort to predicting the bankfull discharge, Q_{bf}, and associated channel geometry at Q_{bf} for the purposes of channel study, classification, and design. In a study comparing various Q_{bf} predictors in coarse and fine bed rivers, I find that the discharge associated with 50% of cumulative sediment yield based on the flow record—Q_{s50}, the half yield discharge—predicts Q_{bf} better than most other predictors, especially in fine-bed rivers. Other predictors include the most effective discharge, Q_{eff}, and the 1.5-year flood.

Using statistical methods to quantify the uncertainty in the sediment load-discharge relationship as well as the empirical flow frequency distribution, I develop methods to propagate uncertainty in estimations of Q_{eff} and Q_{s50}. In an examination of the influence of flow regime non-stationarity on sediment yield metrics, I find that in urbanizing watersheds with increasing trends in flow variance, estimates of Q_{eff} and Qs50 increase dramatically compared to those based on the entire flow period of record. Finally, I estimate Q_{eff} and Q_{s50} using empirical, sediment load data-driven models and physically-based models driven by one-dimensional flow-depth relationships evaluated at a cross section. Physically-based models that match the slope of the sediment load-

discharge relationship performed well. This is the case with total load models for fine bed sites, but generally not the case for bed load models used on coarse bed sites.

All daily flow records and sediment load data as well as all Matlab ® and **R** scripts are contained in the supplementary data.

ACKNOWLEDGEMENTS

It takes a village to complete a PhD. That village starts at home with my incredibly supportive, patient, and loving wife Kari, who provided an ear whenever I had frustrations or breakthroughs with analyses, marveled at a new figure, or practiced her grammar *kung fu* on my writing. Thanks to my baby girl Penelope, for coming into my life last year, giving me perspective on what matters, going to bed promptly at 7:30 pm, and sleeping soundly through the night as I burned the midnight oil to finish this dissertation. Thanks to all of our friends for their generous spirits and help watching that lady bug over the past year.

I thank my advisor Brian Bledsoe for working with me over these past four years. It took some time to generate steam on this project. I appreciate our conversations and brainstorming sessions as we slowly developed and arrived at this present study. Your folksy wisdom, zen proclivities, and appreciation of classical guitar music all enhanced my time here. Thanks also for your flexibility when Penny was born. I look forward to future collaborations.

Thanks to Kevin Werbylo for reaching out to collaborate on what started as a small exploration of the influence of flow regime on sediment yield magnitude frequency in rivers and what eventually turned into my first chapter, which set the stage for the remainder of the dissertation. Thanks to the rest of my committee Mazdak Arabi, Peter Nelson, and Ellen Wohl for providing helpful feedback and support over the past four

years. Thanks to Jorge Ramirez who served as a mentor through the I-WATER IGERT program and beyond. I am thankful for being part of this fellowship and appreciate the friendships and connections I have developed in it.

Thanks to Sam Michels-Boyce who collaborated with me on the question of the significance of bed load transport in fine bed rivers to his master's research. In pursuing his master's on this project, Tyler Rosburg has been a great collaborator and good sounding board along the way.

My funding sources over the last four years began with an NSF IGERT fellowship (Award # 0966346). I am indebted to Jorge and the other I-WATER co-PIs for taking the initiative to apply and administer this fellowship. Karleene Schindler provided excellent and patient administrative support throughout. This was followed by a research assistanceship funded through a Transportation Research Board, National Cooperative Highway Research Program grant (Award # 24-40) awarded to Brian Bledsoe, Peter Nelson, and Dan Baker. Finally, I was awarded an Environmental Protection Agency, Science to Achieve Results graduate student fellowship to finish this work.

For Chapter 1, I gratefully acknowledge Kevin Werbylo with whom this theoretical exploration of MFA began. Kevin wrote the Matlab script that generated and analyzed Q_{eff} samples for the Flow Record Length analysis section. He is also a co-author on the published version of this chapter. This chapter benefitted from discussions with Richard Vogel, Kristin Bunte, and Jose Salas as well as reviews from John Pitlick

and two anonymous reviewers through the Water Resources Research publication process. This work was funded while I was an NSF I-WATER IGERT Fellow.

For Chapter 2, thanks goes to Kristin Bunte and Erich Mueller for sharing bed load data sets they have painstakingly collected in the field (Kristen) or painstakingly amassed and organized (Erich). Thanks also to the U.S. Forest Service Rocky Mountain Research Stations in Fort Collins and Boise for making their bed load data, bed sediment, and channel geometry measurements available online. Peter Nelson and Dan Baker provided feedback and input along the way. They also helped craft the framework of sediment yield metrics and studying the sensitivity of these metrics to driving variables. Portions of this work as well as the work for Chapter 3 was conducted under the support of the Transportation Research Board, National Cooperative Highway Research Program grant 24-40: Design Hydrology for Stream Restoration and Channel Stability at Stream Crossings.

Casey Kramer, Washington State Department of Transport Hydraulics Engineer, originally made the suggestion that I consider how well process-based bankfull discharge predictors performed compared with standard hydrologic predictors. This inspired the focus of Chapter 3. I would also like to thank the helpful comments from Dr. Daniel Baker on the draft manuscript. Thanks goes to Jennifer Hoeting as well as the Colorado State University statistical consulting graduate students for conversations and insight on statistical approaches for quantifying uncertainty in Chapter 4.

TABLE OF CONTENTS

LIST OF SYMBOLS

α	Coefficient for sediment transport rating curve.
β	Exponent for sediment transport rating curve.
λ	Rate parameter of the exponential distribution (1/year).
μ	Mean of untransformed (μ_x) and log-transformed (μ_y) daily flows. Subscripts "2" and "3" indicate the 2nd and 3rd moments of a probability density function.
ϱ_Q	Empirical probability density value (e.g., histogram) (probability/m^3/s).
σ	Standard deviation of untransformed (σ_x) and log-transformed (σ_y) daily flows.
τ_*	Shield dimensionless shear stress. Subscript "*c*" denotes critical value for sediment entrainment.
Φ	Cumulative normal distribution function.
a	Coefficient for at-a-station hydraulic geometry relation. Subscripts "*cli*" and "*fp*" denote in-channel and overbank or floodplain values.
b	Exponent for at-a-station hydraulic geometry relation. Subscripts "*cli*" and "*fp*" denote in-channel and overbank or floodplain values.
C_v	Coefficient of variation of daily flows.
D_s	Sediment grain size (m). Subscript "50" denotes the median grain size value.
F_x	Cumulative distribution function for random variable x.
f_x	Probability density function for random variable x.
$f+$	Fraction of sediment transported by discharges greater than the effective discharge.
G	Specific gravity of sediment.
h	Flow depth (m).
k	Sediment transport relation coefficient.
M	Rank.
p	Probability.
Q	Discharge rate (m^3/s).
$Q_{1.5}$	1.5-year return interval flood peak discharge (m^3/s).
Q_2	2-year return interval flood peak discharge (m^3/s).

Q_{bf} Bankfull discharge (m^3/s).

Q_{cf} Channel forming discharge (m^3/s).

Q_{eff} Effective discharge (m^3/s).

Q_{mean} Mean annual discharge (m^3/s).

Q_s Sediment discharge rate (tonnes/day or kg/sec).

Q_{s25} Discharge associated with 25% of cumulative sediment load (m^3/s).

Q_{s50} Half-yield discharge, discharge associated with 50% of cumulative sediment load (m^3/s).

Q_{s75} Discharge associated with 75% of cumulative sediment load (m^3/s).

RI Return interval of a discharge value (yr).

s Standard deviation of daily flow (m^3/s).

$\overline{T}$ Mean inter-arrival time of flood events $\geq Q_{s50}$ (year).

$\overline{x}$ Mean of daily flow (m^3/s).

BIOGRAPHY

Joel came to Colorado State University from the hot and humid south where people mostly worry about what to do with all the water falling out of the sky; of course that is changing these days. He took a circuitous path to arrive at hydrology and fluvial geomorphology as a profession, starting out remediating old industrial sites along the Hudson River and looking wistfully out at the water, which sometimes flowed south and sometimes north. A brief stint with a conservation organization and some time at a municipal water utility made him realize that his calling was to work on the technical aspects of water resources and watershed management.

In his search for a graduate program, he discovered the field of fluvial geomorphology and was hooked. Joel studied with Martin Doyle at the University of North Carolina at Chapel Hill (now at Duke) in a truly interdisciplinary group of ecologists, geographers, and hydrologists. There he worked on a number of projects related to assessing the efficacy and outcomes of North Carolina's state-run stream and wetland mitigation program. His master's work involved a hydraulic analysis of stream restoration's potential to attenuate flood waves. After two years at an environmental engineering firm navigating the turbid waters of Atlanta, he and his wife turned their gazes west to her home state.

Now at CSU and settled in to Fort Collins, Joel plans to prolong living the dream here by working as a soft money researcher for as long as possible. Ultimately, he would enjoy a stable and well-paying job as a research hydrologist with a federal agency or, perhaps, the hectic but rewarding life as a professor somewhere. In the meantime, he will enjoy his soon to be augmented free time with his wife, baby daughter, and friends in the great outdoors of Colorado.

INTRODUCTION

Rivers transport sediment supplied from upstream sometimes continuously, and sometimes in fits and spurts depending on the river's flow regime, the size and quantity of the sediment delivered from upstream, and the geomorphic and geographic setting of the river. For example, low gradient rivers with fine beds tend to continuously transport sediment along their beds and in suspension. When floods occur in these rivers the rate and quantity of transport increases nonlinearly with discharge, as is common in most rivers. In coarse bed rivers, the bed material may only mobilized during infrequent high flow events. The magnitude and frequency of sediment transport in rivers, therefore, is a function of the size of sediment in a river's bed, the size and quantity of sediment supplied from upstream, and the frequency distribution or flow regime [*Vogel et al.*, 2003; *Soar and Thorne*, 2011; *Hassan et al.*, 2014; *Sholtes et al.*, 2014]. These processes interact with river channel boundary conditions such as vegetation, surficial lithology, and valley shape to produce an emergent channel form.

In their foundational paper on the topic, "The Magnitude and Frequency of Geomorphic Work", Wolman and Miller [1960] explain their theory that geomorphic events of intermediate frequency perform the most work over time using a metaphor derived, perhaps, from a Brother's Grimm children's tale and excerpted from their paper below [p. 73].

A dwarf, a man, and a huge giant are having a woodcutting contest. Because of metabolic peculiarities, individual chopping rates are roughly inverse to their size. The dwarf works steadily and is rarely seen to rest. However, his progress is slow, for even little trees take a long time, and there are many big ones which he cannot dent with his axe. The man is a strong fellow and a hard worker, but he takes a day off now and then. His vigorous and persistent labors are highly effective, but there are some trees that defy his best efforts. The giant is tremendously strong, but he spends most of his time sleeping. Whenever he is on the job, his actions are frequently capricious. Sometimes he throws away his axe and dashes wildly into the woods, where he breaks the trees or pulls them up by the roots. On the rare occasions when he encounters a tree too big for him, he ominously mentions his family of brothers-all bigger, and stronger, and sleepier.

In this metaphor, the man represents intermediate magnitude floods. However, as demonstrated in this dissertation, the man is not always the most effective at transporting sediment, and in some rivers the dwarf and giant win out over time. The research presented in this dissertation asks the following overarching question related to the dwarf, the man, and the giant: What influences how much and how often sediment is transported in a river? The "what" part of this question relates to physical drivers that influence sediment yield (integration of sediment transport over time) such as the flow regime and channel boundary conditions, as suggested above. How much and how often sediment is transported—or the magnitude and frequency of sediment transport in rivers—is of general scientific and management interest as it influences channel form, water quality, aquatic habitat, and channel restoration and design considerations. These factors are

Adapted from Grimm & Grimm [1884].

sensitive to changes in flow regime and sediment supply, making sediment transport magnitude-frequency analysis (MFA) an important tool in river management [*Tilleard*, 1999; *Kondolf et al.*, 2006; *Soar and Thorne*, 2011; *Wohl et al.*, 2015]. Here, I quantify the magnitude and frequency of sediment transport using sediment yield metrics, which integrate the relationship between flow regime and sediment transport (see Chapter 2, Sections 1 and 2).

Though sediment yield MFA is a well-trodden area of study [c.f., *Wolman and Miller*, 1960; *Benson and Thomas*, 1966; *Pickup and Warner*, 1976; *Wolman and Gerson*, 1978; *Andrews*, 1980; *Ashmore and Day*, 1988; *Biedenharn and Thorne*, 1994; *Nash*, 1994; *Emmett and Wolman*, 2001; *Vogel et al.*, 2003; *Simon et al.*, 2004; *Goodwin*, 2004; *Barry et al.*, 2008; *Soar and Thorne*, 2011; *Bunte et al.*, 2014; *Hassan et al.*, 2014], there are some significant open questions in this field. All previous work focuses on MFA in one type of system; for example coarse bed, snowmelt-driven mountain streams [*Emmett and Wolman*, 2001; *Bunte et al.*, 2014] or flashy, sand bed streams [*Soar and Thorne*, 2001], and has not yet integrated observations and relationships across river types. The ability of theoretical relations [*Nash*, 1994; *Vogel et al.*, 2003; *Goodwin*, 2004] to accurately quantify sediment yield magnitude and frequency has not been adequately studied. Finally, though much work has been conducted to quantify the uncertainty of sediment yield estimates, none has explicitly quantified the uncertainty of the magnitude and frequency of sediment transport relationship. This dissertation fills these knowledge and research gaps.

In Chapter 1, I use theoretical representations of the flow regime and sediment transport relation to explore how flow variability, channel morphology, and bed sediment size all influence the magnitude and frequency of sediment transport in rivers. This work adds physical complexity to these theoretical approaches resulting in new mechanistic understandings of the controls of sediment transport magnitude and frequency in rivers. I also explore how well a theoretical, continuous probability density function (PDF) used to represent the flow regime (flow frequency distribution) of a river in MFA compares with discrete and finite flow records in estimating sediment yield metrics.

Chapter 2 extends and validates the theoretical study by exploring similar relationships between sediment yield metrics and both driving and boundary condition variables using concurrent flow records and sediment load data sets from fine bed, suspended load-dominated and coarse bed, bed-load dominated rivers across the U.S.

Using the same data set, I characterize the ability of dominant discharge estimates based on hydrology (the 1.5 and 2 year recurrence interval flood peaks) and sediment yield (the most effective discharge, Q_{eff}, and the discharge associated with 50% of cumulative sediment yield, or the half-yield discharge, Q_{s50}) to predict bankfull discharge in Chapter 3. The dominant discharge is a theoretical single flow rate that over time would create the existing channel form [*Soar and Thorne*, 2011]. The bankfull discharge is that which just fills the channel before spilling onto the floodplain in rivers with developed floodplains [*Wolman and Leopold*, 1957; *Williams*, 1978], and has

important channel design implications. I compare predictive abilities of these various bankfull discharge predictors between coarse and fine bed sites.

Finally, in Chapter 4 I develop methods for quantifying prediction and confidence intervals for sediment yield metrics Q_{eff} and Q_{s50}. I also explore the influence of other forms of uncertainty on these metrics such as a changing flow regime due to urbanization and modeling sediment transport at a site where bed material load data do not exist.

The four chapters of this dissertation build from one another to provide a holistic and comprehensive treatment of sediment yield magnitude and frequency analysis. They provide new insight on the relationships between physical drivers of sediment transport in rivers and sediment yield; they uncover physical mechanisms behind these relationships heretofore not published; and they provide new tools to conduct MFA, predict bankfull discharge, and quantify the uncertainty in sediment yield-based dominant discharge estimators.

CHAPTER 1

Theoretical Approaches to Sediment Transport Magnitude-Frequency Analysis

Summary

Theoretical approaches to magnitude-frequency analysis (MFA) of sediment transport in channels couple continuous flow probability density functions (PDFs) with power law flow-sediment transport relations (rating curves) to produce closed-form equations relating MFA metrics such as the effective discharge, Q_{eff}, and fraction of sediment transported by discharges greater than Q_{eff}, $f+$, to statistical moments of the flow PDF and rating curve parameters. These approaches have proven useful in understanding the theoretical drivers behind the magnitude and frequency of sediment transport. However, some of their basic assumptions and findings may not apply to natural rivers and streams with more complex flow-sediment transport relationships or

---

Sholtes, J., K. Werbylo, and B. Bledsoe (2014), Physical context for theoretical approaches to sediment transport magnitude-frequency analysis in alluvial channels, Water Resources Research, 50, doi:10.1002/2014WR015639.

Joel S Sholtes conceived the study as it is presented in the paper. Developed models for broken power law and entrainment threshold analysis. Analyzed all output data, created figures, and wrote the manuscript. Kevin Werbylo proposed initial concept of utilizing theoretical approaches to MFA to consider the influence of different flow regimes. Assisted with study design, developed code for record-length analysis, discussed the results and implications, contributed to writing methods, and edited the manuscript. Brian P. Bledsoe assisted in study design, discussed results, contributed to discussion and implications, and edited the manuscript.

management and design scenarios, which have finite time horizons. I use simple numerical experiments to test the validity of theoretical MFA approaches in predicting the magnitude and frequency of sediment transport. Median values of Q_{eff} and $f+$ generated from repeated, synthetic, finite flow series diverge from those produced with theoretical approaches using the same underlying flow PDF. The closed-form relation for $f+$ is a monotonically-increasing function of flow variance. However, using finite flow series, I find that $f+$ increases with flow variance to a threshold that increases with flow record length. By introducing a sediment entrainment threshold, I present a physical mechanism for the observed diverging relationship between Q_{eff} and flow variance in fine and coarse bed channels. My work shows that through complex and threshold-driven relationships sediment transport mode, channel morphology, flow variance, and flow record length all interact to influence estimates of what flow frequencies are most responsible for transporting sediment in alluvial channels.

1 Introduction

To what discharge or range of discharges does a river adjust its dimensions to balance the inputs of flow and sediment while maintaining a dynamically stable form? This question underlies research conducted by generations of geomorphologists and engineers on the relationship between alluvial channel form, sediment transport, and flow regime [*Mackin*, 1948b; *Wolman and Miller*, 1960; *Pickup and Warner*, 1976; *Hey*

and Thorne, 1986; *Doyle et al.*, 2007]. Alluvial channels are those with boundaries that adjust in response to erosion and deposition of sediment. Wolman and Miller [1960] introduced the hypothesis that the theoretical channel-forming discharge is some intermediate, near-bankfull discharge that, over time, performs the most work (i.e., transports the most sediment). They define this discharge as the most "effective" discharge, Q_{eff}. Since then, scores of studies searching for a relationship between channel form and Q_{eff} have been published. Some workers have found a strong (e.g., 1:1) relationship between the bankfull discharge, Q_{bf}, and Q_{eff} [*Andrews*, 1980; *Andrews and Nankervis*, 1995; *Hey*, 1996; *Torizzo and Pitlick*, 2004] while others have found a wide range of variability in the $Q_{bf}-Q_{eff}$ relationship [*Pickup and Warner*, 1976; *Nolan et al.*, 1987; *Soar and Thorne*, 2001]. Nevertheless, the concept of effective discharge —and the analytical framework of magnitude and frequency analysis of sediment transport—has provided a valuable tool for examining relationships between channel form and process.

Much work has been conducted to operationalize and standardize empirical magnitude-frequency analysis (MFA) for use on rivers and streams with flow records and measured or modeled sediment transport [e.g., *Benson and Thomas*, 1966; *Biedenharn et al.*, 2000]. Empirical MFA involves representing a daily or sub-daily flow record as an empirical probability distribution through either binning the flows in a histogram [*Beidenharn et al.* 2000; *Soar and Thorne* 2001] or numerically differentiating the empirical cumulative distribution function of the flows [*Orndoff and Whiting*, 1999]. This empirical probability distribution is then multiplied by a sediment transport-

discharge relation, which may either be a statistical regression, or a site-calibrated sediment transport equation [e.g., *Hey*, 1996] to create an empirical effectiveness histogram or curve.

While Wolman and Miller [1960] originally suggested that a continuous, theoretical probability density function (PDF) could be used to represent the flow regime, it was not until three decades later that this theoretical approach to MFA was formalized [*Nash*, 1994; *Vogel et al.*, 2003; *Goodwin*, 2004; *Quader and Guo*, 2009; *Klonsky and Vogel*, 2011]. The theoretical approach to MFA involves multiplying an assumed continuous PDF or one that is fit to the flow distribution (e.g., the log-normal or gamma distribution) with a sediment-transport relation, which may be as simple as a power law function that relates sediment transport to flow, or a more complex and threshold driven relation. Metrics based on the resulting effectiveness curve equation may then be derived by analytical integration. The appeal of the theoretical approach to MFA lies in the ability to generate easily applied, closed-form solutions to MFA metrics such as Q_{eff} [*Vogel et al.*, 2003; *Goodwin*, 2004] and the amount of sediment transported by discharges greater than Q_{eff}, $f+$ [*Vogel et al.*, 2003; *Goodwin*, 2004]. With these, one can expediently determine the relationship between MFA metrics, and attributes of the flow regime (e.g., coefficient of variation, skewness, etc.) and/or sediment transport mode (e.g., empirical sediment rating curve exponent, and critical shear stress for bed mobilization). Furthermore, one could use these relations to predict how a channel

might respond to a change in flow variability or sediment supply due to environmental change assuming a correlation between Q_{eff}, or another MFA metric, and Q_{bf}.

Using the theoretical approach, Vogel et al. [2003] found that Q_{eff} often takes on a relatively low value (and $f+$ a large value) and is responsible for relatively little load transport over time while larger, less frequent discharges are often responsible for the majority of load transport in rivers. They argue that Q_{eff} may not be a useful metric when considering what flows are responsible for transporting the bulk of suspended sediment in a channel. It should be noted that Vogel et al. [2003] were more interested in total river load in general (solutes, suspended sediment, etc.), and not specifically in geomorphically significant flows. From a geomorphic perspective, many empirical MFA studies have found correspondence between Q_{eff} and Q_{bf}, suggesting that some relationships exist between the discharge range that maximizes the effectiveness of sediment transport and channel form in certain channel types [*Wolman and Miller*, 1960; *Carling*, 1988; *Andrews and Nankervis*, 1995; *Hey*, 1996; *Emmett and Wolman*, 2001]. Here, I explore why theoretical and empirical approaches can produce contradictory results.

The present study takes a dualistic approach to investigate claims on the magnitude and frequency of sediment transport in channels based on theoretical, closed-form solutions to MFA metrics. I utilize the analytical framework of the theoretical approaches to study how adding complexity to them changes the predicted relationships between flow regime, sediment transport mode, and MFA metrics. For this first

objective, I begin by considering the influence of flow and sediment transport mode on MFA metrics using the original theoretical approaches (Sections 3.1 & 4.1). As discussed above, I acknowledge the limitations of these approaches; however, I find it illustrative to begin this study by exploring the relationships they produce. To add complexity to these approaches, I introduce a compound channel form (Sections 3.3, & 4.3) and a threshold for sediment entrainment (Sections 3.4 & 4.4) and consider the influence of flow variability and sediment transport mode on MFA metrics calculated from these updated theoretical approaches. For the second objective, I test the assumptions of the theoretical approaches themselves by considering how MFA metrics calculated from theoretical approaches, which use continuous PDFs to represent the flow record, compare with those calculated with a synthetic empirical approach using discrete, finite, flow records sampled from those same PDFs (Sections 3.2 & 4.2).

I begin with a more thorough introduction to theoretical MFA approaches and outline my methods for accomplishing the objectives stated above. I end with a discussion of how and why results from theoretical and empirical approaches diverge. I also explore how theoretical approaches can be extended to incorporate a higher degree of physical realism, which in turn allows them to be used to evaluate more complex relationships between channel form and the magnitude and frequency of sediment transport.

2 Theoretical Framework

This investigation follows and expands upon the analytical framework of previous theoretical MFA work [*Nash*, 1994; *Vogel et al.*, 2003; *Goodwin*, 2004]. Consistent with this previous work, I initially represent the sediment transport-discharge relationship as a power law: $Q_s = \alpha Q^{\beta}$, where Q_s has units of mass/time, specifically (tonnes/day). In this sediment rating curve α is a scaling coefficient that is positively related to the magnitude of sediment flux and drainage area [*Syvitski et al.*, 2000; *Barry et al.*, 2004]. Implicit in this rating curve is a discharge–bed shear stress relationship. It has been shown that the value of α does not affect the value of Q_{eff} or other normalized MFA metrics [*Nash*, 1994; *Goodwin*, 2004], so it will not be specifically considered in this study. The rating curve exponent, β, is positively correlated to the size of the largest bed particles (D_{84}) [*Emmett and Wolman*, 2001], bed armoring [*Dietrich et al.*, 1989; *Barry et al.*, 2004], and dependent upon sediment transport measurement technique [*Bunte et al.*, 2004], as well as channel morphology (i.e., stage-discharge relationship) [*Hey*, 1996] among other factors.

The mechanisms by which sediment moves through a channel (e.g., in suspension or along the bed) should inform the type of transport relation used. Where sediment transport measurements exist, a statistical regression may be used, often taking the form of a power law function (sediment rating curve). Where empirical sediment rating curves are not available, semi-empirical, sediment transport relations, calibrated to the

hydraulics and sediment of the channel of interest, are relied upon. Barry et al. [2008] found that the calculated value of Q_{eff} is insensitive to the type of transport equation used in bed load channels.

Many continuous probability distribution functions have been used to represent daily stream flow, which are generally highly positively skewed, including the two-parameter lognormal, gamma, Generalized Pareto, exponential, as well as broken power law functions [e.g., *Vogel et al.*, 2003; *Goodwin,* 2004; *Archfield et al.*, 2007; *Quader and Guo* 2009; *Segura and Pitlick*, 2010]. In general, continuous PDFs fit natural flow records with mixed results, especially in the right tail of the distribution and in multi-modal cases [*Nash*, 1994; *Segura and Pitlick*, 2010]. Nash [1994] found that on large rivers the lognormal distribution fit daily flows well in some circumstances and poorly in others due to the multimodal nature of some flow records, as well as skewness and kurtosis combinations that exceeded what is possible with the lognormal distribution. Quader and Guo [2009] tested the fit of the exponential distribution on daily flows, finding that it performs the best in smaller streams but found poor fits between flow records and continuous PDFs in general, especially among streams with intermittent flow. Segura and Pitlick [2010] found that a broken power law function better fit the frequency distribution of daily flows in snowmelt-dominated streams, as compared to the exponential and lognormal distributions. While it does not fit daily flow distributions well in some cases, I chose to work with the two-parameter lognormal distribution function due to its demonstrated ability to represent skewed daily stream flow

distributions in many cases [*Limbrunner et al.*, 2000], its relative parsimony, and its historical use in generating theoretical MFA relationships [*Chow*, 1964].

$$f(Q) = \frac{1}{Q\sqrt{2\pi\sigma_y^2}} \exp\left\{ -\frac{1}{2\sigma_y^2}\left[\ln(Q) - \mu_y\right]^2 \right\} \tag{1.1}$$

Here, Q represents the average daily flow value (m^3/s), and μ_y and σ_y are the mean and standard deviation of the logarithm of the average daily flows, respectively. Using other skewed, continuous PDFs such as the gamma distribution produced qualitatively similar theoretical relationships as the lognormal distribution. It is possible for the exponential distribution to have a relatively thick right tail for large values of C_v when fit using the method of moments. This can lead to a negative relationship between $f+$ and C_v (opposite of the relationship produced using lognormal or gamma PDFs); however, such thick right tails may not be realistic for natural flow regimes. It should be noted that a sub-daily time resolution may be more appropriate for analyzing sediment yield in rivers whose discharge may vary widely within a day such as those with small drainage areas and flashy hydrology [*Biedenharn et al.*, 2000]; however, for the purposes of this study, I only consider flow regimes with daily time resolution.

Flow records are samples of the underlying population distribution of the flow regime and are discrete and finite in nature. This is particularly evident in the right tail of the distribution where continuous PDFs may over-represent the discrete, sporadic occurrence of infrequent flood events. Even if a flow record perfectly represents a sample from a certain probability density function, an infinite sample size would be required

before the empirical PDF would match the shape of theoretical PDF. As the period of record length increases past 50 to 100 years and beyond, assumptions of channel equilibrium and flow regime stationarity inherent in MFA may be violated. As such, continuous PDFs will always approximate finite flow records due to their discrete nature. Nevertheless, results from MFA using continuous PDFs can yield important insights about the relationships between flow regime and the magnitude and frequency of sediment transport [*Quader and Guo*, 2009; *Klonsky and Vogel*, 2011].

Vogel et al. [2003] and Goodwin [2004] demonstrate that a closed-form solution for the effective discharge can be derived by multiplying a continuous PDF with a sediment-rating curve to create the effectiveness curve. The flow that coincides with the peak of the effectiveness curve, found by taking its derivative, is known as the effective discharge. The resulting expression is a parsimonious, closed-form function of the rating curve exponent, β, and the mean and variance of the logarithms of daily flow when the lognormal PDF is used:

$$Q_{eff} = \exp\left[\mu_y + \sigma_y^2(\beta - 1)\right] \tag{1.2}$$

Many methods exist to calculate the value of Q_{eff} directly–or empirically—from a flow record and either a measured sediment-rating curve or calibrated sediment transport relation [e.g., *Hey*, 1996; *Biedenharn et al.*, 2000; *Soar and Thorne*, 2001]. Generally, Q_{eff} is equal to the median value of the discharges contained in the maximum effectiveness histogram bin, which is the product of a daily flow histogram and the sediment transport relation. It can also be determined with an empirical kernel density

function [*Klonsky and Vogel*, 2011] or as the maximum finite difference derivative of the empirical cumulative distribution form of the effectiveness curve [*Orndorff and Whiting*, 1999].

Based on the lognormal distribution for daily flows, the return interval in years of Q_{eff} is:

$$RI = \frac{1/365}{1-\Phi\left[\frac{\ln(Q_{eff})-\mu_y}{\sigma_y}\right]} \tag{1.3}$$

where the expression $\Phi[\ ]$ represents the standard normal cumulative distribution function (CDF) [*Vogel et al.*, 2003]. Here, RI represents the return interval in years calculated from the daily flow series PDF. I do not use a nonparametric or empirical alternative to equation (1.3) in this study because I are sampling from the lognormal distribution. Additionally, Vogel et al. [2003] derived a closed-form solution for the fraction of average total sediment load transported by discharges greater than Q_{eff}, $f+$:

$$f+ = 1-\Phi\left[-\sqrt{\ln(1+C_v{}^2)}\right] \tag{1.4}$$

where C_v is the coefficient of variation of the untransformed daily flows (σ_x/μ_x). This function monotonically increases with C_v with an asymptote at unity. The empirical analog to the theoretical approach simply involves dividing the total amount of sediment transported on each day summed over a flow record by the amount of sediment transported by flows greater than Q_{eff}.

A final metric I explore characterizes the spread in the range of flows responsible for transporting the middle 50% of sediment centered on Q_{eff}. I refer to this as the sediment yield interquartile range, and calculate it numerically without a closed-form solution. A smaller value for this metrics means that a smaller range of flows transports this central 50% of sediment yield, in which case a single discharge metrics may be suitable for channel design where sediment continuity is a concern. A larger number indicates that a wider range of flows is responsible for sediment continuity and a more sophisticated approach to channel design may be necessary.

3 Data and Methods

3.1 Flow Regime Analysis

I begin by considering the range of variance in natural flow regimes. Poff [1996] conducted an analysis of the statistical properties of daily flows in unregulated streams and rivers in the conterminous United States. He created flow regime categories by grouping rivers by various statistical properties. I select several of his flow regime categories representing the range of variance he reports from groundwater and snowmelt-driven hydrology to flashy and intermittent hydrology ($1 < C_v < 5$). To understand how flow regime variance—represented by the coefficient of variation of the average daily flow—affects the magnitude and frequency of sediment transport, I solve

equations 1.2, 1.3, and 1.4 for this range of values of C_v. I also use this range of C_v values to inform the subsequent analyses.

3.2 Flow Record Length

My first test of the theoretical approach to magnitude frequency analysis (MFA) compares values and return intervals of Q_{eff} and values of $f+$ generated from equations 1.2, 1.3, and 1.4 with those generated from synthetic daily flow records of varying length (10 years, 100 years, 1,000 years, and 100,000 years) sampled from the lognormal distribution. I create these extremely long flow records (large sample sizes) to examine how empirical MFA metrics compare to theoretical values as the flow record sample approaches the continuous, underlying population distribution (the lognormal PDF) used in the theoretical approach. Using 1,000 to 100,000 year records will increase the probability of sampling a large and rare event, but these large events will receive less weight in the empirical density function for large sample sizes, and hence less influence on MFA. In fact, a large flood sampled in a short flow record, will have an overwhelming influence on MFA because it will receive more weight in the histogram (higher density) due to the smaller sample size. To generate synthetic daily flow records for each combination of C_v value (0.5 to 5) and flow record length (RL) considered, I used a uniform distribution to randomly sample the two-parameter lognormal CDF specified by a constant mean (μ_x) of 2 m^3/s (arbitrary value) and C_v values ranging from 0.5 to 5. For each flow record length, I created 100 trials of RL*365 random samples

from the lognormal CDF for every value of C_v. The mean and variance of the lognormal distribution are calculated by the method of moments where the values in parentheses are untransformed [*Yevjevich*, 2010]:

$$\mu_y = \frac{1}{2}\ln\left(\frac{\mu_x^2}{1+C_v{}^2}\right) \tag{1.5}$$

$$\sigma_y^2 = \ln\left(1+C_v{}^2\right) \tag{1.6}$$

Next, I created an empirical flow PDF or histogram of the synthetic flow record. Much consideration has been given to the number of histogram bins and method for calculating the bin intervals in effective discharge analysis with suggestions ranging from 25 to 100 equally-spaced (arithmetic) discharge classes and discouraging the use of logarithmic classes [*Biedenharn et al.*, 2000; *Soar and Thorne*, 2001]. More rigorous statistical approaches have been suggested by Orndoff and Whiting [1999] who use a numerical differentiation of the empirical flow CDF, and Klonksy and Vogel [2011] who recommend using a kernel density function. For simplicity, I use the general approach outlined by Biedenharn et al. [2000]. I modify their method slightly to best represent flow record lengths ranging from 10 year to 100,000 year by using a constant 50 equally-space arithmetic bins to create histograms of daily flow. Additionally, I do not modify the width of discharge bin classes such that no bins contain zero flows as per Biedenharn et al. [2000]. Sensitivity analysis indicates that relative relationships among the MFA metrics and C_v, β, and *RL* variables are not affected by the number of bins (bin width) used for $25 \leq \#\ of\ bins \leq 100$. The midpoints of each histogram bin are then

multiplied by sediment-rating curves of the form $Q_s = \alpha Q^{\beta}$ to generate the synthetic "empirical" effectiveness histograms. The median value of all the daily discharges contained in the maximum effectiveness histogram bin represents the effective discharge.

The coefficient of the rating curve, α was arbitrarily set to 0.02. The value of α does not affect the value of Q_{eff} [*Nash*, 1994; *Goodwin*, 2004] or normalized MFA metrics such as *f+*; therefore, keeping this value constant and arbitrary was deemed reasonable. I consider values of the exponent β from 0.5 to 5. This range represents the spectrum of observed sediment-rating curve exponent values where smaller values as low as 1 are generally associated with suspended sediment transport [*Nash*, 1994; *Syvitski et al.*, 2000]. Values less than 1 are uncommon. Larger values of β up to and greater than 5 are generally associated with bed load transport [*Emmett and Wolman*, 2001; *King et al.*, 2004]. These ranges are not exhaustive; indeed, values of β up to and greater than 10 have been reported for bed load transport in mountain streams with relatively low transport stages [*Bunte et al.*, 2004]. However, the range of β selected for this study serves to illustrate the relationship between sediment transport mode, as represented by the rating curve exponent, β, over the range of flow regimes.

I summarize the empirical MFA metric results as a function of C_v, β, and *RL* by reporting median values from the 100 trials. Increasing the number of trials from 100 to 1,000 and 10,000 does not significantly alter the median value of the MFA metrics, nor does it influence the trends and relationships reported here.

3.3 Compound Channel Form

Next, I compare theoretical approaches to MFA derived from the single power law (SPL) sediment-rating curve function—equations 1.2 to 1.4—to those generated using a piecewise or broken power law (BPL) function that represents a compound channel form consistent with many natural channel cross sections. Compound channels exhibit a break in lateral slope between the channel and the floodplain and hence a break in transport effectiveness [*Hey*, 1996] (Figure 1.1). I consider how flow variance interacts with compound channel form to drive sediment transport effectiveness.

I use an at-a-station hydraulic geometry relation of the form $h = aQ^b$ to relate flow depth, h, to discharge for both in channel and overbank flows. Values of a and b were chosen to generally reflect reported values for in-channel hydraulic geometry relations [*Knighton*, 1998, p.173]. I set the value of the in-channel coefficient, a_{ch}, to 0.2 and the value of the exponent, b_{ch}, was set to 0.4. To maintain continuity from in-channel to overbank flows, the value of the coefficient for overbank flows, a_{fp}, is a function of the coefficient for in-channel flows, as well as the exponents for both overbank and in-channel flows: $a_{fp} = a_{ch} Q_{bf}^{\left(b_{ch} - b_{fp}\right)}$, where Q_{bf} is the bankfull discharge. For this analysis, Q_{bf} was arbitrarily chosen to be 10 m^3/s, consistent with an intermediately-sized channel. I vary the value of the overbank flow exponent, b_{fp}, from 0.1 to 0.3 to test the sensitivity of the analysis to the difference in lateral slope between the channel banks and the floodplain. These at-a-station hydraulic geometry parameter values for overbank flows correspond to those reported for stage-discharge relationships

in compound channels elsewhere [*Ackers*, 1993; *Shiono et al.*, 1999]. I use downstream hydraulic geometry relations to calculate channel width and slope as a function of Q_{bf} developed from coarse-bedded streams in the Rocky Mountains, Colorado by Torrizo and Pitlick [2004].

The statistical properties of the flow regime must be related to Q_{bf} in a non-arbitrary manner. That is, the flow regime must "fit" the channel geometry represented by the value of Q_{bf}. To do this, I used a single log-linear regression between mean annual discharge and Q_{bf} (n = 10, R^2 = 0.92) from the streams studied by Torrizo and Pitlick [2004]:

$$\mu_x = 0.151 Q_{bf}^{0.873} \tag{1.7}$$

The relationship between mean daily discharge and Q_{bf} used in this analysis is unique to the Colorado Rocky Mountains where it was developed. As before, I maintain μ_x constant and vary C_v from 0.5 to 5. I acknowledge that flow regime variability can influence channel form. Varying flow variability while maintaining a constant channel form is a simplification used in this study.

The single power law sediment-rating curve assumes a single stage discharge relationship. To incorporate a compound channel form I use a simplified, non-sediment entrainment threshold version of the Einstein-Brown (EB) equation as reported in Brown [1950] because it has a form similar to a power law sediment-rating curve:

$$Q_s = k_1 \tau_*^3 \qquad \tau_* = \frac{hS}{(G-1)D_s} \tag{1.8}$$

In equation 1.8, k_1 is a constant coefficient, which converts dimensionless unit width, volumetric sediment flux to total sediment discharge (tonnes/day) , G is the specific gravity of the sediment (set to 2.65), and D_s is the characteristic sediment diameter. The independent variable in this equation, τ_*, is the dimensionless Shields parameter, which is a linear function of depth, h for wide rectangular channels, and friction slope, S. Hence, with depth defined as a power law function of discharge, and Q_s defined as a power law function of τ_*, Q_s in (8) can now be defined as a power law function of discharge. This is a continuous relationship in the SPL case and a broken or piecewise relationship in the BPL case. Results using (8) can be directly compared to the power law sediment-rating curve of the form $Q_s = \alpha Q^{\beta}$ used in theoretical MFA approaches:

$$Q_s = \frac{k_1 a^3 S^3}{\left[(G-1)D_s\right]^3} Q^{3b} \tag{1.9}$$

where a and b are equal to a_{ch} and b_{ch} for $Q \leq Q_{bf}$ and equal to a_{fp} and b_{fp} for $Q > Q_{bf}$. I arbitrarily chose a grain size of 10 mm (medium gravel) for this analysis. Sensitivity analysis demonstrates that magnitude-frequency analysis metrics are not sensitive to the grain size using this simplified EB relation. I chose this form of sediment transport relation because it represents the sediment transport-discharge relationship in a non-arbitrary manner and can be directly compared to SPL-based theoretical MFA metrics as shown in equation 1.9 (Figure 1.1).

The majority of previous work has found the value of Q_{eff} to be less than or equal to Q_{bf} in alluvial channels [*Pickup and Warner*, 1976; *Andrews and Nankervis*, 1995; *Soar and Thorne*, 2001] with the exception of Bunte et al. [2014]. In the present analysis, Q_{eff} was always less than Q_{bf}, therefore the only MFA metric that was affected by the BPL sediment flux-discharge relationship was the fraction of sediment transported above Q_{eff}, $f+$. I generate effectiveness curves using finite approximations of the continuous lognormal PDF. To compare values of $f+$ for the SPL and BPL scenarios directly, I use the area under the SPL effectiveness curve as the denominator of $f+$.

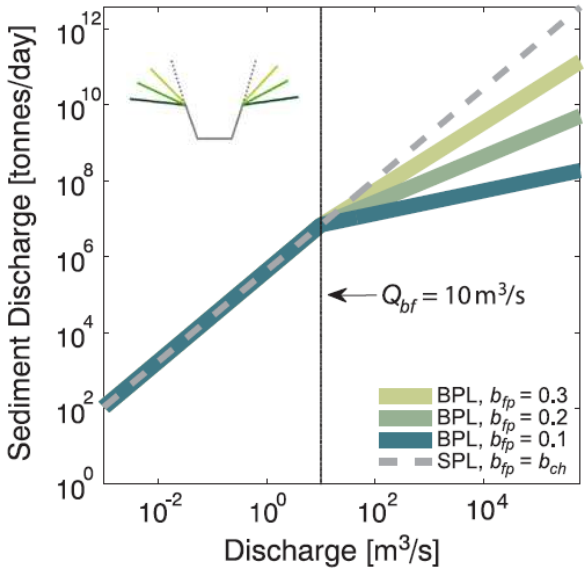

Figure 1.1 Log-linear sediment-rating curves for single power law (SPL, broken line) and broken power law (BPL, solid lines) at-a-station hydraulic geometry relationships for in-channel (left of vertical line) and overbank flows (right of vertical line) with varying degrees of floodplain lateral slope.

3.4 Sediment Entrainment Threshold

In Section 3.3 I considered the influence of compound channel form on MFA metrics without considering a threshold for sediment entrainment. Here I explore how the presence or absence of a threshold affects the values of MFA metrics compared to those derived by equations 1.2, 1.3, and 1.4. Using the same numerical analysis framework in Section 3.3, I introduce a final sediment transport relation that includes a threshold for sediment entrainment: the Meyer-Peter and Müller (MPM) relation for uniformly-sized sediment in transport as bed load [*Meyer-Peter and Müller*, 1948].

$$Q_s = k_2\left(\tau_* - \tau_{c^*}\right)^{1.5} \tag{1.10}$$

The constant, k_2, is similar in concept and units to k_1. Additionally, τ_{c^*} represents the critical value of dimensionless shear stress for sediment entrainment (set to 0.047). It is a threshold value of dimensionless shear stress below which no sediment transport occurs. I chose MPM because it of its parsimony, which serves this illustration of the influence of a threshold of sediment transport on MFA metrics. Similar trends between MFA metrics and C_v result when a more complex bedload equation is used [e.g., *Parker*, 1979].

I vary the size of sediment considered from 1 mm (coarse sand) to 64 mm (very coarse gravel), which, for a given channel geometry, increases the flow depth and discharge necessary for sediment entrainment. Using MPM, (10), and finite approximations of lognormal PDFs representing daily flows with C_v values ranging from 0.5 to 5, I generate finite approximations of theoretical effectiveness curves as before. I

calculate values of the MFA metrics using MPM rather than a sediment-rating curve with no threshold for sediment transport (e.g., Sections 3.1 to 3.3) and compare these with values from their theoretically derived counterparts.

4 Results and Discussion

4.1 Flow Regime Analysis

I begin by considering the range of variance in natural flow regimes. Poff [1996] conducted an analysis of the statistical properties of daily flows in unregulated streams and rivers in the conterminous United States. He created flow regime categories by grouping rivers by various statistical properties. I select several of his flow regime categories representing the range of variance he reports (Table 1.1). The values reflected in Table 1.1 represent averages from all stream gages grouped in each category.

To understand how flow regime variance— represented by the coefficient of variation of the average daily flow—affects the magnitude and frequency of sediment transport, I solve equations 1.2, 1.3, and 1.4 for the range of values of C_v and μ_x

Table 1.1 Statistical properties of daily flow regime categories from Poff [1996].

	Groundwater (GW)	Snowmelt (SN)	Perennial Runoff (PR)	Intermittent Runoff (IR)	Harsh Intermittent (HI)
n	55	22	209	20	7
C_v	1.1	1.3	1.7	3.5	4.8
μ_x	17.5	23.7	13.0	5.2	0.4

represented in Table 1.1 fit to lognormal PDFs (Figure 1.2a). I also use this range of C_v values to inform the subsequent analyses.

As described by equation 1.4, $f+$ increases in an asymptotic manner with C_v and is not a function of β (Figure 1.2b). As C_v increases, the flow PDF and effectiveness curve become more positively skewed and the tails thicker. That is, smaller discharges become more frequent and large discharges become slightly more frequent. This translates to a value of Q_{eff} that decreases with increasing C_v, in a relative sense. That is, Q_{eff} occupies an increasingly smaller position of cumulative sediment transport and the area of the effectiveness curve to the left of Q_{eff} decreases (see Figure 1.9, left panel) while the value of $f+$ increases. In their analysis of sand bed streams, Soar and Thorne [2001] found an increasing relationship between $f+$ and a metric for flow variance;

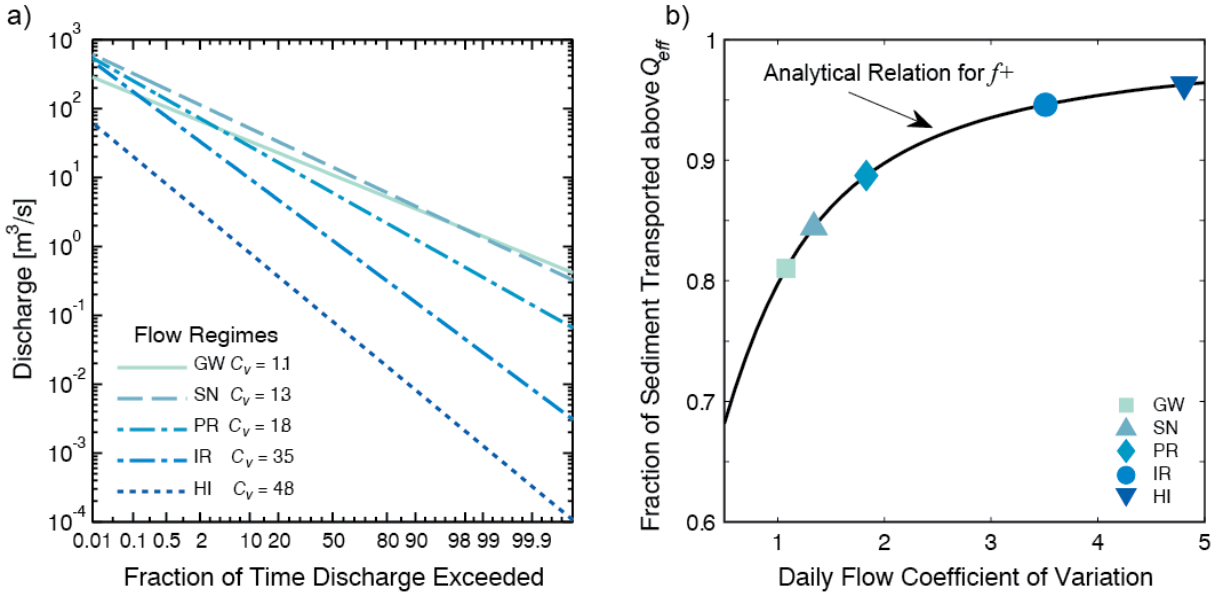

Figure 1.2 a) Lognormal flow duration curves fitted to the Poff et al. [1996] flow regime categories. b) theoretical relation for $f+$ and $f+$ values plotted for flow regime categories.

however, work by Bunte et al. [2014] in coarse bedded streams suggests otherwise. I explore this divergence in sediment transport and MFA metric behavior between fine and coarse bed streams in Section 4.4, below.

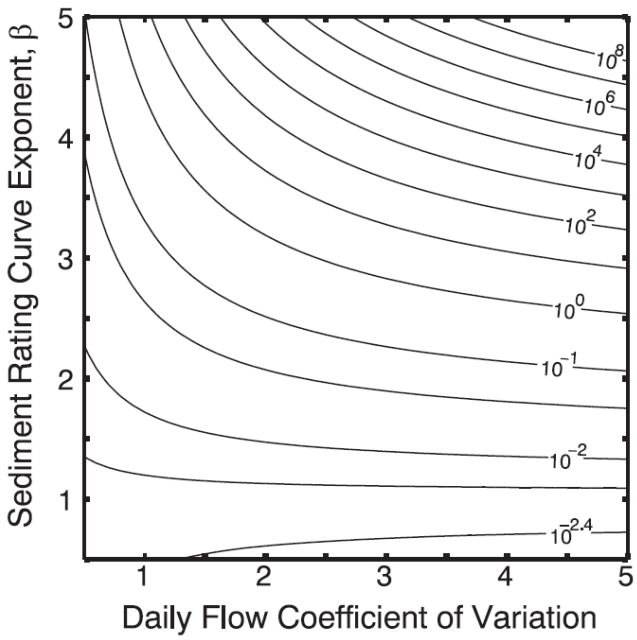

Figure 1.3 Return Interval (year) of Q_{eff} for $\mu_x = 2$ m^3/s as a function of β and C_v.

The relationship between RI as a function of β and C_v indicates that as β increases, RI increases for constant C_v, but more so for $C_v > 2$ (Figure 1.3). As C_v increases with constant β, RI increases for $\beta > 2$ (representative of the bed load-dominated domain), and is relatively constant for $\beta < 2$. The theoretical relation plotted in Figure 1.2 precludes the possibility of RI approximating the 1.5 year flow event for $\beta \geq 2.5$. The 1.5 year event is often cited as the median or average return interval for Q_{eff} or Q_{bf} though with questionable merit as discussed by Doyle et al. [2007]. While these general trends may translate to physical systems in some cases, the absolute values of RI shown in Figure 1.3 diverge from those reported for North American streams, calculated using empirical methods, which generally fall in the range of 0.5 to 2 year [*Pickup and Warner*, 1976; *Andrews*, 1980; *Nash*, 1994; *Emmett and Wolman*, 2001]. However, recent work by Bunte et al. [2014] using different bed load measurement techniques suggests that in coarse bedded streams with very large sediment-rating curve

exponents ($\beta > 5$), the largest flows are likely the most effective over time. While this theoretical relation may provide information about the general relationships between sediment transport mode, flow variance, and the magnitude of Q_{eff}, it is limited in its applicability to the physical world, especially for large β and C_v values.

4.2 Flow Record Length Analysis

In the previous section, I considered the influence of C_v on MFA metrics using theoretical approaches alone, which use continuous PDFs to represent daily flows. Here I compare values of MFA metrics generated from theoretical approaches with those generated from synthetic, finite flow records sampled from the same underlying daily flow PDF (empirical approach). I begin this discussion by considering samples of effectiveness histograms representing a range of β and C_v values and flow record lengths (Figure 1.4). The effectiveness histograms plotted in the top 3 rows of Figure 1.4 represent a single 100 year flow record chosen randomly from the 100 trials conducted for each plotted value of C_v. As both β and C_v increase, larger, less frequent flows transport relatively more sediment over time. The effective discharge, or the median value of the flows in the bin with the maximum effectiveness value, tends to fall in the first flow bin for $C_v > 1$ and $\beta < 2$. The effective discharge tends to fall in the last flow bin for $\beta \geq 3$ over all values of C_v. At some threshold value of β, Q_{eff} jumps from a very frequent flow value to a very infrequent value in the right tail of the effectiveness

histogram, sometimes falling in the last flow bin. This jump, or threshold, can be seen in the contour plots of *f+* and *RI*, plotted as functions of β and C_v (Figure 1.5).

The number of years in a flow record also plays a role in the relationships between β and C_v and the MFA metrics *f+* and *RI.* Consider effectiveness histograms generated from flow records with $C_v = 1$ and lengths varying from 10 years to 100,000 years (bottom 3 rows, Figure 1.4). As the flow record length increases, the synthetic daily flow histogram more closely replicates the continuous function that is the product of the sediment-rating curve and the lognormal flow PDF underlying theoretical MFA approaches. This gives more weight to more frequent flows near the flow distribution peak. Less frequent flows in the tails of the distribution carry more weight in shorter flow records, which have fewer flows in each bin. This effect becomes more pronounced in the effectiveness histograms as the value of β increases for shorter flow records (Figure 1.4). The effective discharge calculated from shorter flow records is more sensitive to the occurrence of a rare flow event overwhelming sediment yield.

I continue this record length analysis by considering the relationship between MFA metrics *f+* (Figure 1.5 top row) and *RI* (Figure 1.5 bottom row) as a function of β and C_v. Moving from bottom to top in each subplot in the upper row of Figure 1.5, *f+* increases with β to a maximum value at $\beta \approx 1.8$ for the 10 year flow record up to $\beta \approx 3.8$ for the 100,000 year flow record.

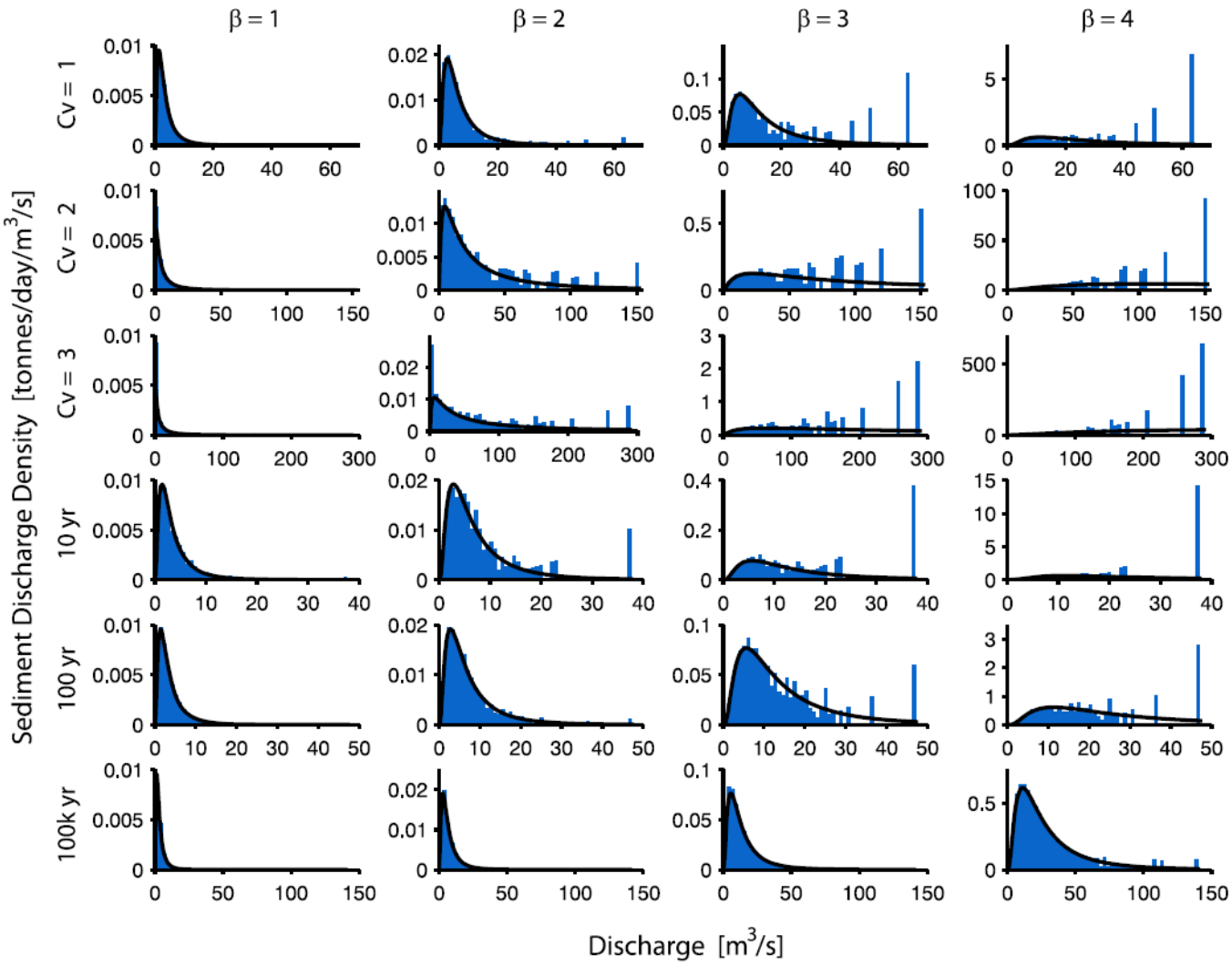

Figure 1.4 A random sample of effectiveness histograms for a range of β and C_v values for a 100 year flow record (top three rows) and a range of record lengths for $C_v = 1$ (bottom three rows) along with theoretical effectiveness curve (solid black curve). Flow samples are identical moving across columns. Flow samples change moving down rows as C_v and record length increase. Note that for $\beta \geq 3$, the largest discharge bin generally becomes the most effective. This is more apparent for larger values of C_v and for shorter flow record lengths.

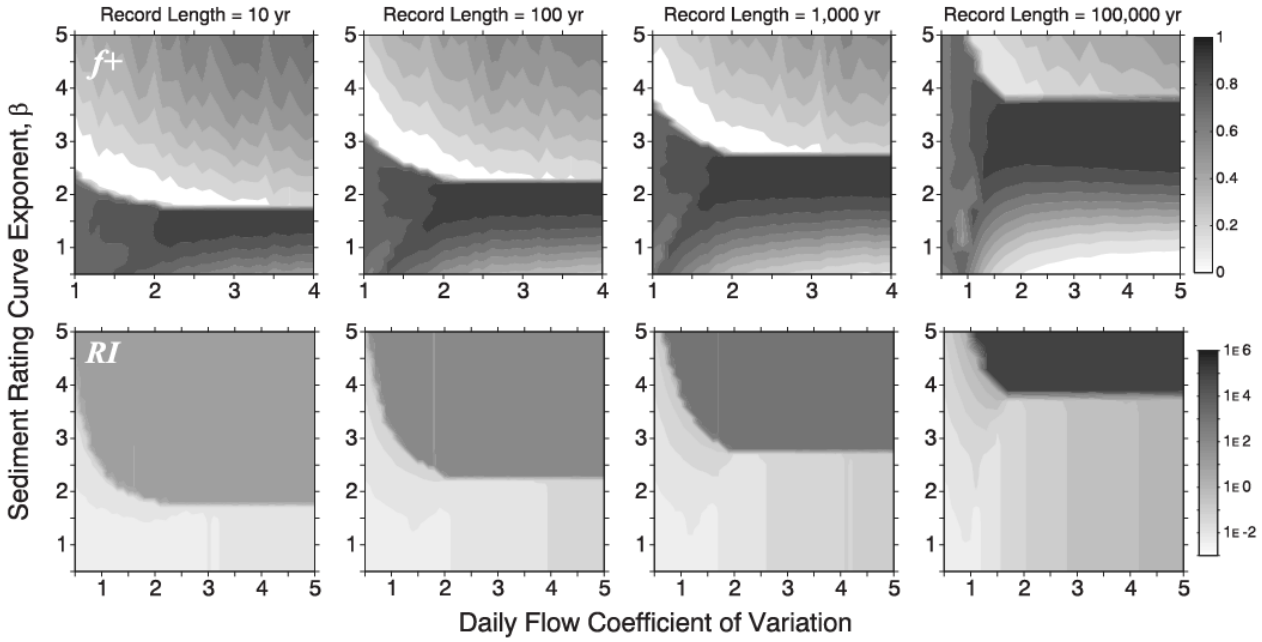

Figure 1.5 Contour plots of values of the fraction of sediment transported above Q_{eff} (*f+, top* row) as well as the return interval of Q_{eff} (RI, bottom row) in years as a function of β, Cv, and length of flow record. Contour values represent the median value of *f+* (top row) and RI (bottom row) of 100 trials of each flow record length.

After this β threshold is reached, $f+$ drops precipitously to nearly zero when Q_{eff} falls into the largest discharge bin in the effectiveness histogram (see Figure 1.4). As β continues to increase, more weight is given to infrequent flows in the right hand tails of the flow probability distribution resulting in more sediment being transported at larger discharges (some greater than Q_{eff}) and a slow increase in $f+$ occurs after this threshold. The threshold described here begins at $\beta \approx 2.4$ for the 10 year records up to $\beta > 5$ for the 100,000 year records at $C_v = 0.5$ and decays to a constant $\beta \approx 1.8$ to 3.8 at C_v values that range from approximately 2.1 to 1.8 for the 10 year and 100,000 year record lengths, respectively.

The value of $f+$ is less sensitive to C_v than to β. In the case of relatively shorter flow records (e.g., 10 year to 100 year), a more sparse distribution of flows allows a few large, infrequent flows to overwhelm the total sediment transport at smaller values of β. In the realm of existing flow record lengths (10 year to 100 year) the behaviors of $f+$ and RI as functions of β and C_v transition smoothly from the values shown in Figure 1.5 for the 10 year to the 100 year plots.

The theoretical relation for $f+$ described by equation 1.4 is only a function of C_v and does not resemble the behavior plotted in Figure 1.5, top row. A horizontal line at intermediate values of β (below the threshold) tracks the approximate trend described by equation 1.4 of $f+$ increasing asymptotically to unity with increasing C_v. The difference between the two descriptions of $f+$ lies in the difference between discrete flow series and flow series represented by continuous PDFs, as well as the definition of Q_{eff}. Even though the discrete, synthetic flow series generated for this study are derived from the same underlying PDF as equations 1.2) to 1.4, they behave differently than continuous PDFs in MFA in large part due to the lack of a continuous right tail in the flow distribution (histogram) of finite records (Figure 1.4). This lack of continuity in the tail of empirical records of course depends on sample size. Assuming, for example, that a river's flow regime perfectly fits the lognormal distribution, given a long enough period, the discrete flow record will match the continuous distribution. However, over engineering time frames (often 50 – 100 years), this is likely not the case. The return interval of Q_{eff} (RI, calculated with equation 1.3 for median values of Q_{eff} from 100

trials) behaves in a similar manner as $f+$ in terms of the threshold effect in the β direction (Figure 1.5, bottom row). Here, RI remains fairly constant with β until the threshold is reached. After which RI rapidly jumps to a much larger value as Q_{eff} occurs in the uppermost discharge bins of the effectiveness histograms.

The record length results show that use of a continuous flow PDF inherent in theoretical MFA weights sediment transport to the tails of the flow PDF and overestimates their influence. Theoretical approaches do not capture the variability and sensitivity of MFA to finite flow records, especially for larger C_v and β values. I find that the need for a longer flow record becomes more important as the variability of the flows increases as well as for values of β greater than approximately 2. This demonstrates that caution should be used when calculating effective discharge in systems with shorter flow records and highly variable flow conditions. For example, one relatively large flow event in the right tail of 10-year flow record is the most effective for $\beta = 3$ and $C_v = 1$. While a very infrequent flow may be the calculated effective discharge, consideration should also be given to the effectiveness peak of the more frequent flows, or a range of flows, when designing a channel for sediment continuity.

4.3 Compound Channel Analysis

Next, I consider the influence of compound channel form on MFA by using a sediment-discharge rating curve for two cases: 1) a single power law (SPL) function for all discharge values, and 2) a piecewise or broken power law (BPL) function, which

incorporates a break in the stage-discharge relationship at Q_{bf} to simulate overbank flows.

Using the SPL under case 1, a continuously increasing relationship between $f+$ and C_v is predicted, which coincides with the theoretical solution for $f+$ described by equation 1.4. However, if I assume that shear stress on the channel bed increases at a slower rate with discharge for overbank flows than for in-channel flows, as with the BPL sediment transport relation in case 2, then a decreasing relationship is predicted between C_v and $f+$ after a peak in $f+$ at $C_v \approx 1.5$ to 2.0 (Figure 1.6a). The location of this peak depends on the degree of difference between channel bank slope and floodplain lateral slope. As the value of b_{fp} decreases the lateral floodplain slope becomes milder relative to the channel bank slope, and the amount of sediment transported at a given overbank discharge decreases. This reduces the relative influence of larger, infrequent flows.

In case 1, Q_{eff} reduces in absolute magnitude with increasing C_v resulting in more sediment being transported at flows greater than Q_{eff} and an increase in $f+$ (e.g., Figure 1.9, left panel). In case 2, Q_{eff} behaves the same way with C_v since it is less than Q_{bf} where the break in at-a-station overbank hydraulic geometry occurs. For a given value of C_v, $f+$ is smaller in case 2 than in case 1 because less sediment is transported overall by overbank flows. The fraction of sediment transported above Q_{eff} continues to decline with increasing C_v in case 2 as overbank floods become more frequent, but less effective when compared to case 1. This relationship may change if a threshold for sediment transport is introduced, which is explored by itself in the next section.

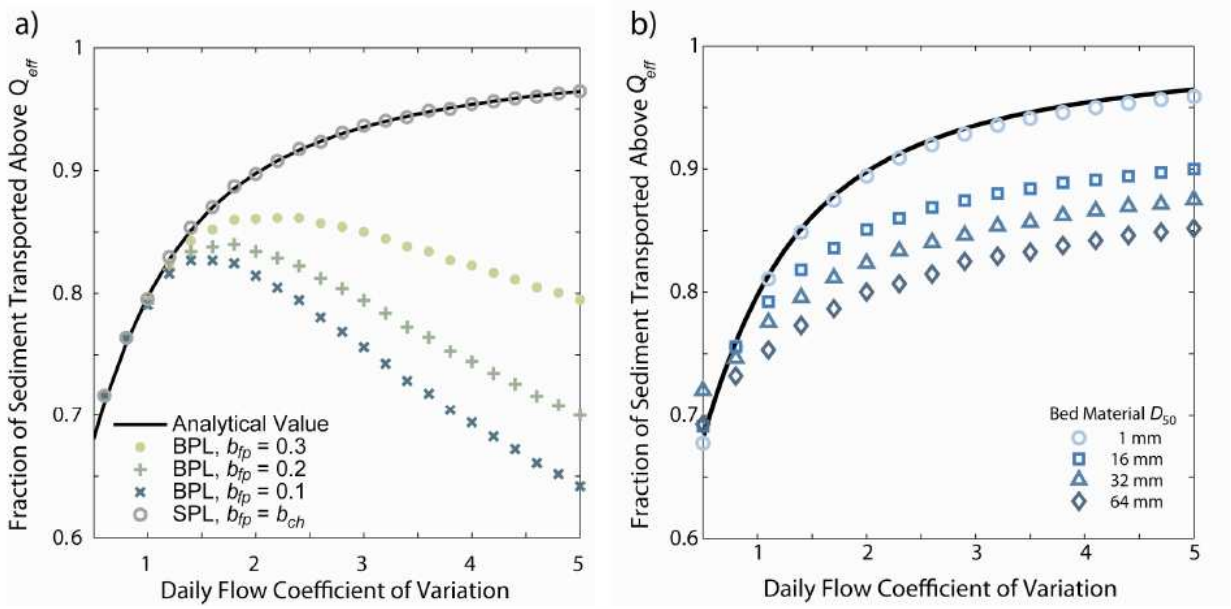

Figure 1.6 a) The fraction of sediment transported by discharges greater than Q_{eff}, *f+*, for the single power law (SPL) and broken power law (BPL) at-a-station hydraulic geometry relationships. b) Values of *f+* for a range of grain sizes in a non-compound channel using an entrainment threshold for sediment transport.

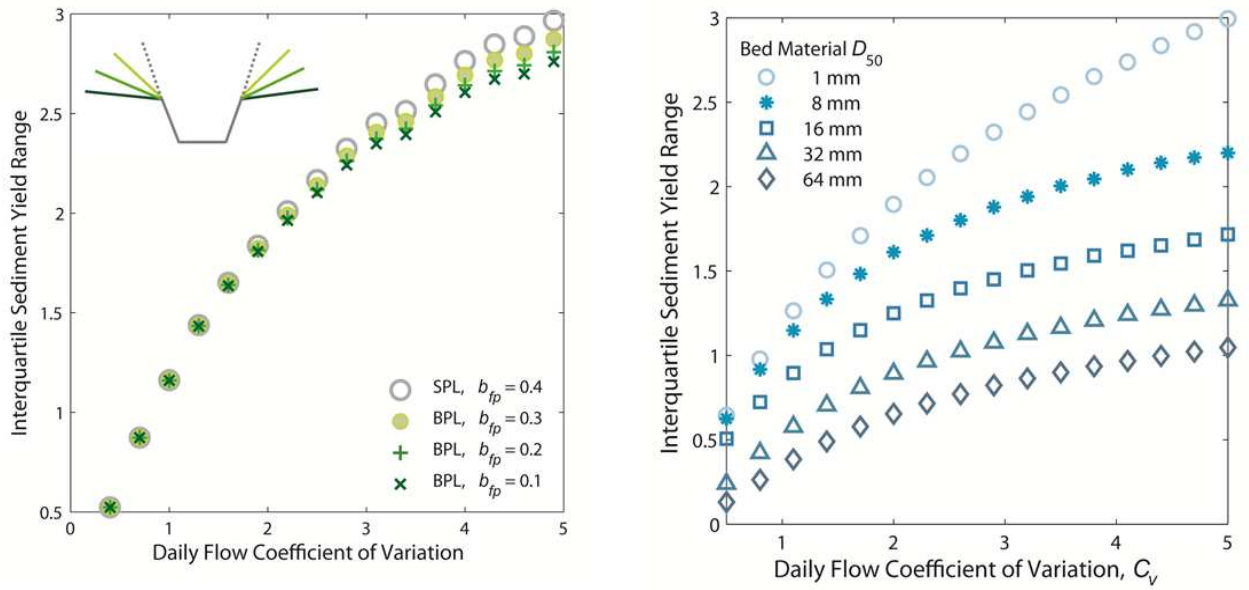

Figure 1.7 Interquartile sediment yield range centered on Q_{eff} (*Qeff.spread*) as a function of C_v and a) compound channel form as well as b) grain size.

It is often the case that breaks in stage-discharge relationships are not explicitly incorporated in MFA [e.g., *Andrews*, 1980; *Nash*, 1994]. However, as Hey [1996], and others studying the hydraulics of compound channels [*Knight and Demetriou*, 1983] note, single stage-discharge or stage-shear stress relationships may not accurately capture the hydraulics of natural rivers with floodplains. Of course, the question of capacity-limited sediment transport at large flows is more complex than treated herein. For example, fine sediment-limited systems can develop armor layers [*Dietrich et al.*, 1989], which can lead to discontinuous flow-sediment transport relationships before and after armor layer breakup [*Jackson and Beschta*, 1982]. Nevertheless, this simple computational experiment has demonstrated that explicitly incorporating floodplain morphology and overbank flows can substantially influence calculations of the magnitude and frequency of sediment transport in natural rivers. I have shown that flow variability interacts with floodplains to reduce the influence of large infrequent flows on long-term sediment transport in channels.

Compound channel form plays a negligible role on influencing Q_{eff} for $Q_{eff} \leq Q_{bf}$. If $Q_{eff} > Q_{bf}$, then it will play a larger role in that as more flow has access to the floodplain (shallower sloped floodplain, short banks) then $Qeff.spread$ will increase but only for very large values of C_v (very flashy systems).

4.4 Sediment Entrainment Threshold Analysis

The final element of physical context I introduce to the theoretical MFA approach is a threshold for sediment entrainment. Sediment transport operating with a threshold interacts with flow distributions in ways that depart from the simplistic sediment-rating curve. For distributions with low C_v, large flows are relatively rare. Transport of coarse sediment classes—and the most effective discharge for these sediment size classes—occur primarily in the right tail of the flow distribution resulting in a very large RI (Figure 1.8b). With increasing C_v, flows less than the threshold for sediment entrainment become more frequent pushing the bulk of sediment transport further out into the right tail of the flow distribution and increasing the absolute value of Q_{eff} (Figure 1.8a). However, as C_v increases in coarse-bedded rivers, RI drops precipitously with increasing C_v as the larger flows necessary to move coarser sediment become more common (Figure 1.8b). In contrast, in fine grain streams with very low or negligible entrainment thresholds the peak of the effectiveness curve follows that of the flow distribution as C_v increases. This means that the absolute value of Q_{eff} decreases with increasing C_v (Figure 1.8a & b; Figure 1.9, left panel). This reverse in the relationship between C_v and Q_{eff} between coarse and fine sediment can be seen by examining the peak of effectiveness curves for a range of sediment sizes and C_v values (Figure 1.9).

I find a reduction in $f+$ as a function of C_v for values generated with the threshold-type sediment transport relation compared to what equation 1.4 predicts

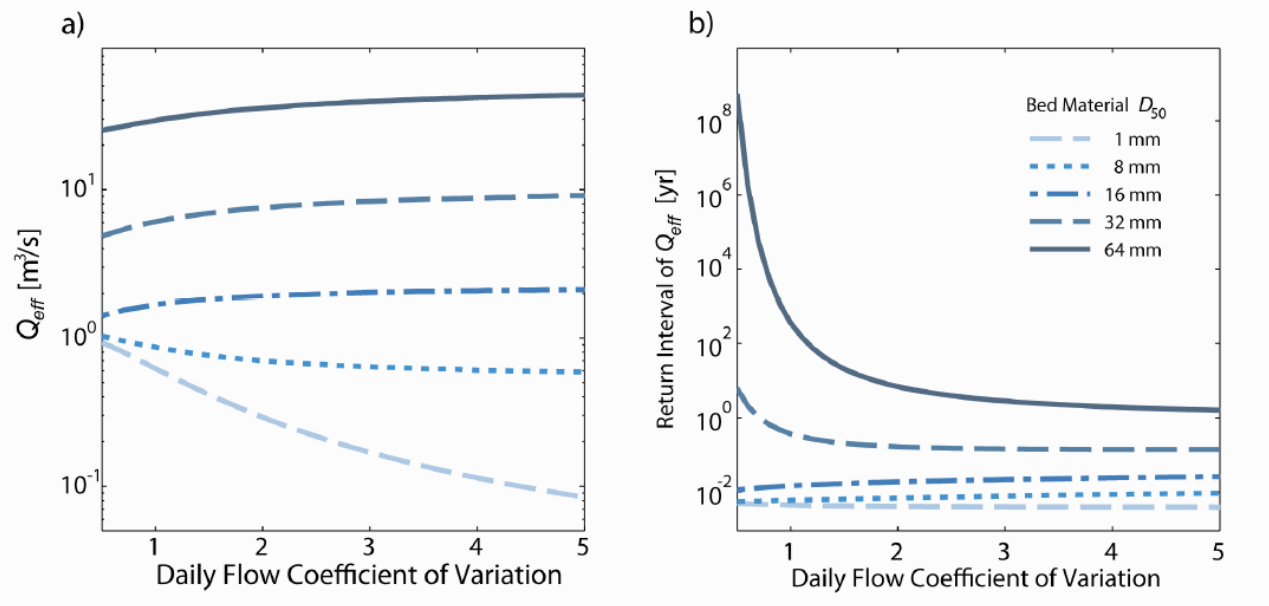

Figure 1.8 a) The value of Q_{eff} as a function of C_v and sediment grain size, D_{50}. b) The return interval of Q_{eff} in years as a function of the same. Note that the Q_{eff}–C_v relationship decreases for relatively small sediment (sand to fine gravel) but increases for large sediment sizes (medium gravel to small cobble).

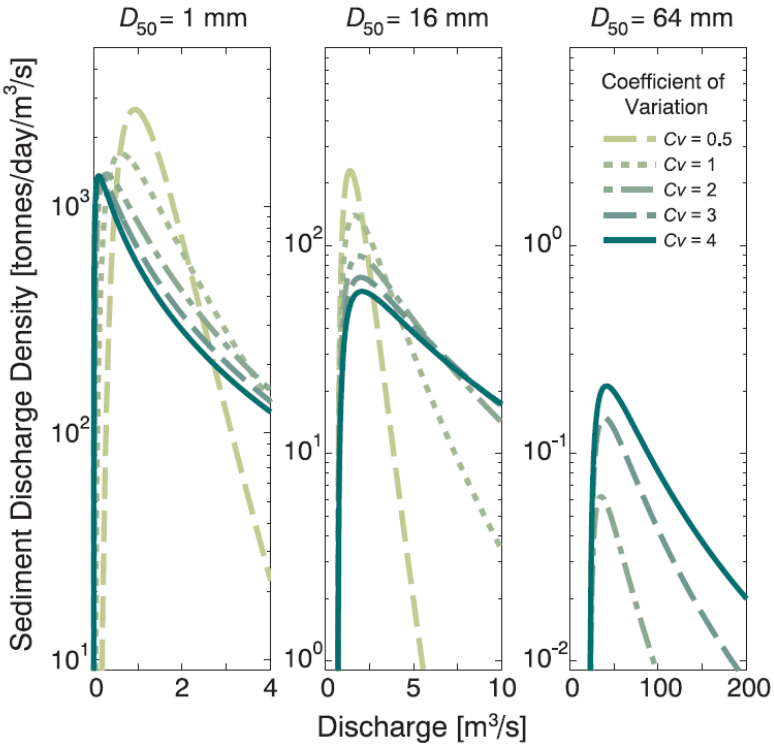

Figure 1.9 Effectiveness curves for a range of grain sizes and C_v values. Note that the discharge associated with the peaks of these curves, Q_{eff}, decreases with increasing C_v for small grain sizes and increases with increasing C_v for large grain sizes.

(Figure 1.6b). This difference increases with grain size. The threshold for fine-grained sediment (1 mm to 8 mm in this example) is relatively small and the sediment transport relation for this size class approximates the single power law, sediment-rating curve used in equation 1.4. Therefore, the $f+ - C_v$ relationship for sand size material (1 mm) approximates the theoretical relation equation 1.4. However, as sediment size increases (> 1 mm in this example), the $f+ - C_v$ relationship increasingly falls below the theoretical relation, though parallels its shape. This is due to the Q_{eff}–C_v relationship previously discussed: as C_v increases more flows occur below the threshold of entrainment for coarser sediment resulting in less sediment transport overall. This combination of effects results in increasingly smaller values of $f+$ as grain size and C_v increase.

Sediment yield interquartile range increases with C_v but decreases with increasing grain size. This means that fine sediment (i.e., sand) dominates the bed, a larger range of flows is responsible for sediment transport and continuity, whereas this range tightens for gravel to cobble bed streams.

The divergence in trends in absolute value of Q_{eff} and C_v between streams with fine versus coarse sediment has been documented in these stream types separately in the literature. Work by Bunte et al. [2014] in bed load-dominated gravel and cobble streams suggests that as flow variance increases so does Q_{eff} such that for certain large values of flow variance, Q_{eff} may be the largest discharge on record (assuming that sediment is never supply limited in these streams). In sand bed streams dominated by suspended

load, Soar et al. [2005] found a decreasing relationship between the ratio Q_{eff}/Q_{bf} and flow variance using a different metric of flow variance: Q_2/Q_{mean}, where Q_2 is the two year flood based on the maximum annual flood series and Q_{mean} is the mean annual discharge. Here I present a physical mechanism for this diverging relationship across sediment size classes due to the relationship between flow variability and the magnitude and frequency of flows greater than the threshold for sediment entrainment.

5 Conclusion

Magnitude-frequency analysis (MFA) conducted with theoretical, closed-form equations 1.2, 1.3, and 1.4 provides valuable insight about the general relationships between sediment transport mode, flow variance, and the magnitude of the effective discharge, Q_{eff}, to generate hypotheses about the physical world. However, these theoretical approaches fall short of capturing important physical processes and complexities inherent in rivers and streams, and may not apply to actual river management scenarios, which have finite time horizons. In this study, I have used simple numerical experiments to test the validity of theoretical MFA approaches in predicting the magnitude and frequency of sediment transport. I have also used the analytical framework implicit in these approaches to study the influence of compound channel form and a threshold for sediment entrainment on the magnitude and frequency of sediment transport.

Theoretical MFA relations predict a monotonic increase in the absolute value, as well as the return interval (RI), of the effective discharge, Q_{eff}, with increasing flow coefficient of variation, C_v, and sediment-rating curve exponent, β using equations 1.2 and 1.3 (Figure 1.3). The fraction of sediment transported by discharges greater than Q_{eff}, $f+$, as predicted by equation 1.4, monotonically increases with C_v and approaches unity asymptotically for large values of C_v (Figure 1.6, solid line). In this study, I demonstrate that even modest modifications to the assumptions contained in these theoretical approaches result in divergent relationships among flow variance, sediment transport mode, and values of MFA metrics. I find the following:

1. Median values of MFA metrics RI and $f+$ from finite flow records sampled from the same continuous flow probability density function used in the theoretical MFA relations demonstrate complex, non-monotonic, and threshold-driven relationships as a function of C_v, β, and the length of the flow record (Figure 1.5) not reflected in the theoretical relations for these metrics.
2. Introducing compound channel morphology by creating a break in the stage-discharge relationship at the bankfull discharge causes the $f+ - C_v$ relationship to fall well below that predicted by equation 1.4. The value of $f+$ increases up to an intermediate value of C_v and then decreases for larger values of C_v (Figure 1.6a). This outcome is due to the reduction in effectiveness of overbank flows with the existence of a floodplain. It is sensitive to the difference between channel bank slope and floodplain lateral slope.

3. Inclusion of a threshold for sediment entrainment results in a divergent relationship between Q_{eff} and C_v between fine and coarse-grain channels. In channels with fine-grained sediment, the absolute value of Q_{eff} decreases with increasing C_v while the value of $f+$ follows equation 1.4 closely. In channels with coarse-grained sediment and larger entrainment thresholds, the absolute value of Q_{eff} increases with C_v and the value of $f+$ falls below that predicted by equation 1.4 (Figures 1.6b, 1.8, and 1.9).

This divergence in the Q_{eff}–C_v relationship for fine vs. coarse sediment has been observed separately in coarse bed [*Bunte et al.*, 2014] and fine bed streams [*Soar et al.*, 2005]. As the flow distribution becomes more positively skewed with increasing C_v smaller flows become more frequent resulting in Q_{eff} reducing with C_v in fine-grained streams with low sediment entrainment thresholds. In coarse-grained streams, these more frequent small flows associated with larger C_v fall below the entrainment threshold. Flows in the tails of the distribution then dominate sediment transport and, because the flow PDF tail thickens with increasing C_v, Q_{eff} also increases.

Magnitude-frequency analysis of sediment transport in rivers provides a process-based, analytical tool for river scientists and managers to characterize what flow or range of flows is most responsible for transporting sediment and maintaining sediment continuity in a channel. These approaches may be applied practically (e.g., channel design and environmental flow studies) and academically (e.g., dynamic equilibrium theory). My study indicates that the empirical approach to MFA, which is based on a

finite flow record, should be relied on for practical questions with engineering time horizons (50 to 100 years). However, in applying the empirical approach to systems with shorter flow records ($>$ 10 years) that have larger C_v values and/or β values ($>$ 2) a few large flows can overwhelm MFA resulting in very large estimates of Q_{eff}. Depending on the question of interest, this result may or may not be appropriate to consider in the long-term sediment yield of a river.

Theoretical MFA approaches are useful for predicting general relationships between aspects of the flow regime, sediment transport mode, and sediment yield in research settings. I found that their assumptions limit their use primarily to cases where sediment entrainment thresholds are non-existent or are very small (e.g., wash or dissolved load) when a sediment rating curve is utilized, where compound channel form is lacking, or where only in-channel flows are considered. The values and behaviors of metrics based on integrals of continuous and infinite PDFs such as $f+$ diverge from those generated from discrete and finite records in large part due to the lack of a continuous right tail in the flow distribution of finite records (Figure 1.4). This lack of continuity in the right tail of empirical records is of course a phenomenon of sample size. This study indicates that use of a continuous theoretical flow PDFs over weights sediment transport in the tails and overestimates their influence under engineering time-frames (often 50 – 100 years) when compared to empirical distributions of finite flow records.

Future work will more closely consider the interaction between channel form, flow regime, and sediment transport mode. The behavior of MFA metrics using different probability distributions other than the two-parameter log normal distribution as well as the use of bed load vs. total load sediment transport equations will be considered. These and other metrics generated from MFA have the potential to inform general geomorphic theory as well as process-based channel design.

CHAPTER 2

The Magnitude and Frequency of Sediment Transport in Alluvial Rivers

Summary

What flow or range of flows is most responsible for transporting sediment and maintaining sediment continuity in a river over human time scales? This question has inspired scores of studies considering the magnitude and frequency of sediment transport (MFA) in rivers and has been a part of the ongoing debate regarding process vs. form-based approaches to stable channel design. I consider this question using bed material load data collected near stream gages across a spectrum of stream types ($n = 153$ sites): from flashy sand bed streams dominated by suspended load to snow-melt gravel and cobble streams dominated by bed load. Using the sediment yield density curve, which is the product of the flow frequency distribution and a sediment transport relationship, I calculate sediment yield metrics describing the magnitude, frequency, and range of flows most responsible for sediment transport over the hydrologic period of

---

Chapter not yet published. Joel Sholtes collected the data from publications and online sources, conducted all of the research, analysis, and writing on this chapter with input and feedback from his advisor. Brian Bledsoe, Peter Nelson, and Daniel Baker co-authored the research proposal that funded a portion of this work. The basic framework for exploring the influence of sediment yield drivers on sediment yield metrics was proposed by them.

record. I then characterize relationships among sediment yield metrics, driving, and boundary variables such as flow variability and bed material properties.

I find that sediment yield in fine bed, suspended load-dominated streams is more sensitive to metrics describing flow variability, whereas in coarse bed, bed load-dominated streams sediment yield is more sensitive to physical aspects of the channel and bed sediment size. Though some differences were observed between fine and coarse bed sites, sediment yield metrics respond in a continuum from flashy hydrology and fine bed streams to stable hydrology and coarse bed streams. This work expands on previous MFA studies by applying a uniform method of bed material magnitude and frequency yield analysis across a wide range—and a large number—of river types to characterize the relationships among properties of the flow regime, bed material, and the range, magnitude, and frequency of the most effective flows. The empirical relations characterized in this chapter compare favorably with theoretical relationships derived in Chapter 1. By considering the magnitude and frequency of sediment transport using the same methodology for fine and coarse bed rivers, this study bridges and extends our understanding of relationships between physical drivers and sediment yield in fine and coarse bed rivers.

1 Introduction

How much and how often sediment moves in a river has preoccupied river engineers and geomorphologists for generations. While the scope of this question is vast, many workers focus on linking channel form, that is, bankfull geometry, to one or more dominant discharges. This vein of inquiry originated with the pioneers of fluvial geomorphology as well as river and canal engineering. Gilbert [1914] and Mackin [1948a], among others, introduced the theory of graded rivers postulating that rivers in dynamic equilibrium adjust their slope and dimensions over time in response to flow and sediment inputs. Rivers in "grade", it is thought, maintain a stable slope and continuity between inputs and outputs of sediment over time given a stationary flow regime. While it has its detractors [e.g., *Kesseli*, 1941] and limitations [*Graf*, 1983; *Pizzuto*, 1994] this theory has proven to be a useful conceptual model for understanding and predicting channel response to the drivers of flow and sediment as well as channel design.

In the mid-20$^{\text{th}}$ century, the U.S. Geological Survey's network of stream gages was over a half-century-old and a large-scale suspended sediment flux data collection effort was underway. Graded river concepts linking channel form with process could directly be tested *in-situ* using these data. With Wolman and Miller's [1960] influential paper on the magnitude and frequency of geomorphic work, a new direction of inquiry opened where daily or sub-daily flow records were combined with newly available long-term daily sediment flux records to calculate the effective discharge, Q_{eff}, or the

discharge that transports the most sediment over time. More recent magnitude-frequency analysis methods use various empirical representations of the flow frequency distribution or a fitted probability distribution function to represent the flow regime [*Nash*, 1994; *Vogel et al.*, 2003; *Goodwin*, 2004] along with flow resistance and sediment transport relations, which translate flow rate or depth to sediment transport capacity [*Hey*, 1996; *Barry et al.*, 2008; *Hassan et al.*, 2014]. The product of these two results in the sediment yield density curve (yield curve), which describes average magnitude and frequency of sediment transport conditions over the flow record (Figure 2.1).

Magnitude-frequency analysis (MFA) of sediment transport in rivers and its relationship with flow regime and channel boundary conditions comprises the framework for the present study. Previous MFA work has only focused on fine bed, suspended

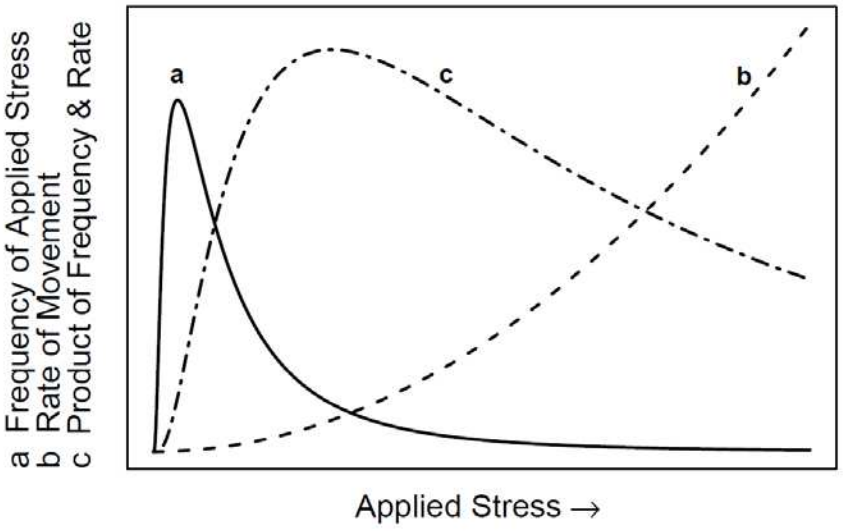

Figure 2.1 Conceptual diagram of lognormal stress (flow) distribution (a), power law sediment rating curve (b), and sediment yield curve (c), which is the product of (a) and (b).

load-dominated [*Wolman and Miller*, 1960; *Nash*, 1994; *Vogel et al.*, 2003; *Simon et al.*, 2004; *Crowder and Knapp*, 2005] or coarse bed, bed load-dominated streams [*Carling*, 1988; *Emmett and Wolman*, 2001; *Barry et al.*, 2008; *Hassan et al.*, 2014], limiting their conclusions about the magnitude and frequency of sediment transport in all rivers and streams. In an often-cited study, Andrews [1980] combined measured suspended load and modeled bed load to estimate total load for his MFA in the Yampa River Basin, Colorado including the wash load component of the suspended load (< 0.0625 mm). Andrews found that Q_{eff} approximates Q_{bf} across all drainage scales. Some have argued that because sediment in transport smaller than the sand-silt threshold (0.0625 mm) is almost always in suspension and not found in appreciable quantities in the channel bed, this wash load material does not greatly influence channel form [*Brownlie*, 1981; *Hey*, 1996; *Soar and Thorne*, 2011]. Therefore, it should not be considered in MFA or total sediment load computations in fine bed rivers if the research question is concerned with the relationship between sediment yield and channel form. If landscape denudation rates or water quality are of concern, then including wash load in this analysis is called for [*Wolman and Miller*, 1960; *Simon et al.*, 2004].

Empirical MFA lacks a comprehensive and standardized consideration of the relationship of flow regime and sediment transport mode with sediment yield across the spectrum of single-thread, alluvial river types. To standardize MFA in this study, I only consider bed material load (sand size and greater). After comparing several methods for representing the flow frequency distribution, I choose one approach to represent the flow

frequency distribution at a site across all sites. Using sediment load and flow data for coarse and fine bed streams, I characterize relationships of flow regime and physical sediment and channel properties with metrics describing the magnitude and frequency of sediment transport, introduced in Section 2. Where applicable, I compare results from this empirical analysis with the theoretical relationships I found in Chapter 1.

This work extends our current understanding of how much sediment is transported by what flow frequencies, and bridges this understanding across a spectrum of river types using previously published and new sediment yield metrics. It characterizes what flows or range of flows are most important in shaping channels and maintaining mass balance in a channel through sediment transport. It also compares these empirical relationships with the theoretical ones derived in Chapter 1.

2 Magnitude-Frequency Analysis Background

The sediment yield metrics I use to characterize the magnitude and frequency of sediment transport in rivers include previously-published metrics such as the effective discharge [*Andrews*, 1980]; the fraction of sediment transported by discharges greater than Q_{eff}, $f+$ [*Vogel et al.*, 2003]; as well as the half yield discharge, Q_{s50}, which is the discharge above and below which the a cumulative 50% of sediment yield occurs on average [*Emmett and Wolman*, 2001; *Vogel et al.*, 2003] (Figure 2.2). A sediment yield metric introduced in this study is the spread of sediment yield, which I define as the

difference between the discharges that bracket 50% of cumulative sediment transported centered on either Q_{eff} or Q_{s50} and normalized by those respective discharges. The sediment yield spread can also be thought of as a normalized interquartile range, IQR. Note that in some cases where the values of Q_{eff} or Q_{s50} are very small or very large, the yield spread metric may not cover a full 50% of sediment yield as the lower or upper bounds of the sediment yield curves might be limiting. I also analyze percentiles and return intervals of these discharge-based sediment yield metrics.

Relationships comparing both physical sediment properties and attributes of the flow regime with the sediment yield metrics described above have been reported in the literature for certain metrics in certain river types. For example, studies on the influence of sediment transport characteristics on the magnitude and frequency of sediment transport have demonstrated that as the value of the exponent of the power law sediment rating curve function increases for a particular channel (β in $Q_s = \alpha Q^{\beta}$,

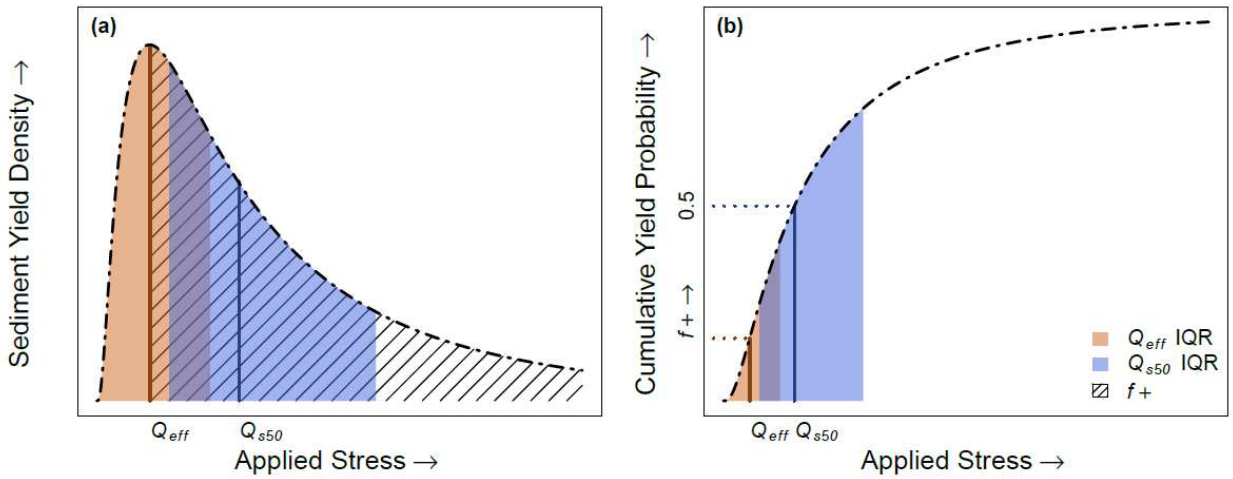

Figure 2.2 Conceptual diagrams of sediment yield metrics plotted on sediment yield density (a) and cumulative probability (b) curves. The shaded areas delineate the bounds of the cumulative 50% of sediment transported centered on Q_{eff} (orange) and Q_{s50} (blue), or normalized IQR.

where Q_s is the sediment transport rate and Q is the water discharge) more sediment is transported over time by less frequent, higher magnitude flows [*Nash*, 1994; *Vogel et al.*, 2003; *Bunte et al.*, 2014]. That is, larger exponent values, which tend to be associated with larger sediment sizes, and larger thresholds for entrainment, weight sediment transport and effective discharge towards these larger, infrequent flow events. The magnitude and frequency of sediment transport in channels with larger rating curve exponent values may be more sensitive to flow variability and changes in flow variability as the right tail of the flow distribution becomes more dominant [*Chapter 1*; *Sholtes et al.*, 2014].

Regarding the influence of flow regime in MFA, previous theoretical work [*Wolman and Miller*, 1960; *Vogel et al.*, 2003; *Goodwin*, 2004] and empirical work [*Pickup and Warner*, 1976; *Nash*, 1994; *Klonsky and Vogel*, 2011] in both sand and gravel dominated systems has found that an increasing relationship exists between estimates of Q_{eff} and variability in the daily flow record. However, other empirical work in sand dominated alluvial channels demonstrates that these relationships might in fact be inverse [*Soar et al.*, 2005]. As demonstrated in Chapter 1 and in Sholtes et al. [2014], by including a threshold for sediment transport in MFA, this divergent relationship between flow variability and Q_{eff} can be explained. As flow variability increases, the mode of the flow distribution becomes smaller and the right tail thicker. The tail of the flow distribution dominates sediment yield in coarse bed systems with larger thresholds for transport, leading to an increase in Q_{eff} with flow variability here. The mode of the

flow distribution dominates sediment transport in fine grain systems with little to no threshold for sediment entrainment, leading to a decrease in Q_{eff} with flow variability.

Some work has suggested that watershed scale relationships exist between sediment transport properties and flow regime. For example, Barry et al. [2004] and Bunte et al. [2014] found that in armored, snowmelt streams an increasing relationship exists between both the coefficient and the exponent of sediment rating curves in coarse bed channels and drainage area. This is likely linked to the reduction in bed grain size moving downstream as well as the increase in fine sediment supply. Andrews [1980] reports a decreasing trend in daily flow skewness and increasing trend in duration of Q_{eff} with drainage area in the snowmelt driven Yampa River Basin. However, he found that the ratio of Q_{eff} to Q_{bf} remained close to unity throughout. Nash [1994] considered the recurrence interval of Q_{eff} in a nationwide survey of suspended-load dominated rivers and found no significant correlation between drainage area and the recurrence interval of Q_{eff}. Finally, Simon et al. [2004] found that Q_{eff} calculated from daily flow records and total suspended load measurements had a recurrence interval that ranged from 1.1 to 1.7 years across a wide range of drainage areas and physiographic regions. Their findings indicate that the frequency of Q_{eff} remains fairly stable across a wide range of drainage areas.

Individual studies on relationships between either flow variability or grain size with the magnitude and frequency of sediment yield in rivers may conflict with one another and general understanding of how these relationships play out across a wide

variety of rivers does not exist. This is partly due to workers' focus on either coarse or fine bed rivers as well as a lack of standardization in methodology, not to mention the complexity in drivers and boundary conditions that create channel form. As Emmett and Wolman [2001, p. 1378-1379] reflected:

> Given this variety and plethora of controls of channel form, it is not surprising that no all-encompassing relationship between morphology and transport has been constructed [*Nash*, 1994]. Parenthetically, it is interesting to note that, despite the accumulation of much data on flow duration, adequate quantitative comparisons remain difficult because comparable data on flow duration, sediment characteristics and transport, and channel characteristics are not reported consistently. This does not imply that consistent data would assure emergence of a universal relationship between sediment transport and river form. Nor, of course, does the absence of universality and the presence of variability imply only uniqueness and disorder. Given the noise, one might marvel at *the order that can be discerned* and used. (emphasis added)

The present study extends on previous work by using consistent data and standardized methods to exploring the magnitude and frequency of sediment transport in a wide range of river types as a function of flow regime and channel boundary conditions. It introduces and characterizes the behavior of new sediment yield metrics, compares empirical results with theoretical ones, and explores how sediment yield metrics behave across coarse and fine bed sites. It is my hope that by asking some new questions about the magnitude and frequency of sediment transport with a standardized methodology I might achieve some "order that can be discerned and used" in science and management of sediment transport in rivers.

3 Data and Methods

Empirical magnitude-frequency analysis of sediment transport in rivers requires 1) either a calibrated sediment transport equation for a particular site or sediment transport–flow measurements, and 2) a relatively long flow record (>10 years, though >20 years is preferable, see Chapter 1). The methods described below primarily focus on how the sites were selected, what types of data are used in this study, how the sediment transport–flow relationships are derived, and how the general MFA is conducted. I also discuss and test several methods for representing the flow distribution in an effort to create an MFA approach that works well across a wide variety of systems. Detailed information on data sources and methods used to estimate Q_{bf} using at-a-station hydraulic geometry—data used in this chapter—is provided in Chapter 3, where the bankfull discharge is a primary focus. Methods utilized to extend the flow records of sites with flows records < 10 years is provided in Appendix 4C.

3.1 Site Selection and Description

I use gaged flow and sediment flux data from 153 sites across the conterminous U.S. and Puerto Rico including 60 coarse bed sites and 93 fine bed sites for which ≥15 paired bed material sediment load-discharge measurements were available near a flow gage with a long-term record (Figure 2.3). In general, these sites were selected because the majority have been previously published in MFA studies or are located along the same river as previously-published sites and deemed to meet the criteria for MFA.

However, because the percent of particles finer than 0.0625 mm (wash load fraction) of suspended load is often not evaluated in suspended load measurements and sites with smaller drainage areas (<100 km^2) are under-represented in published MFA studies, other sites were brought in to this study to augment the data set. I included only alluvial rivers (mobile bed and banks) in dynamic equilibrium with the drivers of flow and sediment supply, meaning measured channel properties are likely to be stable over an engineering time frame (50-100 years). Impacts such as flow regulation, channelization, and land use change can result in transient influences on channel form and are therefore avoided in this study. I used aerial photograph reconnaissance as well as USGS gage notes as a rough method for determining if a river was either regulated or

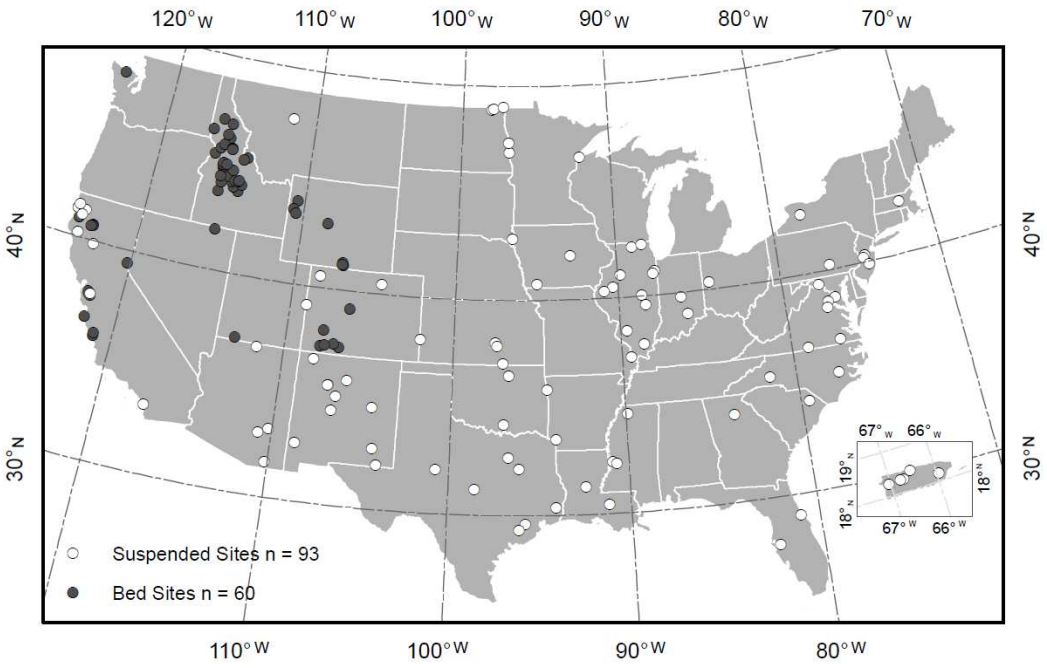

Figure 2.3 Map of co-located bed material load measurements and flow gages for fine bed sites (white circles) and coarse bed sites (black circles) used in Chapter 2.

channelized, and removed it if it was. Site specific information including data sources for sediment load measurements and channel properties is given in Tables 2A.1 and 2A.2 in the Appendix.

Characteristics of each site have been summarized in Figure 2.4 a to f. These plots are symmetrical empirical density functions with box-and-whisker plots inside (black rectangle interquartile range with white dot at the median). The values of the sediment rating curve exponent, β ($Q_s = \alpha Q^{\beta}$) have a median just below 2 for the fine bed sites, and just above two for the coarse bed sites, but the latter have a much greater spread in β and a larger average value of β (Figure 2.4a). While the drainage areas of both types of sites overlap, more sites in the 100 to 1,000 km^2 range exist for coarse bed sites, and more sites in the 10,000 to 100,000 km^2 range exist for the fine bed sites (Figure 2.4b). The difference in drainage area is due to the nature of USGS' suspended sediment monitoring program, which targets larger rivers, as well as the upper limits in drainage area for coarse-bed rivers in the U.S. The majority of the coarse bed sites have a coefficient of variation of daily flow (C_v) that is less than 2, while a much broader range of C_v values exists for the fine bed sites, whose interquartile range falls between 1.5 and 3 (Figure 2.4c). Flow record lengths between the two types of sites are fairly similar with a median record length for fine bed sites of approximately 65 years and 45 years for coarse bed sites (Figure 2.4d). Median grain size data, where available, are also evaluated (Figure 2.4e). I use median grain size values to differentiate

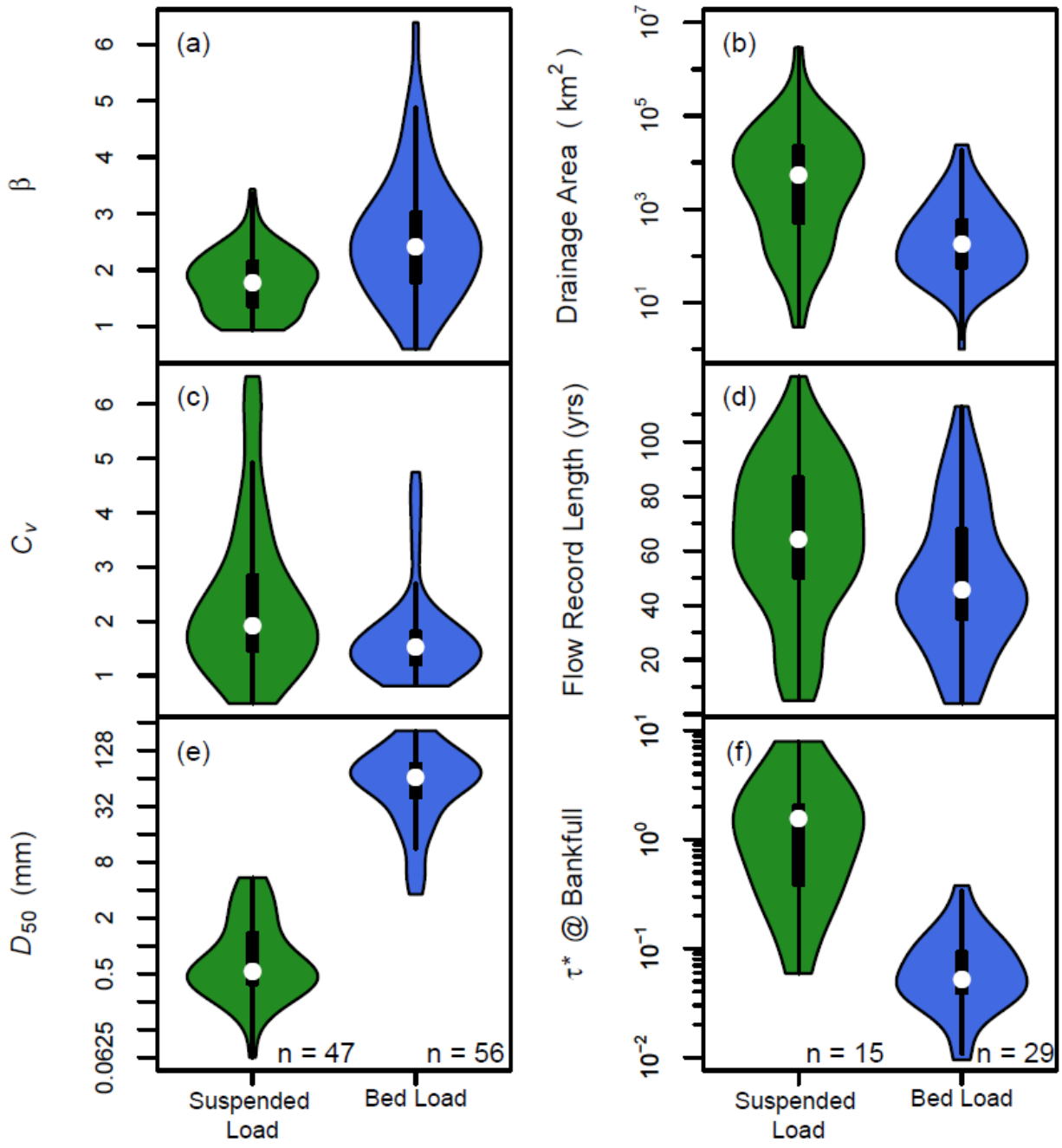

Figure 2.4 Empirical density functions (violin shapes) and interquartile ranges (black rectangles with white median dots) for site attributes. Unless otherwise noted, n = 93 fine load sites and n = 60 coarse bed sites.

between fine-bed, suspended load-dominated sites and coarse bed, bed load-dominated sites. Here I am making the assumption that the suspended load dominates bed material load transport in sites with mostly sand beds, and that bed load dominates bed material transport in sites with gravel and cobble beds. Sites with mixes of sand and gravel in the bed have been avoided because bed material is transported both as bed and suspended load in significant proportions and data for both modes of transport at a particular site are rare.

Although some of the fine bed sites do have an average median bed sediment grain size, D_{50}, in the very fine gravel range (Figure 2.4e). I removed most sites from both fine and coarse bed categories for either being too coarse, or fine, respectively. The average median grain size of some fine bed sites lies in the very fine to fine gravel range (1 to 4 mm); however these sites were kept in the suspended load analysis because several bed sediment samples from these sites have D_{50} values in the sand range. I cut off coarse bed sites at the lower end of the fine gravel range (4 mm). While there are more objective methods for determining the dominate mode of sediment transport based on hydraulic properties and grain size, such as the Rouse number [*Julien*, 2010], calculating these for all sites was not possible given available data.

Data were available for determining the value of dimensionless shear stress, τ^*, at bankfull discharge, where $\tau^* \approx hS \,/\, (1.65D_{50})$ with h the flow depth at bankfull (approximation for hydraulic radius), S the stream bed slope (approximation for the energy slope), and D_{50} the median diameter of the bed material. This parameter is also

helpful for inferring the dominant mode of sediment transport in rivers [*Dade and Friend*, 1998]. Bed load-dominated rivers tend to have values of $\tau^* \leq \tau_c^*$, where τ_c^* is the critical value for incipient motion and ranges from 0.03 to 0.07 [*Buffington and Montgomery*, 1997]. Suspended load-dominated rivers tend to take on values of $\tau^* \geq 1$ at bankfull discharge, and mixed load rivers have values of τ^* that fall between bed- and suspended-load dominated rivers. I estimate values of τ^* for sites having the necessary data (Figure 2.4f), finding that the median value of τ^* for fine bed sites is 1.5 with an inter quartile range, IQR $\in$ (0.4, 2.1), and the median value for coarse bed sites is 0.05 with IQR $\in$ (0.04, 0.1). The lower end of the τ^* values for fine bed sites and the upper end of τ^* values for coarse bed sites falls in the mixed load category, therefore some mixed load sites may exist in this dataset.

3.2 Bed Material Load Data Sources

Sediment moves through rivers by saltating and rolling along the bed as bed load and in suspension in the water column as suspended load. I have divided my sites along these two transport modes terming coarse bed, bed load-dominated sites "coarse bed", and fine bed, suspended load-dominated sites "fine bed". For the purposes of this study, these transport types are estimated using bed load samplers, and depth-integrated suspended load samplers, respectively. Of course, this binary distinction never absolutely exists in the real world. All forms of transport tend to occur in a given river at various points in time whether its bed is coarse or fine, depending on its sediment supply. In

some cases, the total sediment yield in coarse bed rivers can be dominated by fine sediment in suspension [*Whiting et al.*, 1999]. Though fine sediment may travel in suspension in coarse bed rivers, it is the movement of the coarse bed material that ultimately forms the channel boundaries; therefore, I only use bed load measurements to conduct MFA at coarse bed sites. Bed load transport in fine bed rivers also plays an important role in sediment continuity, channel geometry (e.g., slope) [*Hey*, 1996] as well as in flow resistance calculations [*Brownlie*, 1981]. However, it has been shown that bed load in fine bed rivers is approximately a factor (e.g., 10%) of suspended load, and does not significantly influence the slope of the rating curve [*Nash*, 1994; *Michels-Boyce*, 2014b]. Therefore, I limit my MFA in fine bed rivers to suspended sediment measurements only.

I compile paired bed load–instantaneous discharge data sets from a range of sources listed below in Table 2.1. Specific information for all sites is compiled in Appendix 2A. In general, these data were collected using Helley-Smith bed load samplers, which collect grain sizes ranging from approximately 0.2 mm (depending on the mesh size used) to 64 mm, truncating the upper end of sediment size at the gravel-cobble threshold [*Emmett*, 1980]. Bunte and Abt [2009] note that particles larger than 64 mm are rarely sampled in larger bed load traps in small to medium sized streams. However, work by Bunte and her collaborators indicates that the short sampling times associated with the Helley-Smith sampler under-samples coarser particles in general, which move very sporadically. This, in addition to local flow acceleration caused by the

Helley-Smith sampler, can lead to rating curves with milder slopes than those generated from bed load traps [*Bunte et al.*, 2004], a potential downfall. The coarse bed sites utilized in this study have drainage areas ranging from 10 to 10,000 km^2 and are located primarily in the central and northern Rocky Mountain region where the majority of bed load data exist. Some bed load data for sites located in the U.S. Southwest and Pacific Northwest are available through the USGS National Water Inventory System Water Quality Samples for the Nation Database[3]. There is a substantial lack of published or government collected bed load data in the remainder of the country.

A much greater amount of suspended sediment data are available in the U.S. and Puerto Rico. The focus of this study is bed material load, defined here as particle diameters > 0.0625 mm (sand-silt cutoff). Therefore, I limited my search to suspended sediment datasets that contained a minimum of 15 suspended sediment concentration measurements with grain size analysis to determine percent of sediment coarser than 0.0625 mm (sand-sized component). I determined these sites to be primarily sand bed streams either from published bed sediment samples or from aerial photograph reconnaissance. I utilized the USGS Sediment Data Portal[4], Discrete Site data [*USGS*, 2014] for suspended sediment concentration, percent of suspended sediment sample with diameters > 0.0625 mm, and instantaneous discharge data. In some cases, instantaneous discharge data were not available at the time of the sediment concentration

[3] http://nwis.waterdata.usgs.gov/usa/nwis/qwdata
[4] http://cida.usgs.gov/sediment/

measurement. In these cases, average daily flow values were used. Some outliers were removed from the data based on visual assessment and confirmation that data were entered incorrectly (e.g., very large values of sediment transport at very low discharges, or vice sersa).

Table 2.1 Bed material load measurement sources

Reference	Region / Site
Coarse bed Sites	
Andrews [1994]	Sagehen Creek, California
Andrews [2000]	East Fork Virgin River, Utah
Bunte & Abt [2009]	Rocky Mountains, Colorado
Erwin et al. [2011]	Pacific Creek, Wyoming
Jones & Seitz [1980]	Clearwater River, Idaho
King *et al.* [2004]	Rocky Mountains, Idaho
Rankl & Smalley [1992]	Rocky Mountains, Wyoming
Smalley et al. [1994]	Wind River, Wyoming
USFS [2014]	Rocky Mountains, Colorado & Wyoming
USGS NWIS [2014]	California
Fine bed Sites	
Biedenharn & Thorne [1994]	Mississippi River
Crowder and Knapp [2005]	Illinois
Nash [1994]	Conterminous US
Nolan *et al.* [1987]	California
Soar & Thorne [2001]	Midwestern & Eastern US
Watson et al. [1997]	Midwest, US
USGS Sed. Data Portal [2014]	Conterminous US and Puerto Rico

3.3 Physical Site Metrics

Physical site metrics describing channel geometry and bed sediment characteristics of each site were calculated where data were available. Estimates of the median and 84^{th} percentile grain size were based on pebble count data for bed-load sites and from sieved bed sediment samples reported either in the literature or on NWIS. Bankfull discharge was either estimated based on matching a field-identified bankfull

stage with an estimated flow rate from a nearby gage, or from identifying a break in the discharge-channel geometry relationships described in the hydraulic geometry methods for bankfull discharge determination discussed in Williams [1978]. See Chapter 3 for further discussion on bankfull discharge estimation. Bankfull width and average depth were estimated from hydraulic geometry relationships based on site-specific measurements evaluated at the bankfull discharge. Drainage area data were collected from NWIS site descriptions as well as published values. Slope estimates are water surface slope estimates measured in the field at some sites. I used these values to calculate τ^* using the D_{50} of the bed material and the average depth at bankfull.

3.4 Sediment Rating Curve Generation

Much effort has been given to statistically defining an accurate relationship between flow and sediment transport measurements. This can be a painstaking process with consideration of multiple flow-independent variables [*Cohn et al.*, 1989], inter-annual variability and seasonality [*Walling*, 1977a; *Syvitski et al.*, 2000; *Bunte and Abt*, 2009], hysteresis [*Walling*, 1977a; *Moog and Whiting*, 1998], and uncertainty [*Rustomji and Wilkinson*, 2008]. Finding the most accurate model for each site is not a primary goal of this study because I do not attempt to quantify an accurate absolute sediment load. Rather, I calculate metrics based on the sediment yield curve. Due to the broad nature of the present study and the large amount of sites used, a bivariate, log-linear regression equation was used to define the relationship between discharge and sediment

load (kg/sec). Bed load measurements were generally reported as mass/time. Suspended load measurements were reported as concentrations (mass/volume) and were converted to mass/time by multiplying the concentration by the flow rate. Therefore, suspended sediment load observations were more highly correlated with flow than bed load measurements. Sites were culled in which a low log-linear correlation value resulted for sediment load and discharge relationships and/or a log-linear relationship did not appear to be a reasonable fit based on visual assessment. The interquartile range of R^2 values for suspended load sites is 0.65 to 0.86 with a minimum value of 0.22 and a maximum of 0.96. For coarse bed sites, the interquartile range is 0.57 to 0.77 with a maximum of 0.97 and a minimum of 0.25. The F statistic for log-linear model significance is large enough for all models such that all models had significant fits ($R^2 \neq 0$) at the $\alpha = 0.05$ significance level (maximum p value is 0.02). Diagnostic plots for each model are provided in Appendix 2B.

I examined the sensitivity of log-linear regression line slopes (exponent in untransformed power law equations) to two regression methods: the ordinary least squares model (OLS, `lm()` **R** function) and the robust linear model (RLM, `rlm()` **R** function, `MASS` package). A Bayesian log-linear model as well as uncertainty analysis associated with each method are explored in the following chapter.

Each method has particular inherent assumptions, the most restrictive of which are those of OLS, which require residual error to be normally distributed and of equal variance. This method is also sensitive to outliers or largely divergent values at either

end of the independent variable range [*Ott and Longnecker*, 2001, p. 534]. The normally distributed error assumption is relaxed in RLM, which uses a weighting function that gives less weight to data further away from the mean [*Huber and Ronchetti*, 2009].

The two log-linear regression models require re-transformation bias correction factors to account for the lognormally distributed residual error [*Ferguson*, 1986; *Cohn et al.*, 1989]. Because the residual error is not symmetric about the re-transformed power law regression line (assumed to be normal in log-space and log-normal in Cartesian space), an uncorrected power law function calculated from these methods will tend to be downward biased. Here, the quasi maximum likelihood estimate (QMLE) of the bias correction factor [*Cohn et al.*, 1989], introduced by Ferguson [1986] in regards to estimating sediment loads using a power law rating curve, is used to correct for bias:

$$BCF = e^{ks^2/2} \qquad s^2 = \sum_{i=1}^{N} \frac{\left(Y_i - \hat{Y}_i\right)^2}{N-2} \tag{2.1}$$

The s^2 term is simply the variance of the log-transformed residuals, and $k = 1$ for natural logarithms and 5.3 for base 10 logarithms. The terms Y_i and $\hat{Y}_i$ refer to individual sediment load observations and predicted mean values of sediment load from the regression equation at discharge value i, and N is the number of paired discharge-sediment load observations. To eliminate bias in re-transformed load values, the bias correction factor is applied as follows:

$$Q_s = e^{ks^2/2} \alpha Q^{\beta} \tag{2.2}$$

3.5 Hydrology and Hydrologic Metrics

The majority of sediment measurement sites used in this study are co-located with USGS stream gages; therefore, I utilized the National Water Inventory System[5] to acquire average daily flow data for each site. In some cases, daily flow data were supplied by the U.S. Forest Service [*USFS Boise Adjudication Team*, 2014]. Flow data with finer time resolution is preferred in MFA [*Biedenharn et al.*, 2000; *Soar and Thorne*, 2001] due to the non-linear relationship between sediment load and discharge. Average daily flow data can underestimate sediment yields when compared to hourly or 15-minute flow data [*Holmquist-Johnson*, 2002] because these data do not capture intra-daily flow transience such as flood peaks from convective rainfall or the daily flow pulse in snow-melt rivers. However, limiting this study to sites with instantaneous flow data would make comparing the magnitude and frequency of sediment transport in rivers across a spectrum of river types—a primary goal of this study—infeasible due to the shorter record lengths and relative paucity of instantaneous flow data collocated with bed material load data.

Flow data were used in magnitude frequency analysis as described below in Section 3.8. I also calculated metrics from these flow data describing their variability (Table 2.2, below). Flow metrics involving peak flow values such as the 1.5 year return interval (RI) flood magnitude, $Q_{1.5}$, were calculated from the annual maximum

[5] http://waterdata.usgs.gov

instantaneous discharge for each site, where available, using the Weibull plotting method: $RI = m/(n+1)$, where m is the rank of the flood event and n is the number of events on record.

Some sites with bed material load data had relatively short record lengths (<10 year). Generally, longer-term flow records are desirable in MFA to capture a better sample of flow variability at a site [*Biedenharn et al.*, 2000; *Soar and Thorne*, 2001]. To extend the flow records, I first identified USGS stream gages located near gages with shorter records that had coincidental and longer-term flow records. Using the `RecordExtension.R` script created for this purpose, I used the modified MOVE method described by Moog et al. [1999] to extend short term flow records at a sediment measurement site using a statistical relationship between transformed, concurrent flow data at the site and at a nearby gage with a longer record. A detailed description of the methods used to extend flow records at selected sites as well as plots of the output are provided in Appendix 2C.

Various hydrologic metrics describing the variability or flashiness of a flow regime were investigated. Skewness is calculated as $\mu_3 / \mu_2^{3/2}$, where μ_2 and μ_3 are the second and third central moments of the data. The coefficient of variation is calculated as $s/\bar{x}$, where s is the standard deviation of the sample and $\bar{x}$ is its mean. In general, skewness characterizes the level of asymmetry of the data's distribution. Flow data are nearly always positively skewed, meaning that the right tail of the flow distribution is thicker and/or longer than the left (a large quantity of smaller flows occur during base flow

periods punctuated by few large flows during floods, see curve "a" in Figure 2.1,). The C_v is a normalized estimate of the standard deviation and is highly correlated with skewness for these sites. Other flashiness metrics such as the Richards-Baker flashiness index (*flash.RB*) [*Baker et al.*, 2004] and the ratio of $Q_{1.5}$ to mean daily flow (*Q1.5.mean*) related to sediment yield metrics well.

3.6 Magnitude-Frequency Analysis

Magnitude-frequency analysis of sediment transport in rivers considers the product of a continuous or discrete representation of the flow regime (or bed shear stress) probability distribution (e.g., an histogram or a theoretical or empirical density function) with a sediment rating curve for sediment transport function that is either a function of discharge or another hydraulic parameter such as bed shear, stream power, or flow velocity. I have discussed the sediment rating curve methodologies used in this study above and now discuss the procedure for representing the flow regime as a density distribution, calculating the product of the flow density function and the sediment rating curve, and finally calculating metrics based on the sediment yield density and cumulative density functions.

Numerous methods for representing the flow distribution in MFA have been presented. These range from the standard histogram, arithmetic binning method [*Biedenharn et al.*, 2000; *Soar and Thorne*, 2001], to estimating the empirical probability density function using numerical differentiation of the empirical cumulative

distribution function [*Orndorff and Whiting*, 1999; *Emmett and Wolman*, 2001] or using kernel density function [*Klonsky and Vogel*, 2011], to fitting a continuous PDF to the flow data [*Nash*, 1994; *Goodwin*, 2004]. A preliminary analysis of the kernel density function approach to estimating the flow PDF for MFA outlined in Klonsky and Vogel [2011] resulted in peaky sediment yield curves and highly variable estimates of Q_{eff}. I proceeded to assess the flow PDF estimation methods using only the histogram approach, the empirical density function approach, as well as fitting a log-normal PDF to the data (Figure 2.5). I calculated Q_{eff} using all of these methods and examined the sensitivity of each method to flow record length (RL), the sediment rating curve exponent, β, and the daily flow coefficient of variation (C_v). I also examined the difference in estimates among one another as a function of these same variables.

The histogram approach used in this study follows the general procedure outlined in Biedenharn et al. [2000] as well as Soar and Thorne [2001] who recommend starting with 25, equally-spaced bins spanning the range of flows. The density formulation of the histogram is then calculated following equation 2.3:

$$\rho_Q = \frac{n_i}{N\Delta Q} \tag{2.3}$$

where ρ_Q is the probability density of a given discharge bin ($\rho_Q \equiv$ [probability/(m^3/s)]), n_i is the count of observations in bin i, N is the total number of observations, and ΔQ is the bin width. I then calculate Q_{eff} as the median of the discharges contained within the bin with the greatest sediment yield density value, that is, the product of the median

discharge within each histogram bin with the sediment rating curve value at that discharge value. If Q_{eff} falls into the first bin, Biedenharn et al. [2000] recommend dividing that bin in half and recalculating Q_{eff}. I repeated this procedure a maximum of 10 times. Biedenharn et al. [2000] also recommend reducing the number of bins in the tails of the distribution so that it is continuous. I did not apply this rule to our analysis.

The empirical density function approach is described by Orndoff and Whiting [1999] as well as Emmet and Wolman [2001]. First, an empirical cumulative density function (eCDF) is created by plotting the ordered flow observations (Q_i) with their associated cumulative probability values F_n:

$$F_n(Q) = \frac{1}{N}\sum_{i=1}^{N} 1\{Q_i \le Q\} \tag{2.4}$$

where $1\{A\}$ is the indicator function for event A. This can also be done with the `ecdf()` function in **R**. The eCDF is then numerically differentiated to produce an ePDF. Using equally-spaced differentiation nodes produces results very similar to the histogram method described above. Using logarithmically spaced differentiation nodes results in a most continuous and smooth ePDF. I used 50 logarithmically distributed nodes to differentiate using central difference approximation.

Soar and Thorne [2001] warn against logarithmic binning to represent the flow distribution function as it produces bias when compared to arithmetic binning. They

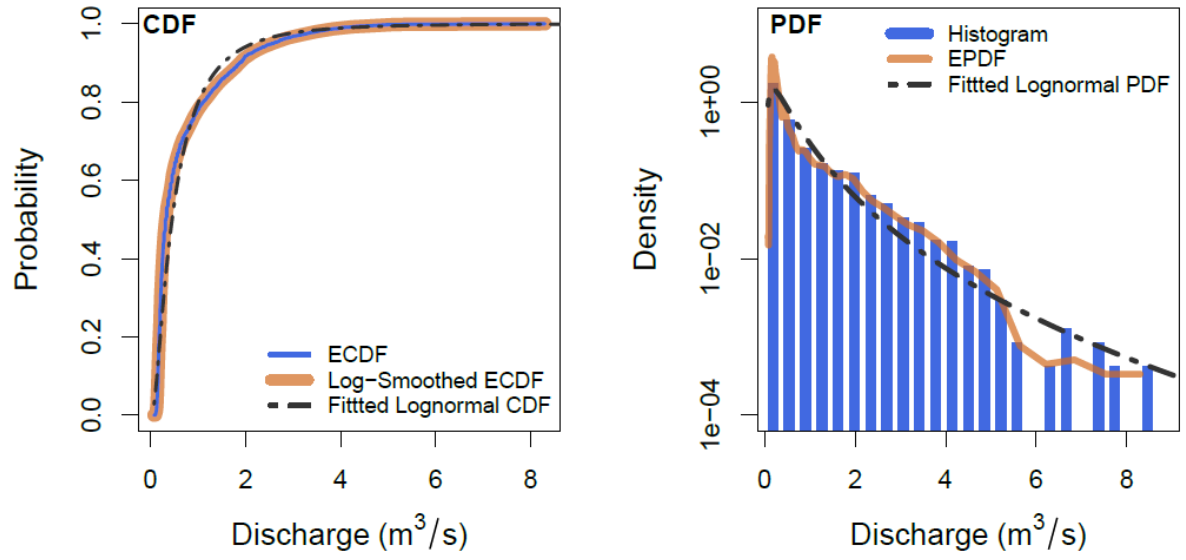

Figure 2.5 Comparison of methods used to represent the flow regime: arithmetically-spaced histogram, empirical cumulative distribution function (eCDF) based on the sorted flow record, a smoothed eCDF using log-spaced evaluation points, and the continuous log-normal distribution function fitted using the method of moments.

argue that because logarithmic bins increase in width with increases discharge values, they will over-estimate the density of larger flows and over-estimate Q_{eff}. The ePDF method with logarithmic differentiation nodes differs mathematically from logarithmic binning. The former is essentially a smoothing method that samples the eCDF constructed from daily flows. The latter estimates the frequency or density of flows within bins that change sizes, which can lead to the bias observed by Soar and Thorne [2001]. This bias was not observed in the present study when comparing estimates of Q_{eff} based on the logarithmic smoothing method with those based on the arithmetic binning method as is discussed in Section 4.1, below. The eCDF of flow records often exhibits steps or jumps within the upper quantiles due to fewer larger flows in the

record (Figure 2.5). This results in singularities (division by zero) or large spikes when numerically differentiating this eCDF to generate the ePDF due to large or infinite slopes in the ePDF. By using logarithmically-spaced evaluation nodes to smooth the ePDF, this method differentiates the eCDF at an interval spacing that better matches its curvature.

Finally, I estimated the flow distribution by fitting the two-parameter continuous log-normal PDF to the flow data using the method of moments [*Yevjevich*, 2010], as discussed in Chapter 1, equations 1.1, 1.5, and 1.6. The lognormal PDF has a long history of representing stream flows in MFA [*Wolman & Miller*, 1960; *Nash*, 1994; *Vogel et al.*, 2003]. However, other skewed, continuous PDFs such as the gamma distribution or a broken power law function may provide a better fit to the data [*Goodwin*, 2004; *Segura and Pitlick*, 2010]. The three representations of the flow distribution used in this study—arithmetically-binned histograms, empirical PDF, and fitted lognormal PDF, are plotted together in Figure 2.5, and Figure 2.6b. As discussed further in the Results section, I calculated all Q_{eff}-related sediment yield metrics using the estimate produced by the ePDF method, as it performed the most well over all sites.

Once the flow distribution function has been calculated, it is multiplied by the sediment transport relation (sediment rating curve in this study, Figure 2.6a) to create the sediment yield density curve (Figure 2.6c). By integrating under the area of this curve, one calculates the average daily sediment yield over the flow record given a daily flow record. One can also calculate MFA metrics from this curve as well as the

cumulative sediment yield curve, calculated from the flow record directly (Figure 2.6d). The effective discharge is estimated as either the median of the discharges contained in the peak sediment yield density bin or the peak value of the eCDF or log-normal sediment yield density curves.

3.7 Sediment Yield Metrics

The previously-described flow and physical metrics are considered driving or independent variables to be related to the response, or dependent variables associated the magnitude frequency analysis. Sediment yield metrics calculated from the magnitude-frequency analysis are listed below in Table 2.2, and include the aforementioned effective discharge, or the peak of the sediment yield density curve, and the fraction of sediment transported by discharges smaller than the effective discharge: *Qeff.*yield, or its compliment, *f+*, as well as the difference in discharges associated with +/- 25% of cumulative sediment transport centered on the effective discharge and normalized by that discharge: *Qeff.spread*. I also calculated discharges and spread associated with the cumulative half yield of sediment transport, Q_{s50}, or the half yield discharge as well as *yield.spread*, which is the difference between the discharges associated with 25% and 75% of cumulative sediment transport normalized by Q_{s50}. Throughout this chapter, I refer to these metrics using italicized abbreviations as shown in Table 2.2.

I calculate the return intervals in years and percentiles of Q_{eff} and Q_{s50} based on the daily flow record, and normalize these values using the $Q_{1.5}$ and mean daily flow for inter-comparison. Figure 2.2, above visually demonstrates some of the sediment yield metrics just discussed. I used **R** to conduct all of the analyses in this study. A list and description of **R** scripts created to implement the analyses for this study along with reproductions of the **R** scripts themselves are included in Appendix 2D.

Table 2.2 Metric Definitions

	Metric	Units	Description
Flow	*yrs*	(yrs)	Number of years on flow record
	mean	(m^3/s)	Mean of daily discharge
	C_v	–	Coefficient of variation of daily flow (s / $\bar{x}$)
	skewness	–	Skewness of daily flow
	spread	–	(75^{th} p-tile flow – 25^{th} p-tile flow) / median flow
	flash.RB	–	Daily flow flashiness metric [*Baker et al.*, 2004]
	$Q_{1.5}$	(m^3/s)	1.5 year return interval flood
	Q1.5.mean	-	$Q_{1.5}$ normalized by the mean of the daily flows
Physical	D_{50}	(mm)	Average median diameter of the bed sediment
	D_{84}	(mm)	84^{th} percentile diameter of the bed sediment
	Q_{bf}	(m^3/s)	Bankfull discharge
	tau.star, τ^*	–	Dimensionless bed grain shear stress at bankfull depth
	w.d	–	Bankfull width to depth ratio
	da.km2	(km^2)	Drainage Area
Yield	*Qs50.RI*	(yrs)	Return interval of half yield discharge (Q_{s50})
	yield.spread	–	(Q_{s75} - Q_{s25}) / Q_{s50}
	Qs50.Q1.5	–	Half yield discharge normalized by $Q_{1.5}$
	Qeff.RI	(yrs)	Return interval of Q_{eff}
	Qeff.spread	–	Similar to *yield.spread*, centered on/normalized by Q_{eff}
	*Qeff.*yield	(%)	Percent of cumulative sediment transport below Q_{eff}
	f+	(%)	Percent of cumulative sediment transport above Q_{eff}
	Qeff.Q1.5	–	Q_{eff} normalized by the $Q_{1.5}$
	Beta, β	–	Sediment rating curve exponent

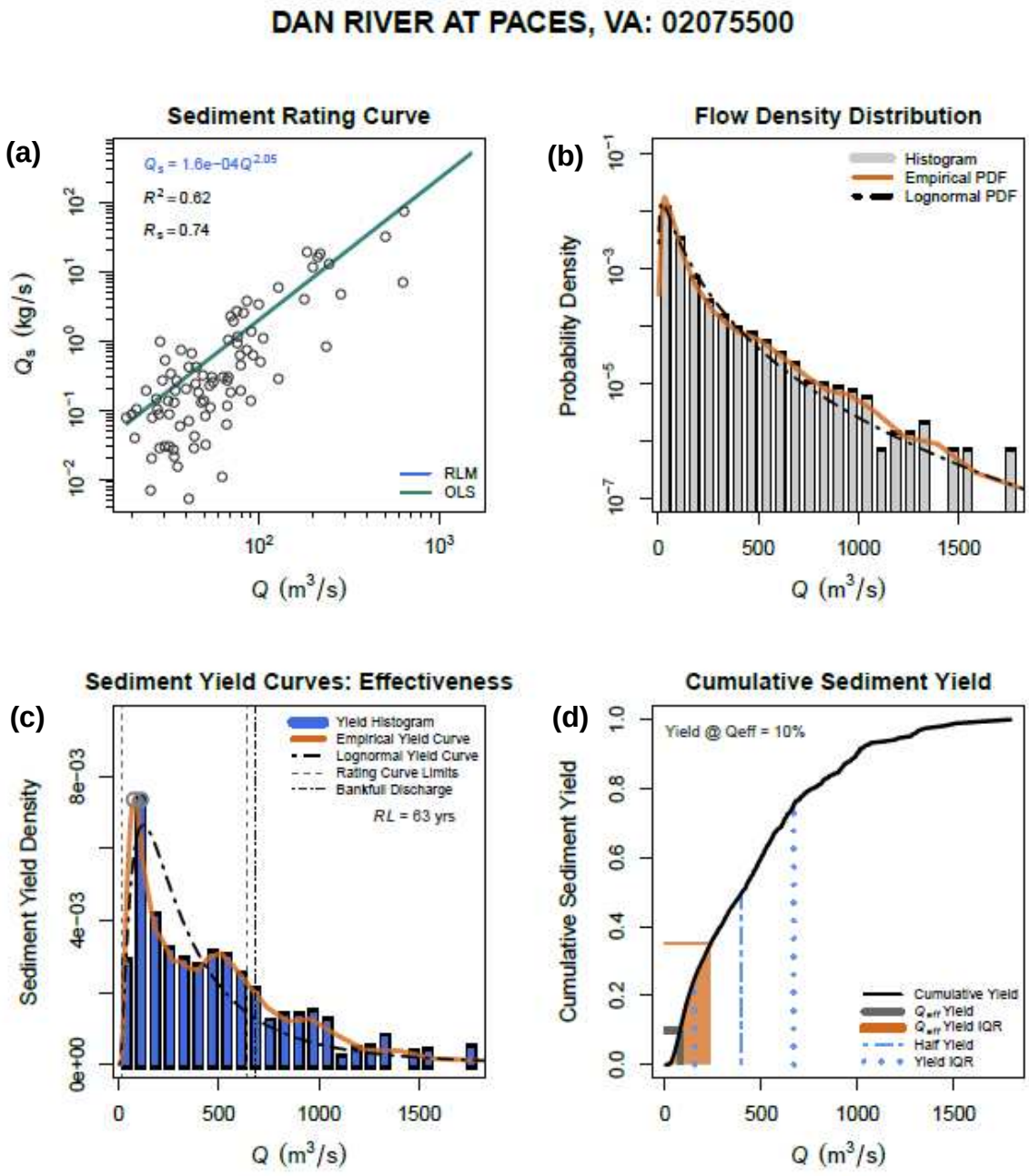

Figure 2.6 Example of MFA methods and output. A) The bias-corrected, log-log linear regression of the sediment rating curve with ordinary least squares line (OLS) and the robust linear regression line (RLM). B) The flow density distribution portrayed as 25 arithmetic bins, and empirical PDF, and a fitted, continuous lognornmal PDF. C) Sediment yield curves from the three methods outlined in B) along with vertical lines indicated Q_{bf} as well as the discharge limits of the sediment load data. D) A cumulative sediment yield curves with various sediment yield metrics.

4 Results

I begin this section by first comparing estimates of Q_{eff} using three methods for characterizing the flow frequency distribution. I then explore the outcomes of the empirical MFA by considering relationships between sediment yield metrics (response variables), and metrics based on the flow regime, bed material size, rating curve exponent, and physical channel properties (driving variables). Metrics used in this analysis are described above in Table 2.2.

4.1 Magnitude-Frequency Analysis Method Assessment

Of the three methods utilized to estimate Q_{eff}, the arithmetic binning method tended to produce the largest estimates, followed by the ePDF method and finally the continuous lognormal PDF method (Figure 2.7). The arithmetic binning method is most sensitive to isolated large flood events in the right tail of the flow distribution, which produced spikes in the sediment yield curve at large discharge values (c.f., Figure 1.4 and discussion in Chapter 1, Section 4.2). This phenomenon is more evident with the binning method for sites with shorter flow records and larger values of β. The ePDF method was less sensitive to these large events in the tail. It smoothes the tail of the flow distribution compared to the histogram method as does the fitted lognormal PDF, which is a continuous distribution function (Figure 2.5).

The fitted lognormal PDF repeatedly under-estimates Q_{eff} relative to the other two methods for fine bed sites and over-estimates Q_{eff} for coarse bed sites when $\beta > 2.5$.

In cases where the rating curve exponent was low (≤ 2) and the flow record only marginally variable, the lognormal approximation method worked well. However, there were many more examples in which it performed poorly relative to the empirical methods. Fitting lognormal distributions using the method of moments produces results that are highly sensitive to the calculated value of the standard deviation of the logs of the samples (equation 1.6). Using the maximum likelihood method to fit this PDF to the data may produce better results because all data are used in the fit as opposed to estimates of only the first two statistical moments of the data as in the method of moments.

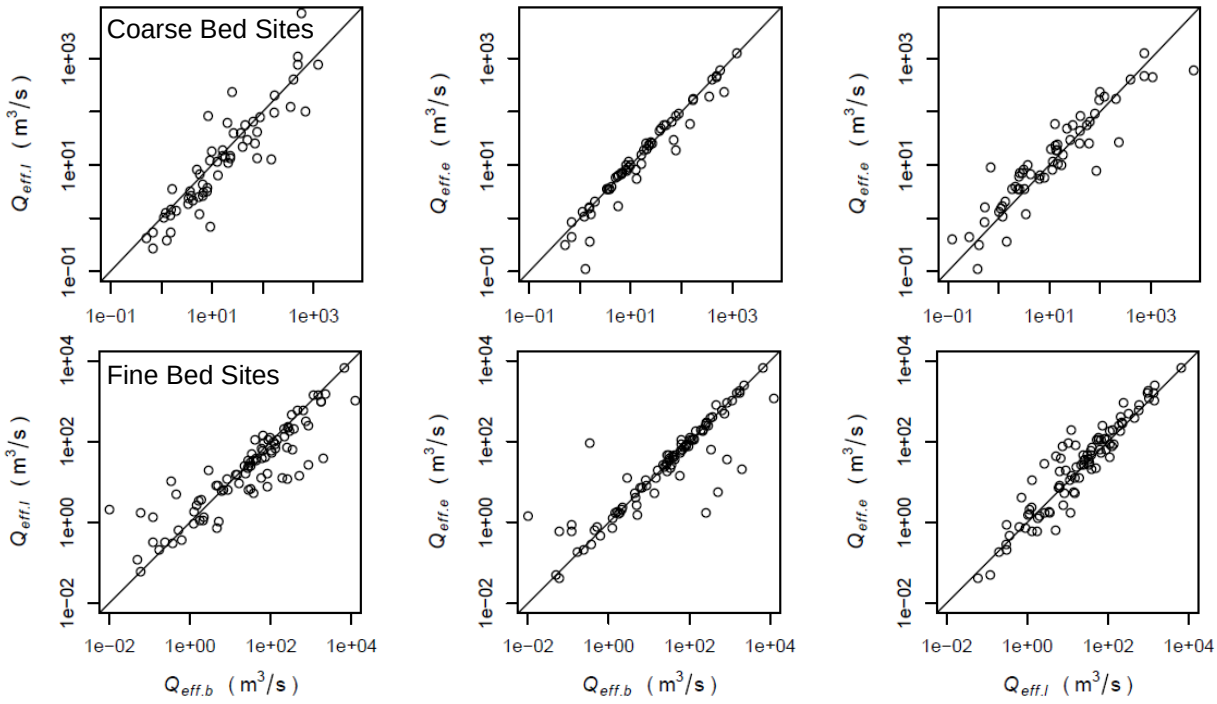

Figure 2.7 Comparison of Q_{eff} calculated from the three MFA methods studied for coarse (top row) and fine bed sites (bottom row): 25 arithmetic bins (*Qeff*.b), an empirical PDF (*Qeff*.e), and a fitted, continuous lognormal PDF (*Qeff*.l).

MFA methods are sensitive to some important independent variables imbedded in the calculation: the sediment rating curve exponent, β, the daily flow coefficient of variation, C_v, and the flow record length, RL, among others (Figure 2.8). I also consider the sensitivity of the difference in estimated values of Q_{eff} between each method by comparing the differences in estimated values of Q_{eff} normalized by mean discharge for all methods. In general, all normalized estimates of Q_{eff} increase with β approximately the same. As β increases, larger, less frequent flows in the tails of the distribution become more effective. As RL increases for coarse bed sites, these less frequent flows tend to have smaller densities making more frequent flows more effective. This produces a slight downward trend in values of Q_{eff} for the two empirical methods in coarse bed sites. No clear relationship exists between RL and normalized Q_{eff} for fine bed sites.

The scatter in the Q_{eff}–C_v relationships increases with C_v. This is due to two opposing trends in the sediment yield curve: as C_v increases, the right tail of the flow distribution becomes thicker and more influential in overall sediment yield. This may result in Q_{eff} taking on a relatively large value for larger values of β. Concurrently, as the flow distribution becomes more positively skewed, smaller discharges also become more influential and the peak of the flow PDF moves to the left towards smaller discharges. For smaller values of β, the sediment yield density curve follows this trend, resulting in smaller discharge values becoming the most effective. The cone-shaped relationship (Figure 2.8, left column) results because of sites with relatively high (> 2)

and relatively low (< 2) values of β, though this relationship mostly shows an increasing trend in coarse bed sites because $\beta > 2$ for the majority of these sites.

Though not plotted here, the magnitude of the difference between normalized estimates of Q_{eff} increases with decreasing RL. This means that as the flow record increases in length, all MFA methods begin to converge in their estimates of Q_{eff}. The differences are the greatest for intermediate values of β where some methods might produce a peak in the sediment yield density curve further out in the tails and some might favor a peak closer to the peak of the flow frequency distribution.

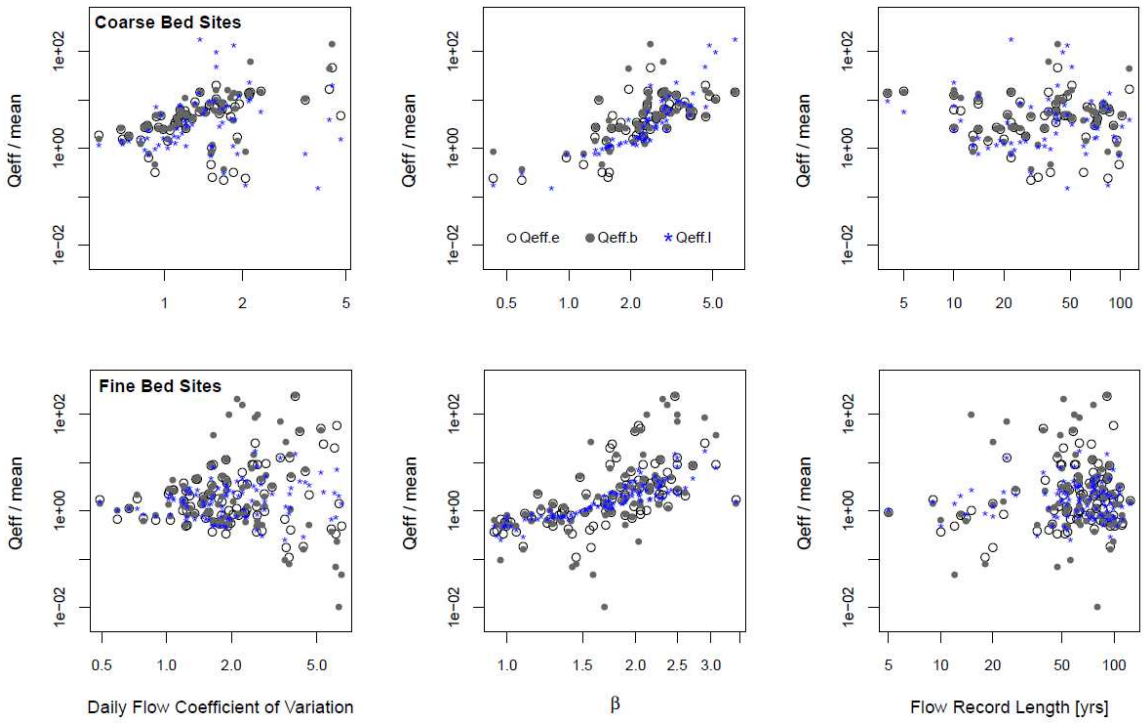

Figure 2.8 Sensitivity of normalized estimates of Q_{eff} as a function of C_v, β, and RL. Values of Q_{eff} are normalized by mean daily flow.

For the remainder of this Chapter, all sediment yield metrics based on Q_{eff} use the estimate produced by the ePDF method. It provides a numerically tractable method for representing the eCDF, which is the best estimate of the flow probability distribution available. The arithmetic binning method does not provide adequate resolution of the low flow range of the flow regime and is susceptible to a few large flows dominating the sediment yield analysis, especially for sites with shorter flow record lengths.

4.2 Empirical Magnitude-Frequency Analysis

I now turn to an exploration of the relationships between driving variable metrics that summarize various aspects of the flow regime (especially flow variability or flashiness, Table 2.2), and physical aspects of the channel and its boundaries (drainage area, sediment transport mode, grain size, the bankfull discharge, and width:depth ratio) with sediment yield response metrics: the metrics based on sediment transport magnitude-frequency analysis (MFA) (Table 2.2). The goal of this exploration is to understand what physical drivers most influence and best predict sediment yield metrics between fine bed and coarse bed rivers. In this section I also compare these empirical relationships with the theoretical relationships found in Chapter 1. An example of the sediment yield analysis for one site is provided above in Section 3, Methods (Figure 2.6). Sediment yield figures for each coarse bed and fine bed site are provided in Appendix 2B.

The values of some sediment yield, flow, and physical metrics span several orders of magnitude; therefore, I begin this exploration by considering log-log linear correlations (Pearson correlation) between driving and response variables. The discussion in Sections 4.2.2 – 4.2.4 in part reference Figure 2.11, below, which shows matrices of the log-linear Pearson correlation coefficient, r, and slope of the relationship between driving and response variables as well as inter-correlations between flow and physical metrics. The size of each circle indicates the relative magnitude of the slope of the log-linear relationship up to a threshold used for plotting purposes. White circles indicate a positive slope and gray a negative slope. The Pearson correlation value is printed in each circle where the slope of the trend is significantly different from zero ($p < 0.05$). I also use scatterplots between driving and response variables to characterize these relationships in more detail below.

4.2.1 Flow Percentiles and Return Intervals of Sediment Yield Metrics

The effective discharge for fine bed sites covers a wide range of percentiles of daily flow; the interquartile range (IQR) of Q_{eff} approximately spans from the 70$^{\text{th}}$ to the 95$^{\text{th}}$ percentile. The IQR of Q_{eff} for coarse bed sites is much narrower, spanning approximately the 92$^{\text{th}}$ to the 99$^{\text{th}}$ percentiles (Figure 2.9).

I also calculate the percentiles of daily flow for the discharge associated with the interquartile range and median of cumulative sediment yield (Q_{S25}, Q_{s50}, Q_{S75}). The Q_{S25}, Q_{s50}, Q_{S75} are calculated by determining the discharge value associated with 25%,

50%, and 75% of cumulative sediment transport over the sorted flow record (Figure 2.2b). The flow interquartile ranges associated with these metrics overlap much more. They expectedly increase up to very high percentiles up to the Q_{S75} where the median values of this metrics fell between the 99th and 100th percentile for both types of sites. The median percentile value of Q_{s50} is 98 for fine and coarse bed sites.

Using the annual maximum flow series for all sites and the Weibull plotting position, I calculate the return interval (RI) of Q_{eff} and Q_{s50}. For many fine bed sites, $Qeff.RI < 1$ year. However, these results are truncated at $RI = 1$ year because I use an annual maximum flood series (not a partial duration series), and do not fit a PDF to the data. The median value of $Qeff.RI$ is < 1 year for fine bed sites and 1.4 years for coarse bed sites, whereas the median value of $Q50.RI$ is 1.2 years and 1.5 years for these two types of sites.

4.2.2 Flow – Sediment Yield Metric Relationships

The skewness and coefficient of variation, C_v, of the daily flow data at each site had the most and the strongest relationships with sediment yield metrics (Figure 2.10, left column). These two flow variability metrics are highly correlated and produce similar relationships with sediment yield metrics. Because C_v was an important variable in Chapter 1, I focus on relationships between sediment yield metrics and C_v herein. Scatter plots for the relationship between C_v and various sediment yield metrics are provided below in Figures 2.12 and 2.13.

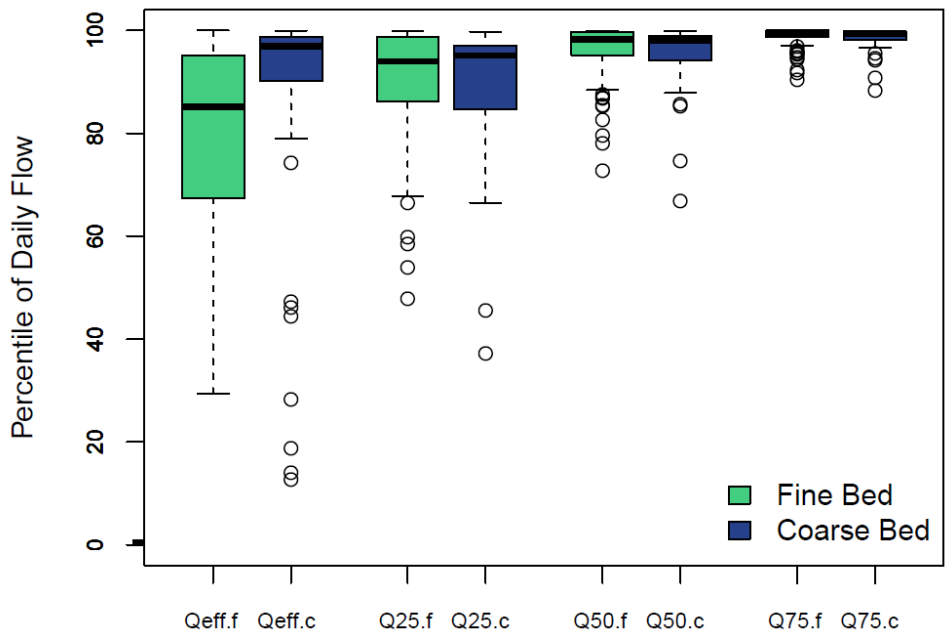

Figure 2.9 Daily flow percentiles for sediment yield metrics for fine bed sites ("f", green), and coarse bed sites ("c", blue).

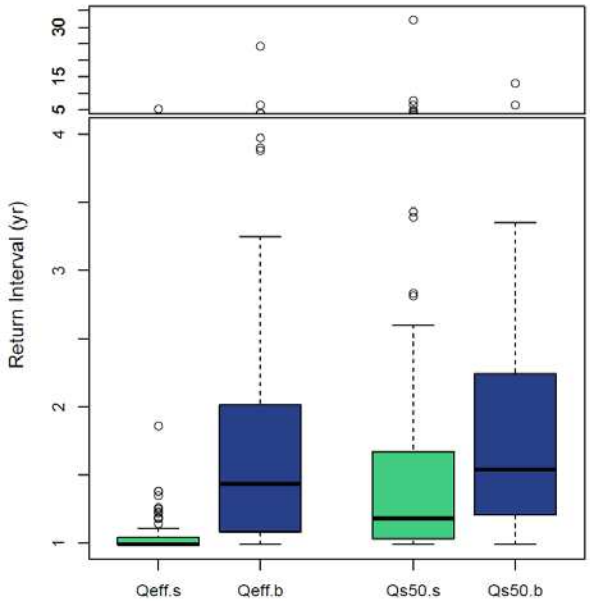

Figure 2.10 Return intervals (years) of sediment yield metrics for fine bed sites (green), and coarse bed sites (blue).

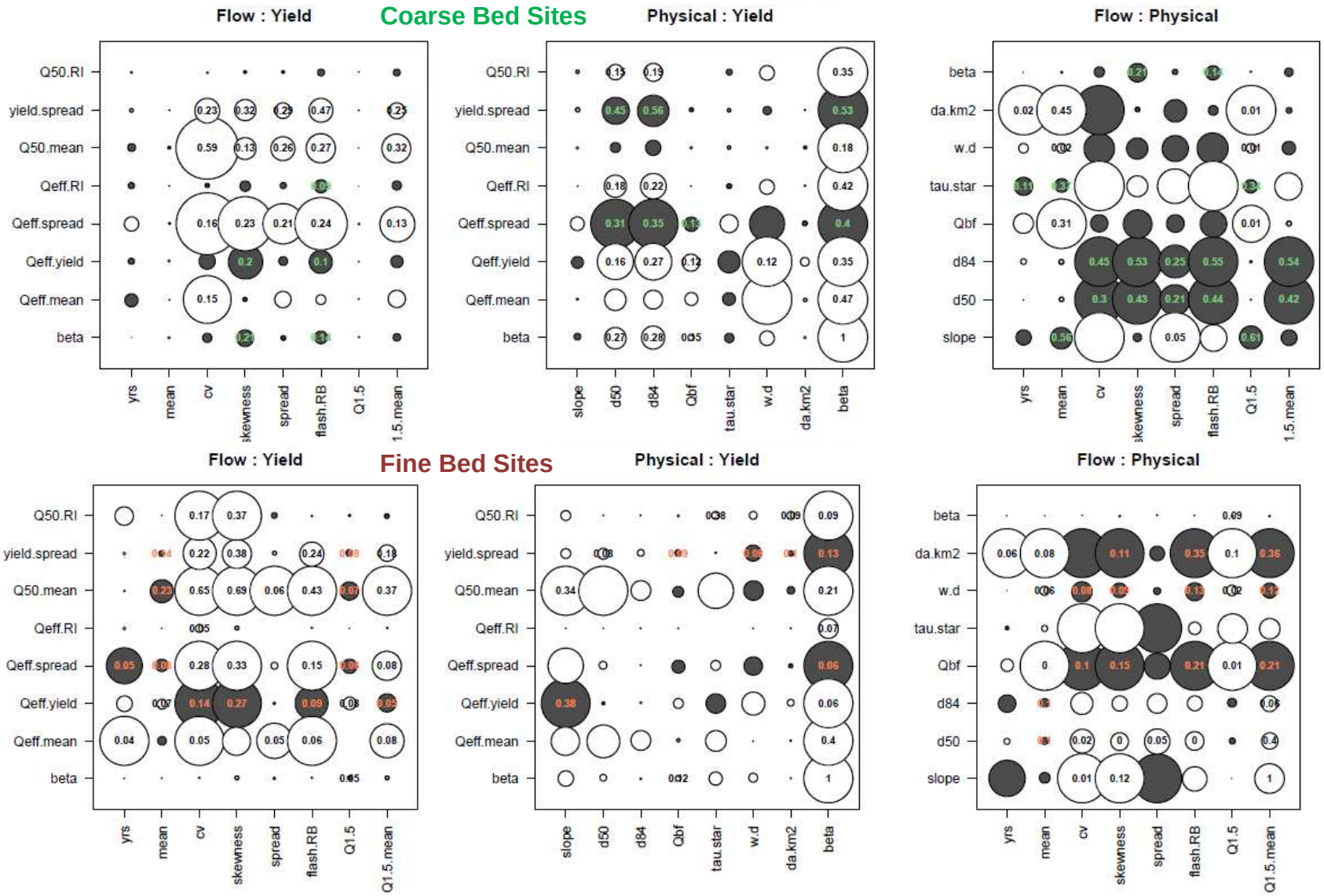

Figure 2.11 Log-linear Pearson correlation and slope matrices among flow, physical, and sediment yield metrics. Circle color indicates positive (white) or negative (grey) slope; numbers indicate Pearson r value and are only printed for slopes significantly different from zero ($p < 0.05$). Size of circles is proportional to the steepness of the slope of the relationship.

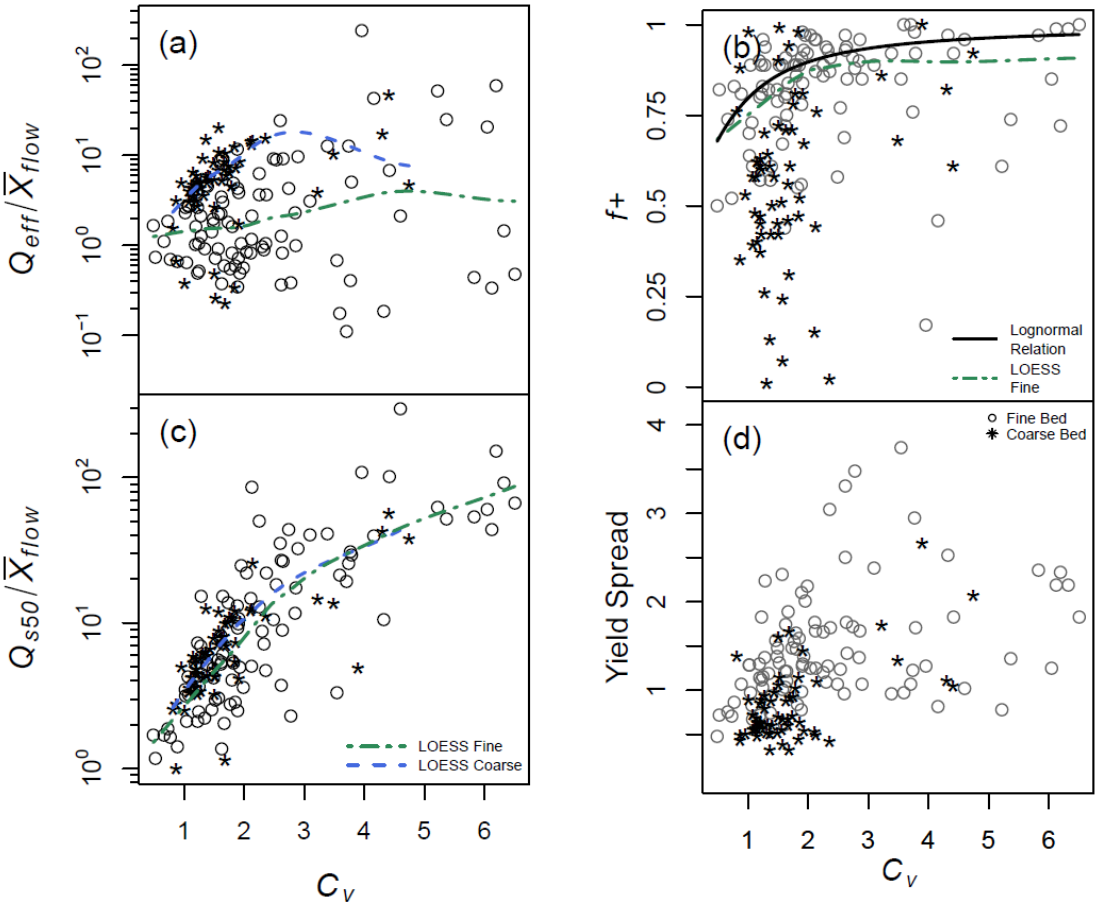

Figure 2.12 Relationships between daily flow coefficient of variation and various sediment yield metrics.

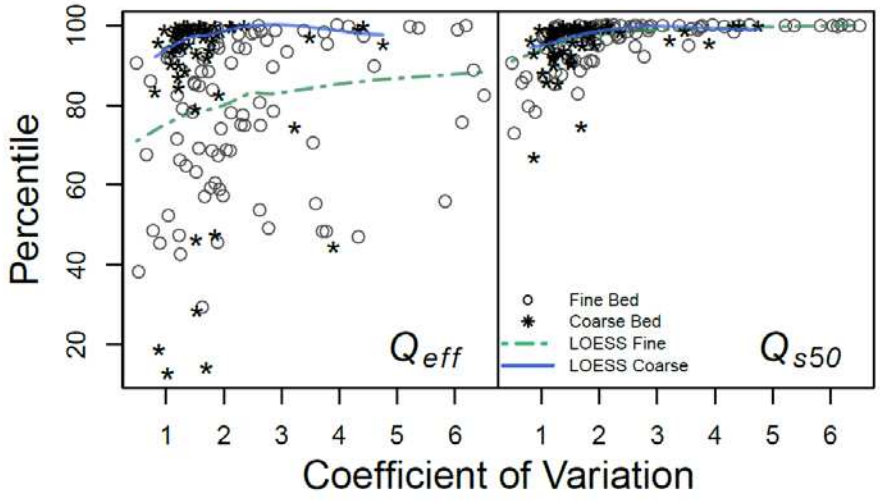

Figure 2.13 Percentile values of Q_{eff} and Q_{s50} as a function of C_v.

A significant increasing relationship is observed between C_v and *Qeff.mean* as well as *Qs*50.*mean*, which are sediment yield metrics normalized by the mean daily discharge. The r value is very small for the *Qeff.mean* relationship (0.16 and 0.05 for coarse and fine bed sites, respectively) and much higher for the *Qs*50.*mean* relationship (0.59 and 0.65, Figure 2.11). When considering the scatterplot of the two relationships, the variability of *Qeff.mean* increases with C_v and little positive or negative trend is apparent (Figure 2.12a). Whereas *Qs*50.*mean* increases tightly with C_v for both types of sites (Figure 2.12c). This means that as flow variability increases, more sediment is transported by flows greater than the mean flow. This is consistent for both types of sites. Trends in the return interval in years of Q_{eff} (*Qeff.RI*) and Q_{s50} (*Qs*50.*RI*) (not plotted) as well as daily flow percentiles (Figure 2.13) reflect this increase with C_v as well. Daily flow percentiles increase with C_v to values > 95 very quickly. This relationship is better defined with Q_{s50}.

A significant decreasing (increasing) relationship is observed between C_v and *Qeff.*yield ($f+$) for both site types ($f+$ is the compliment of *Qeff.*yield). This means that the amount of sediment transported cumulatively below Q_{eff} decreases as flow variability increases. The C_v–$f+$ relationship is plotted in Figure 2.12b. It shows that $f+$ increases sharply with C_v reaching above 90% for $C_v > 3$. The C_v–$f+$ scatterplot for fine bed sites follows the theoretical relationship between flow variability and the effective discharge assuming a continuous lognormal distribution [Vogel et al., 2003] (see also Figure 1.6).

The C_v–$f+$ relationship is highly variable for coarse bed sites but it roughly follows the theoretical relationship (Figure 2.12b).

Though highly scattered, the width or spread of the discharges bracketing 50% of sediment transport centered on and normalized by Q_{eff} (*Qeff.spread*) and Q_{s50} (*yield.spread*) increases with flow variability. As the variability of the flow regime increases, more sediment is transported by a broader range of flows. This relationship is tighter (higher r value) and lower for coarse bed sites, whereas larger values and more scatter are evident with fine bed sites (Figure 2.12d).

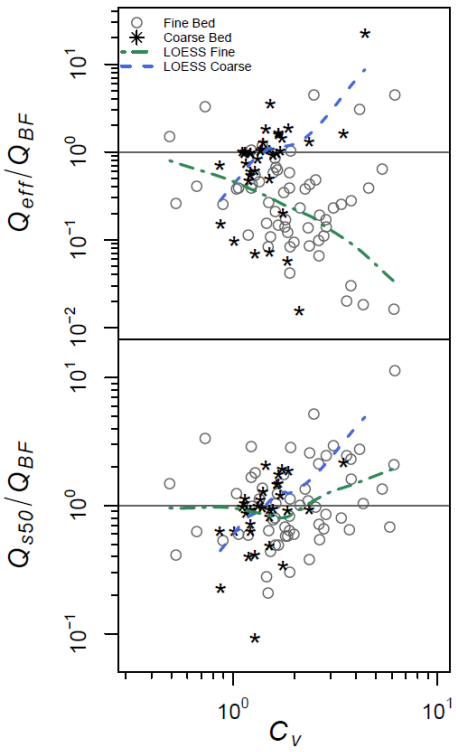

Figure 2.14 Ratios of Q_{eff} and Q_{s50} to Q_{bf} as a function of C_v with LOESS smoothing lines.

The ratios of yield metrics Q_{eff} and Q_{s50} to Q_{bf} plotted against flow variability (C_v) indicates that, for coarse bed sites, as flow variability increases Q_{eff} increases in magnitude relative to Q_{bf} and even exceeds Q_{bf} for large values of C_v (Figure 2.14). However, for fine bed sites, Q_{eff} becomes smaller relative to Q_{bf} as flow variability increases. The general trends for the Q_{s50}:Q_{bf} ratio tends to increase with flow variability for both types of sites. This relationship for Q_{eff} parallels that found in Chapter 1 (Figure 1.8) where Q_{eff} increases with C_v in coarse bed sites and decreases in fine bed sites. The mechanism for this is discussed in more depth in Chapter 1. I do not explicitly consider theoretical relationships for Q_{s50} in Chapter 1; however, I discuss the

general increase in the value of Q_{s50} with flow variability and how it compares with theoretical relationships in the Discussion Section 5.2.4 below.

4.2.3 Physical – Sediment Yield Metric Relationships

I now turn to relationships between sediment yield metrics and physical metrics describing properties of the sediment in the channel (grain size, β), the shear stress experienced by the sediment from flows in the channel (τ^*, β), as well as physical aspects of the channel (slope, width:depth, and drainage area). With the exception of β and slope, most physical and sediment metrics did not greatly influence yield metrics for fine bed sites (Figure 2.11, middle column). In general, the relationships between grain size and sediment yield metrics are more prevalent, steeper, and stronger for coarse bed sites than they are for fine bed sites.

The median and 84$^{\text{th}}$ percentile grain sizes (D_{50} and D_{84}) are highly correlated with one another for both sites and I found similar relationships between both grain sizes and sediment yield metrics. The return interval of both Q_{eff} and Q_{s50} increase with increasing grain size of the bed for coarse bed sites (Figure 2.11, middle column). Both yield spread metrics decrease with increasing grain size in coarse bed sites, but no significant relationships for these metrics occurred for fine bed sites. As the grain size of the bed material increases, a smaller, more infrequent range of flows is responsible for the bulk of sediment transport.

The value of β increases with grain size for coarse bed sites, and may slightly increase with grain size for fine bed sites, but the relationship is highly variable (Figure 2.15). This relationship is steeper for bed load sites. The sediment rating curve exponent is also a function of the flow – shear stress relationship. A larger β value may indicate that the channel is deeper and narrower with a greater sediment transport capacity for a given discharge and/or that it has a greater slope (see Discussion section 5.3.2).

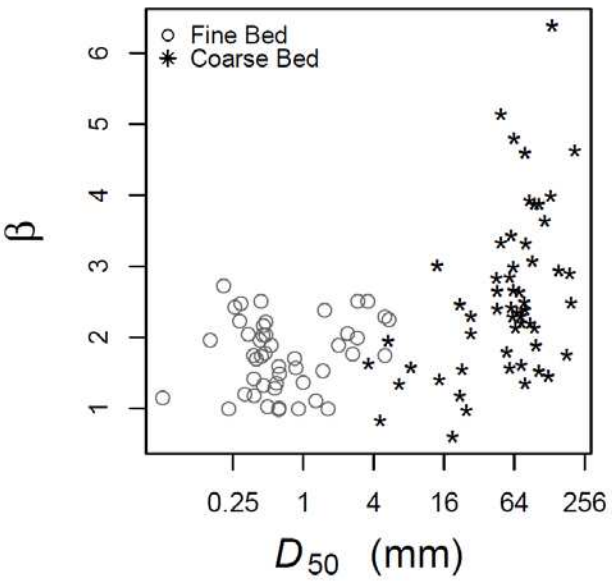

Figure 2.15 Relationship between grain size and sediment rating curve exponent, β for bed load (black stars) and suspended load (open circles).

Nearly all sediment yield metrics have strong relationships with β (Figure 2.11, middle column), though β tends to explain more variance in the sediment yield metrics for coarse bed sites (greater r values). All metrics quantifying the relative magnitude of Q_{s50} and Q_{eff} (*Qeff.mean, Qs50.mean, Q50.RI, Qeff.RI*) increase with β for both types of sites. I plot Q_{s50} normalized by $Q_{1.5}$ as a function of β in Figure 2.16a, below, because there is less variability in the relationship using this normalization compared with using mean discharge. While the Q_{s50}:$Q_{1.5}$ ratio increases with β in general for fine bed sites, there is a large amount of variability. For coarse bed sites, the relationship is steep up until $\beta \approx 2$, and Q_{s50}:$Q_{1.5} \approx 1$ where the slope breaks and becomes milder. Because $Q_{1.5}$ is

a good estimator of Q_{bf} for coarse bed sites, this could indicate that for $\beta > 2$, Q_{s50} exceeds Q_{bf} and less frequent overbank flows are more responsible for sediment transport.

Both the *yield.spread* and *f+* metrics decrease rapidly with increasing β (Figure 2.16b and d). Again, the relationships are strongest for coarse bed sites. The *yield.spread*–β relationship parallels the *yield.spread*–D_{50} relationship for coarse bed sites. As β and grain size increase, the range of flows responsible for the middle 50% of sediment transport decreases. In addition, as β increases the frequency of Q_{eff} and Q_{s50} decrease resulting in less sediment being transported by discharges greater than Q_{eff}; that is, these dominant discharge indices become rarer.

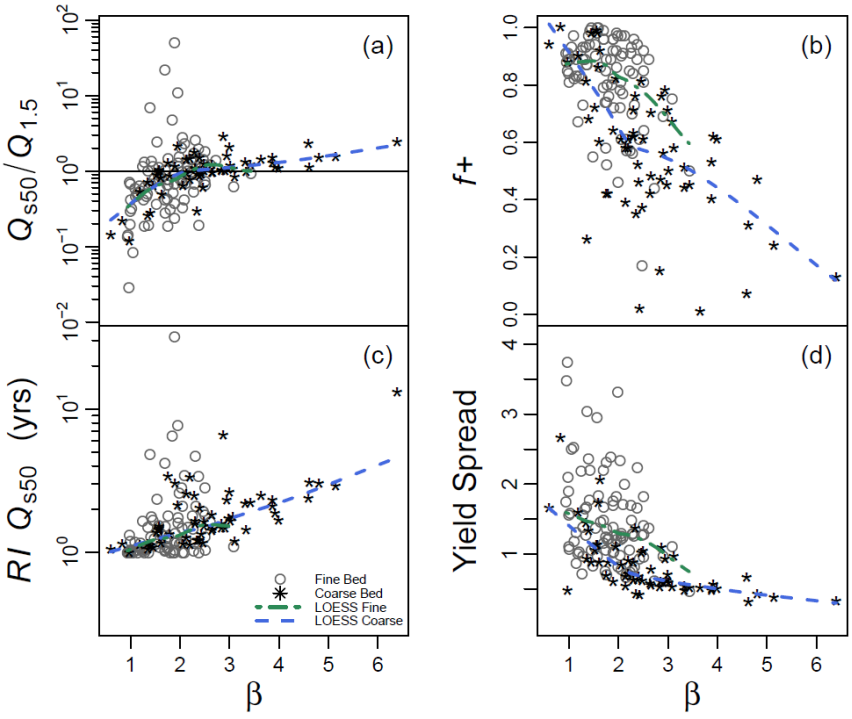

Figure 2.16 Relationships between the sediment rating curve exponent, β, and various sediment yield metrics.

This is reflected in the $RI.Q50 - \beta$ relationship and in the $f+ - \beta$ relationship (Figure 2.16b and c).

Channel geometry-based metrics have some influence on sediment yield metrics (Figure 2.11, middle column). Slope influences sediment yield metrics for fine bed sites. As slope increases, the normalized value of Q_{s50} ($Qs50.mean$) increases, and $Qeff.$yield decreases. In steeper, fine bed rivers, more sediment is transported by less frequent flows (smaller drainage areas with larger flow variability). Stronger relationships between the width:depth ratio ($w.d$) were observed with the coarse bed sites. An increase in $w.d$ leads to an increase in $Qeff.$yield (significant) and $Qeff.mean$ (not significant) and a decrease in both yield spread metrics (not significant) in coarse bed sites. In coarse bed channels with larger $w.d$ values, less frequent flows are more effective. Previous theoretical work has demonstrated that larger values of $w.d$ result from high sediment loads in coarse bed streams [*Parker*, 1979; *Millar*, 2005]. It may be that a more narrow range of infrequent flows are most effective in these channels beginning with those that exceed the threshold for bed entrainment up to and including overbank flows.

4.2.4 Combined Physical and Flow – Sediment Yield Metric Relationships

As discussed above, C_v and β are two key driving variables that explain a large amount of variance in the values of several sediment yield metrics. Therefore, a final set of relationships I consider are yield metrics as a function of combined flow and physical metrics: the product and ratio of C_v and β (Figure 2.17). These combined metrics are

useful because C_v and β both range from 1 to 6 in absolute value. Both normalized values of Q_{eff} and Q_{s50} increase with the product of C_v and β (Figure 2.17a and d). This relationship is very strong for the normalized Q_{s50} values for both types of sites, and for the normalized Q_{eff} values for coarse bed sites only. Klonsky and Vogel [2011] found that Q_{eff} and Q_{s50} normalized by the mean of daily flows both increase with $C_v\beta$ in a fairly tight relationship. I found a similar trend for both types of sites in my data, with the relationship being much steeper for the normalized Q_{s50} for the fine bed sites (Figure 2.17d). Because the maximum values of C_v at fine bed sites are greater than those for the coarse bed sites, flow variability may be dominating this steeper relationship for fine bed sites.

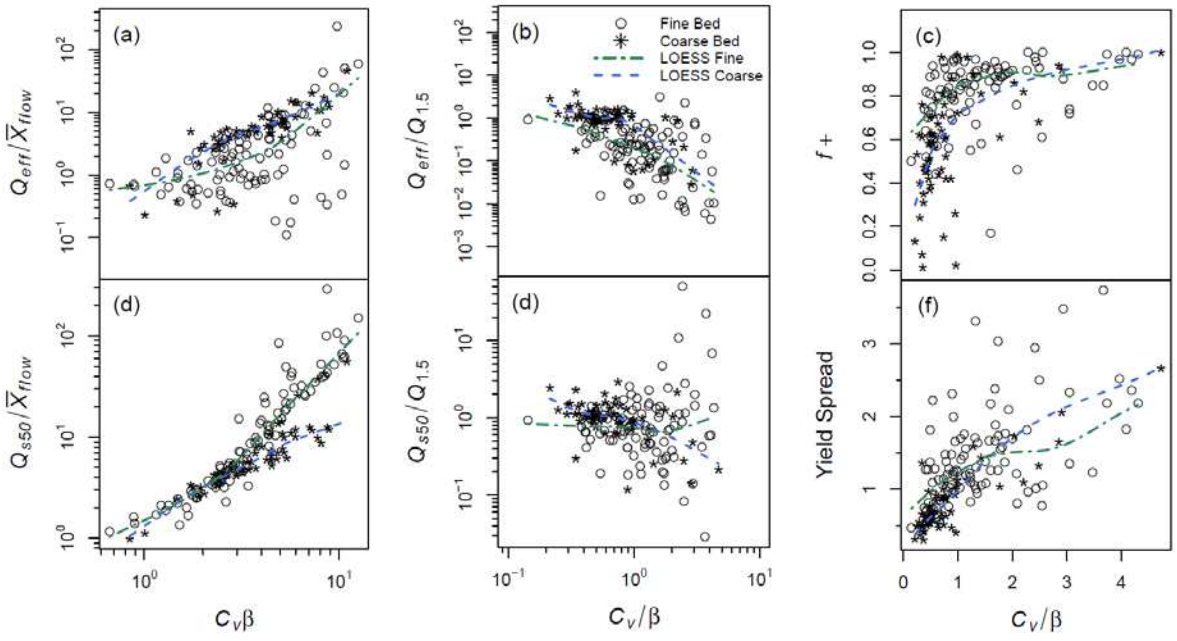

Figure 2.17 Logarithmic scatter plots of relationships between normalized Q_{eff} and Q_{s50} and the product (a and d) or ratio (b and e) of C_v and β. Plots a and d are normalized by mean annual flow and plots b and e are normalized by Q1.5. Plots c and f show scatterplots of the ratio of f+ and yield.spread as a function of the ratio of C_v and β.

The ratio of $C_v : \beta$ is perhaps a more intuitive compound driving variable than its product in that larger values indicate flow variability is high and β low, while smaller values indicate that flow variability is low and β high. I found that normalized Q_{eff} decreases, yield spread increases, and $f+$ increases with increasing C_v/β for both types of sites (Figure 2.17b, c, f). When flow variability dominates the ratio, Q_{eff} becomes smaller and a wider range of flows are responsible for the middle 50% of cumulative sediment yield. When β dominates the ratio, Q_{eff} takes on a larger value and the range of flows responsible for the middle 50% of cumulative sediment transport shrinks.

5 Discussion

5.1 Magnitude-Frequency Analysis Method Assessment

While many MFA methods have been utilized in previous studies—specifically, methods for representing the flow frequency distribution—little consensus exists as to what method is most appropriate despite great efforts to study the robustness and sensitivity of different methodologies [*Orndorff and Whiting*, 1999; *Sichingabula*, 1999; *Biedenharn et al.*, 2000; *Emmett and Wolman*, 2001; *Soar and Thorne*, 2001; *Klonsky and Vogel*, 2011]. Research and recommendations from the U.S. Army Corps of Engineers, Engineering and Research Development Center, Coastal and Hydraulics Laboratory argue that the simple and relatively robust arithmetic binning method provides the least bias and reasonable accuracy [*Biedenharn et al.*, 2000; *Soar and*

Thorne, 2001]. However, this approach requires manual manipulation of bin widths to keep Q_{eff} from falling in the first bin, if deemed appropriate, and to remove empty bins in the tails of the flow distribution. This inserts user bias into the calculation, and is not amenable to MFA across a large number of disparate sites.

Others have brought in more advanced empirical statistical tools [*Orndorff and Whiting*, 1999; *Klonsky and Vogel*, 2011] as well as theoretical statistical approaches [*Nash*, 1994; *Vogel et al.*, 2003; *Goodwin*, 2004] to conduct the analysis. In the present study I have found that a modification to Orndorff and Whiting's [1999] empirical probability density function (ePDF) that utilizes a logarithmic smoothing technique, provides a relatively robust and unbiased methodology that can be used across a wide range of stream types (Figures 2.5, 2.7, and 2.8). This technique avoids the various forms of binning bias discussed by Soar and Thorne [2001] because it is not a logarithmic *binning* procedure. Rather, it uses a logarithmically-spaced window to smooth the empirical cumulative distribution function (eCDF) before it is numerically-differentiated to produce an ePDF. Smoothing the eCDF removes any vertical steps or discontinuities that would lead to singularities in the ePDF. It also creates a continuous tail in the ePDF. Estimates of Q_{eff} produced by this method compared well with the arithmetic binning method favored by some, but had the advantage of being less sensitive to shorter, flashier flow records coupled with larger values of β (c.f., Flow Record Length Analysis, Chapter 1, Section 4.2). I used this ePDF methodology to conduct the magnitude-frequency analysis discussed herein.

Though this component of the present study focuses primarily on methodologies for calculating Q_{eff}, it has also generated insight on the other primary sediment yield metric discussed herein: Q_{s50}. As explored in detail in Chapter 3, Q_{s50} performs well in predicting bankfull discharge—especially in fine bed streams—and therefore serves as a dominant discharge index like Q_{eff}. If a long-term flow record is available for a particular site, calculating Q_{s50} is much more straightforward and less sensitive to the assumptions and methodologies necessary for Q_{eff} as it has the advantage of not requiring a mathematical representation of the flow frequency distribution. One must simply determine the discharge at which 50% of cumulative sediment yield occurs over the sorted flow record. If sediment load data are not available for a particular site, then Q_{s50} must be calculated with a physically-based and site-calibrated sediment transport model. Estimates of Q_{s50} generated from total load models in fine bed streams compare well with those estimated from the empirical regression models used in this chapter as explored in Chapter 4. However, this does not appear to be the case for Q_{s50} estimates made from bed load equations in coarse bed streams. On the whole, Q_{s50} is a mathematically more robust dominant discharge index than Q_{eff}, especially for fine bed rivers. It also have the advantage of predicting Q_{bf} better than Q_{eff} in fine bed rivers (Chapter 3).

5.2 Sediment Yield Metric Relationships

I have presented some of the relationships found in this empirical analysis between the drivers and the response of sediment yield in fine and coarse bed rivers (Figure 2.11). The flow–sediment yield metric relationships observed for fine bed sites tended to be stronger and more prevalent than those of the coarse bed sites, and vice versa for the physical–sediment yield metrics (Figure 2.11). This means that flow variability may exert a stronger control on sediment transport in fine bed rivers and physical boundary properties are more influential on coarse bed rivers.

With some exceptions, the observed relationships were similar in direction of response between both site types, and represented a continuum of responses from, for example, high to low flow variability or from small to large values of β. This is largely because I am using the same representation of the flow-sediment load relationship for fine and coarse bed sites: a single power law function. An alternative method, not feasible given limited data and the large number of sites, would be to represent bed load transport as a threshold function. Most semi-empirical bed load equations represent bed load as a threshold function, which requires site-specific calibration. Where I am able to make direct or near direct comparisons, empirical relationships tended to match the theoretical ones discussed in Chapter 1.

5.2.1 Flow Variability

Results from this empirical analysis confirm previous empirical and theoretical findings that as flow variability (C_v) increases, the frequency of Q_{eff}, as measured by the percentile, decreases (Figure 2.13) [*Wolman and Leopold*, 1957; *Andrews*, 1980; *Soar and Thorne*, 2001; *Vogel et al.*, 2003]. This is also the case for Q_{s50}, for which the relationship is better defined. Normalized values of Q_{eff} and Q_{s50} also increase with flow variability for both types of sites (Figure 2.12 a and c). Theoretical relationships based on power law sediment rating curves with no threshold for entrainment reflect this trend (Figure 1.3 and 2.17, top row). When normalized by Q_{bf}, a diverging relationship between Q_{eff} and C_v was found in fine vs coarse sites as predicted by the theoretical relation with an entrainment threshold (Figure 1.8 a). This is discussed in more detail below in Section 5.2.3.

The empirical relationship between $f+$ and C_v is fairly scattered for both types of sites, but a LOESS empirical regression line for fine bed sites parallels the trend of the theoretical relationship well, which predicts a nonlinear increase if $f+$ with C_v (Figure 2.12b). This means that as flow variability increases, more sediment is transported by flows greater than Q_{eff}. Additionally, though scatter is great, *yield.spread* increases with C_v for both types of sites as well (Figure 2.12d), reflecting the trend of the theoretical relationship (Figure 1.7).

5.2.2 Physical Metrics

The value of the sediment rating curve exponent, β, exerts much influence on sediment yield metrics and on the frequency of the most effective flows for coarse bed sites and less influence on fine bed sites (Figures 2.11 and 2.16). I explore the physical meaning of β in more detail below in Section 5.32. In some cases relationships with β are similar for both types of sites (e.g. *yield.spread*). In this example, these relationships fall on a continuum with coarse bed sites continuing the decreasing relationships where fine bed sites leave off (Figure 2.16d). As the value of β increases, a narrower range of larger flows dominates sediment transport in channels. In the theoretical relationship *yield.spread* decreases with increasing bed sediment size for a given values of C_v (Figure 1.7). The empirical results also reflect this trend with overall values of *yield.spread* being lower for coarse bed sites vs. fine bed sites. Greater values of β result in larger absolute and relative values of Q_{eff} and Q_{s50} as well as the return intervals of these metrics, also resulting in smaller values of $f+$ (Figure 2.15). These empirical relationships parallel theoretical relationships discussed in Chapter 1 (see for example, Figures 1.3, 1.6, and 1.8).

Sediment yield metric relationships with β are stronger for coarse bed sites. This may in part be due to the fact that grain sizes in coarse bed rivers and the shear stress necessary to mobilize the bed can vary by orders of magnitude (i.e., 4 mm to 256 mm), resulting in a wider range and greater values of β. Whereas in fine bed rivers, sand-sized particles (0.063 mm to 2 mm) are often in motion over a wider range of flows. This is

evident in the value of τ_c^* for fine bed sites, for which a majority are above the critical value range for incipient motion at Q_{bf} ($\tau_c^* \in \{0.03, 0.07\}$, Figure 2.4f). An additional explanation lies in transport capacity and supply limitation. Often, larger grain sizes in coarse bed rivers are transport capacity limited as opposed to supply limited [*Montgomery and Buffington*, 1997]. In supply limited conditions, often found in lower gradient, fine bed rivers, the grain size of the bed is less influential on the discharge–sediment load relationship as is indicated in Figure 2.15.

5.2.3 Comparing Coarse and Fine Bed Sites

Many of the relationships discussed above are qualitatively similar—or at least fall on the same spectrum of response—between the two types of sites due to the character of the empirical model used to represent the Q-Q_s relationship for both coarse and fine bed sites. In some cases a well-defined relationship exists for one type of site and not another (e.g., $f+$ vs. C_v for fine bed sites and β vs. $Q_{s50 \cdot RI}$ and *yield.spread* for coarse bed sites). In general, physical metrics tend to explain the variance in relationships with sediment yield metrics in coarse bed sites, whereas flow variability trends to explain more variance in fine bed sites.

Additionally, some *differences* in sediment yield metric relationships between the two types of sites are observed as well. A divergent relationship is observed with flow variability and the ratio of Q_{eff} : Q_{bf} (Figure 2.14). In fine bed sites, this ratio decreases with C_v, meaning Q_{bf} becomes larger relative to Q_{eff}. The opposite is true for coarse bed

sites. The normalized values of Q_{s50} increase with C_v for both fine (weak to nonexistent relationship) and coarse bed sites (stronger relationship).

Soar and Thorne [2001] found a similar relationship for fine bed sites in their study of Midwestern and Eastern U.S. sand bed streams. In coarse-bed, semi-alluvial streams in the U.S. Rocky Mountains, Bunte et al. [2014] found that $Q_{eff} \gg Q_{bf}$ and in many cases was equal to the maximum discharge value. Interpretation of their work also suggests that Q_{eff} should increase with flow variability in these coarse sites. This finding relates to the value of the sediment rating curve exponent: very large values of β lead to very infrequent flows being more effective, especially with increasing flow variability (Chapter 1). Note that the sediment load measurement technique can influence this value as well, especially for bed load sites [*Bunte and Abt*, 2009]. As flow variability increases in coarse bed streams, Q_{eff} takes on larger and larger values. The flow-sediment load relationships for coarse bed streams observed in this study are generated from Helley-Smith bed load measurements and do not have such steep rating curves as those reported by Bunte et al. [2014], who use bed load traps and longer sampling times [*Bunte et al.*, 2004]. Nevertheless, I observe that Q_{eff} increases relative to Q_{bf}, and even exceeds Q_{bf}, in coarse bed streams and this relationship is due to larger values of β.

These empirical results compare well with theoretical findings (Figures 1.9 and 2.18). When considering the theoretical relationship among Q_{eff}, C_v, and β in which a generic rating curve with no threshold is multiplied by the continuous lognormal PDF to represent the flow distribution (See Chapter 1, Section 2), both Q_{eff} and Q_{s50} generally

monotonically increase with C_v and β, though the rate of increase in each is smaller at lower values of C_v and β (Figure 2.18a and b). For very small values of β (< 1.25, in this example), Q_{eff} actually decreases with C_v. When a sediment load–discharge relationship that includes an entrainment threshold is introduced, such as Parker [1979], Q_{eff} is no longer a monotonically-increasing function of C_v and, in this case, D_{50} (Figure 2.18c). Rather, Q_{eff} increases with C_v for larger sediment sizes, and decreases for smaller

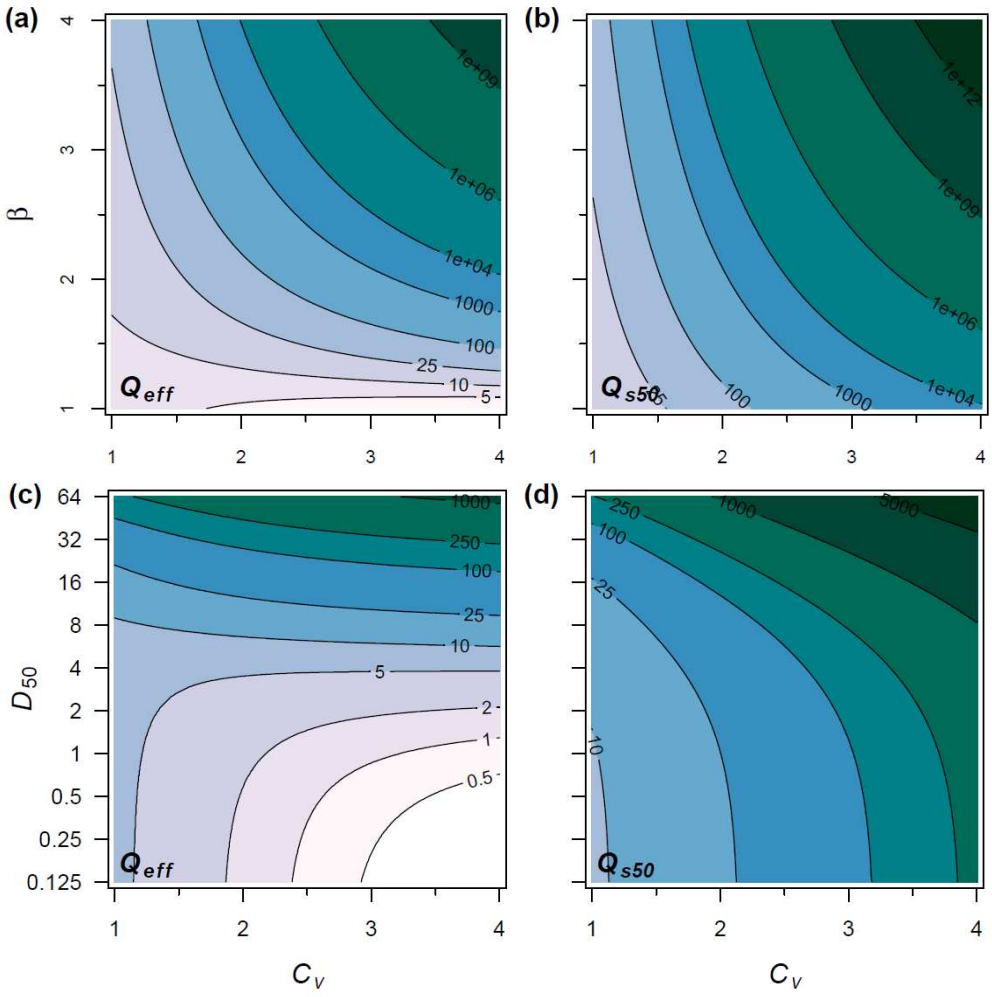

Figure 2.18 Contour plots of relationships between C_v, β, Q_{eff}, and Q_{s50} using a generic rating curve function to represent the sediment load–discharge relationship and a lognormal PDF to represent the flow distribution (a and b), and an entrainment threshold function [*Parker*, 1979] to represent the sediment load–discharge relationship (c and d).

sizes. Though it is quantitatively different from the relationship among Q_{s50}, C_v, and β, Q_{s50} increases monotonically with C_V and D_{50} as well when an entrainment threshold is introduced.

5.3 Unpackaging the Primary Driving Variables of Sediment Yield

Two primary driving variables that most influence sediment yield metrics have been identified in this study: C_V and β. In this section I unpackage some of the physical properties behind these two metrics and relate these to physically-meaningful river processes.

5.3.1 Coefficient of Variation

The coefficient of variation of daily flows, the standard deviation divided by the mean, has been used throughout this dissertation to describe flow variability. This has been a useful metric because it is normalized and can be used to compare flow variability across a wide range of sites. It is also highly correlated with other variability metrics, such as skewness and flashiness (*flash.RB*). However, a value of C_V for a specific river does not translate directly into an understanding of that river's flow regime. Therefore, I briefly explore the nature of C_V and what it means for the flow regimes of the rivers used in this study.

The relationship between the two components of C_V—standard deviation, s, and mean, $\bar{x}$ —have a very tight and increasing log-linear relationship for the study sites (s as a function of $\bar{x}$). This means that the absolute value of s increases nonlinearly with

the absolute value of $\bar{x}$. However, upon normalization of s by $\bar{x}$ no correlation exists between C_v and $\bar{x}$ or drainage area, indicating that the normalization is effective in spite of the nonlinear relationship between these two variables. One way to understand C_v is in terms of flashiness, a term often used regarding flow regime [*Baker et al.*, 2004; *Walsh et al.*, 2005]. A flashy river is one in which base flows dominate and large peak flows punctuate. As the flashiness (and C_v) of a flow regime increases, the base flows tend to become smaller and the magnitude of a given flood frequency become larger. This phenomenon occurs with urbanization [*Konrad et al.*, 2005; *Walsh et al.*, 2005] and also naturally in arid environments [*Graf*, 1983].

Another way to conceptualize C_v is in terms of the temporal nature of floods. Wolman and Gerson [1978] expanded on Wolman and Miller's [1960] consideration of the long-term effectiveness of geomorphically significant events. Wolman and Gerson explore the relationship between the temporal sequencing of these events and the recovery, or relaxation time of a river following these events. Inter-arrival times of many natural and social phenomena follow an exponential distribution [*Kirby*, 1969; *Barabási*, 2005] with $\lambda = 1 / \overline{T}$, where $\overline{T}$ is the mean of the inter-arrival time:

$$f_T = \lambda e^{-\lambda T} \tag{2.5}$$

I calculate $\overline{T}$ for flood events greater than or equal to the Q_{s50} across all sites. The average inter-arrival time of these flood events increases nonlinearly with C_v and skewness (Figure 2.19) for both types of sites. Therefore, as C_v increases so does the

time between geomorphically significant events. Depending on the regional climate, this may mean that rivers with large C_v may spend more time outside of "equilibrium" form. In humid climates with abundant riparian vegetation, river morphology is less sensitive to the timing of geomorphic events due to shorter recovery times [*Wolman and Gerson*, 1978]. However, in arid and semi-arid climates this is often not the case as lack of vegetation results in long recovery times [*Wolman and Gerson*, 1978; *Graf*, 1983].

5.3.2 Sediment Rating Curve Exponent

Inluences on the sediment rating curve exponent, β, have received some attention limited to coarse bed sites. Emmett and Wolman [2001] observed an increasing relationships between β and the D_{84} of the bed in coarse bed sites. In formulating their generic sediment rating curve transport function for bed load, Barry et al [2004]

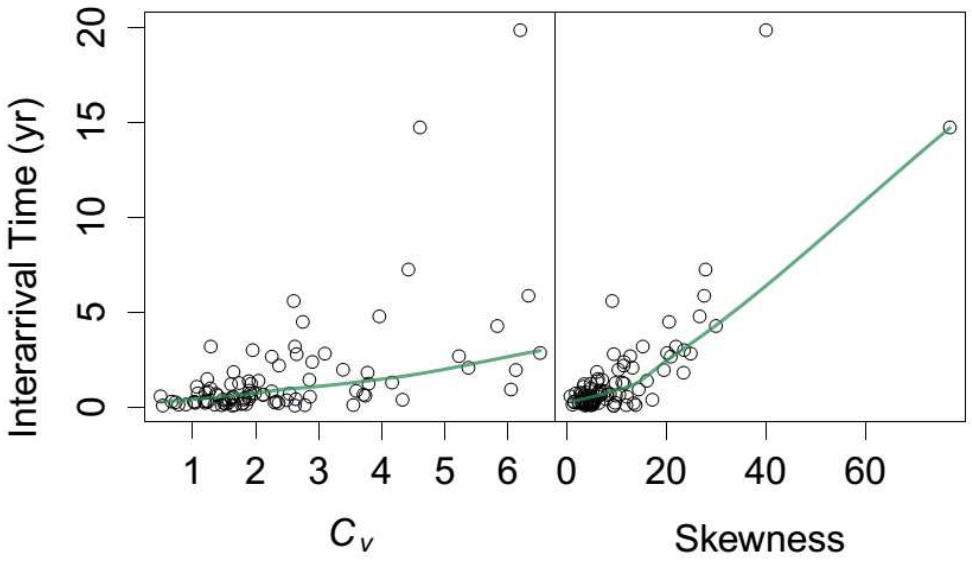

Figure 2.19 Plots of mean inter-arrival time of flood events with magnitudes $\geq Q_{s50}$ as a function of C_v and skewness for fine bed sites only with LOESS smoothing lines (green).

use a metric related to bed armoring to calibrate the exponent value. They found that β values increase with the amoring ratio. Larger armoring ratios mean that the bed grain-size distribution is coarser than that of the subsurface and can indicate sediment supply-limited conditions [*Dietrich et al.*, 1989].

I explore the influence of sediment supply, represented as the fraction of sand in the bed, on β using the Wilcock and Kenworthy [2002] transport relation in a synthetic channel. When fine sediment supply is relatively large, the slope of the Q-Q_s relationship—and hence β—decreases (Figure 2.20). This holds for all grain sizes, especially at smaller discharge values, as more sand is available in the bed for transport at these smaller discharges. The largest change in slope of the Q-Q_s relationship occurs in rivers with bed material in the large gravel and cobble size classes.

The overall slope of the sediment rating curve decreases as a function of channel slope using the Parker [1979] bedload transport relation (Figure 2.21). Especially for coarser bed material. With a larger slope, greater bed shear stress occurs at all discharge values (larger τ^* values) and more sediment is in transport over the range of discharges. Bunte et al. [2014] found that in small mountain streams, β increases with drainage area (hence increases with decreasing slope overall). However, when plotted directly with slope, they find a variable relationship between β and slope that is dependent on process domain [*Montgomery and Buffington*, 1997]. This relationship increases from pool-riffle to plane bed channels (low to medium slope) then decreases from plane bed towards step-pool channels (medium to high slope).

Channel geometry, such as the width-to-depth ratio as well as the amount of vegetation roughness along the banks also likely influence β, as these features influence channel hydraulics [*Darby and Thorne*, 1996; *Bledsoe et al.*, 2011]. The influence of in-channel hydraulics on bed shear stress and ultimately the Q-Q_s relationship is outside of the scope of this Chapter; however previous work on this topic does provide some clues.

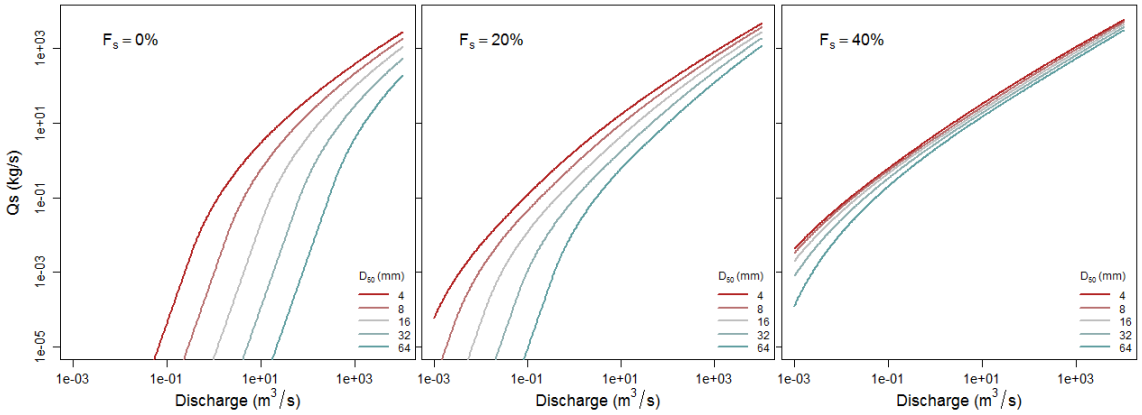

Figure 2.19 Sediment rating curves for a range of median grain sizes for a synthetic channel using the Wilcock and Kenworthy [2002] two-fraction sediment transport capacioty transport model with increasing fractions of sand in the bed.

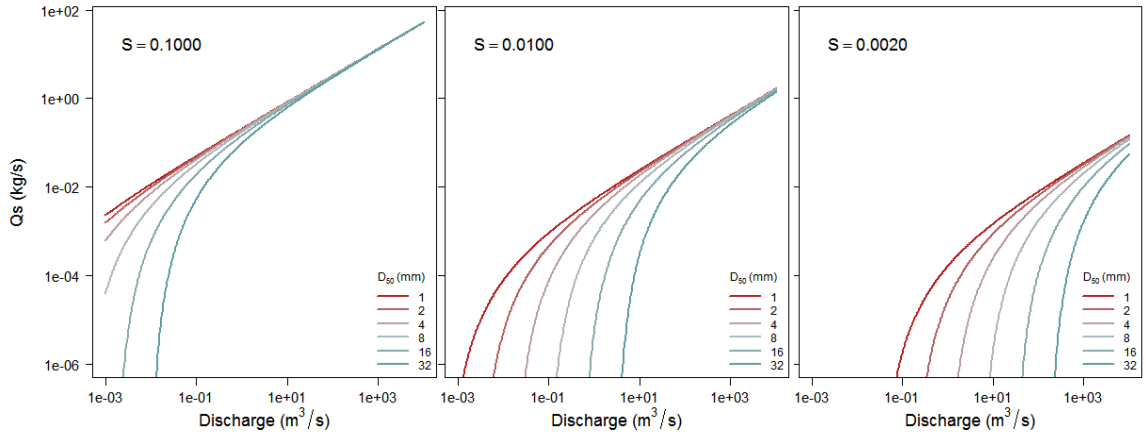

Figure 2.20 Sediment rating curves for a range of median grain sizes for a synthetic channel using the Parker [1979] gravel bed load transport capacity model with increasing values of slope.

Andrews [1984] found that τ^* values associated with the D_{50} at bankfull discharge were appreciably greater in coarse bed channels with thick bank vegetation over those with thin vegetation. Carling [1983] found that the threshold shear stress for initation of motion of coarse bed material was greater in a narrow stream ($w.d < 11$) than in a wide stream ($w.d > 11$). These studies suggest that in narrower, deeper, channels with thick bank vegetation, shear stress more is concentrated on the bed resulting in more scour, leaving behind larger material in the bed. Such channels would likely have steeper Q-Q_s relationships and larger values of β over wider channels assuming they are transport capacity limited.

6 Conclusion

In this chapter, I have tested and applied a robust and consistent magnitude frequency analysis of sediment transport (MFA) methodology to explore empirical relationships between the drivers of sediment yield in rivers, namely the flow regime and physical properties of the bed sediment and channel geometry, and the magnitude and frequency of sediment transport described by various metrics derived from the sediment yield curve (Table 2.2, Figure 2.2). I conduct this analysis for 153 sites across the conterminous U.S. and in Puerto Rico on fine and coarse bed rivers where bed material transport data were available adjacent to a stream gage with a long-term flow record. I

also compare empirical relationships derived in this chapter the theoretical relationships derived in Chapter 1.

A comparison of MFA methods indicates that a logarithmically-smoothed empirical PDF, modified from Orndorf and Whiting [1999] best represents the flow regime and is less susceptible to isolated flood events overriding the sediment yield density curve for shorter flow records. In general, estimating Q_{eff} is very sensitive to the MFA methodology used. The value of Q_{eff} tends to produce very scattered relationships with physical and flow related metrics. The half-yield discharge, Q_{s50}, tends to have stronger relationships with driving variables, and is less sensitive to the MFA methodology. In addition, it tends to predict the bankfull discharge better than Q_{eff} across a wide range of river types as discussed in Chapter 3. However, unlike Q_{eff}, Q_{s50} is calculated from a cumulative sediment yield record and therefore is more sensitive to the sediment transport model used if sediment transport measurements are not available and a physically-based model is required. This is due to cumulative error and is especially sensitive for coarse bed sites as is explored in Chapter 4.

This analysis indicates that the magnitude and frequency of sediment transport in all river types is sensitive to the variability of the flow regime. In fine bed rivers, sediment yield metrics are more sensitive and more closely correlated with flow variability than in coarse bed rivers. As flow variability increases, the range of discharges responsible for the bulk of sediment transport increases and more sediment is transported by discharges greater than the effective discharge, Q_{eff} (Figure 2.12b & d).

This is especially true in fine bed rivers where the Q_{eff} : Q_{bf} ratio decreases with flow variability (Figure 2.14), whereas this ratio increases with flow variability for coarse bed rivers following theoretical predictions (e.g., Figure 2.18c). The bankfull discharge is likely to be greater than Q_{eff} in fine bed rivers, and may be greater, equal, or much smaller than Q_{eff} depending on the coarseness of the bed and steepness of the rating curve.

Bed sediment grain size plays a dominant role in sediment yield in coarse bed rivers. The median grain size of the bed is positively correlated with the steepness of the sediment rating curve, β, at coarse bed sites (Figure 2.15); however, its value incorporates more physical attributes of the channel and geomorphic setting than grain size alone (c.f., Section 2, Chapter 1 and Section 5.3, above). For small values of β (e.g., < 2), generally associated with fine bed rivers, a larger range of discharges is responsible for sediment yield (Figure 2.16d). This range of flows narrows as the grain size of the bed—and the value of β—increases. In coarse bed rivers, with large values of β, a narrower range of less frequent flows dominates sediment yield (Figure 2.16c & d). The most effective discharge also increases in magnitude and decreases in frequency as grain size increases. Combining driving metrics C_v and β help explain much of the variance in normalized values of Q_{eff} and Q_{s50} as well as other sediment yield metrics (Figure 2.17). The empirical relations derived in this chapter among sediment yield metrics, β, and C_v compare favorably with the theoretical relationships of Chapter 1.

Sediment yield in all river types is in some part sensitive to all aspects of the physical drivers and boundary conditions rivers experience: flow regime, sediment supply caliber and quantity, as well as channel geometry. Often, relationships between sediment yield metrics and these physical drivers reflect a continuum from fine to coarse bed rivers (e.g., Figures 2.12, 2.13, 2.16, and 2.17). However, in other cases, such as the ratio of Q_{eff}:Q_{bf} plotted against C_v, different relationships follow between coarse and fine bed rivers (Figure 2.14). In all, flow variability and the slope of the rating curve (in part influenced by bed material caliber) are controlling variables for MFA metrics.

By considering the magnitude and frequency of sediment transport using the same methodology for fine and coarse bed rivers, this study bridges our understanding of relationships between physical drivers and sediment yield in fine and coarse bed rivers. It confirms and extends the understanding of the relative importance of the drivers of sediment yield in rivers by analyzing previously-published relationships in both fine and coarse bed rivers as well as exploring relationships with new sediment yield metrics. Finally, this work provides empirical validation of many of the theoretical relationships derived in Chapter 1.

Channel form and geometry data were difficult to acquire for this large number of sites. The available channel geometry data ($w.d$ and slope), did not yield any meaningful relationships with yield metrics. As discussed by Emmett and Wolman [2001], links between the magnitude and frequency of sediment yield and channel form are as of yet uncharacterized. Future work in this area could study the relationships between, for

example, downstream hydraulic geometry and trends in yield metrics across geographically disperse watersheds. Additionally, assuming a relationship between dominant discharge metrics, Q_{eff} and Q_{s50} and the bankfull discharge [e.g., *Tilleard*, 1999; *Dodov and Foufoula-Georgiou*, 2005] could provide a powerful tool for exploring the channel form sensitivity to changes in the discharge-sediment transport relationship as well as the flow frequency distribution as a result of environmental change.

CHAPTER 3

The Half-Yield Discharge: A Process-Based Predictor of Bankfull Discharge

Summary

The river management and restoration community has given much effort to predicting the bankfull discharge, Q_{bf}, and associated channel geometry at Q_{bf} for the purposes of channel study, classification, and design. Four types Q_{bf} prediction methods predominate: (1) direct estimation based on field indicators of bankfull stage, (2) use of regional downstream hydraulic geometry statistical relations, (3) use of an annual flood with a specified return interval based on the annual maximum flood series (e.g., the 1.5 to 2 year flood) or regional flood peak statistical relations, and (4) process-based approaches that incorporate the magnitude and frequency of sediment transport such as the most effective discharge: Q_{eff}. I calculate process-based Q_{bf} predictors using bed material sediment transport data from 98 gaged sites across the U.S. including coarse bed, bed load-dominated channels and fine bed, suspended load-dominated channels with drainage areas ranging from 1 to $3x10^6$ km^2. I compare these values with estimates

---

Sholtes, J., and B. Bledsoe (In 2nd Review), The Half Yield Discharge: a Process-based predictor of bankfull discharge. Journal of Hydraulic Engineering.

Joel S. Sholtes conceived the study, collected and analyzed the data, wrote the manuscript. Brian Bledsoe reviewed manuscript and provided feedback on applications and presentation of the findings.

of Q_{bf} made from field measurements of bankfull indicators. I find that the discharge associated with 50% of cumulative sediment yield based on the flow record—Q_{s50}: the half yield discharge—predicts Q_{bf} better than most other methods, especially in fine-bed rivers. When compared to Q_{eff} and the 1.5 and 2 year floods, Q_{s50} is the least biased estimator of Q_{bf} and has the lowest mean absolute percent error and root mean square error for fine bed sites. Both process-based predictors and the 1.5 year flood perform well in coarse bed sites. I characterize the behavior of Q_{s50}, a process-based predictor of Q_{bf} to highlight circumstances in which sediment yield analysis may be important in estimating the bankfull discharge. My finding represents a novel estimator of Q_{bf} for fine bed rivers not previously discussed in this context.

1 Introduction

Stable river form over engineering time frames (50 - 100 years) results from the balance of flow regime, sediment supply, and imposed valley slope with the resisting forces of boundary materials in the bed and banks and vegetation [*Lane*, 1954; *Schumm and Lichty*, 1965; *Millar*, 2005]. Though no one discharge is entirely responsible for river form, the bankfull discharge, Q_{bf}, defined conceptually herein as the discharge which just fills the channel before spilling on to the floodplain [*Wolman and Leopold*, 1957; *Williams*, 1978], is one of several important channel geometry and design metrics. This is due to its connection with the dominant or channel forming discharge concept rooted

in river regime theory [*Inglis*, 1949; *Benson and Thomas*, 1966; *Carling*, 1988; *Soar and Thorne*, 2011] and early floodplain formation and hydraulic geometry studies [*Leopold and Maddock*, 1953; *Wolman and Leopold*, 1957; *Hey and Thorne*, 1986]. In some cases, Q_{bf} may have the properties of a dominant discharge in alluvial rivers in that sediment transport effectiveness is at a maximum at bankfull [*Wolman and Leopold*, 1957; *Andrews*, 1980]. For this reason, Q_{bf} or a proxy for Q_{bf} such as a flood of a certain annual return interval are often used as a design discharge for channel restoration and management [*Hey and Thorne*, 1986; *Shields et al.*, 2003; *Doyle et al.*, 2007]. I refer readers to excellent reviews of dominant discharge concepts and methods for estimating it for channel design by Doyle et al. [2007] and Soar and Thorne [2011].

Four predominant approaches to estimating the dominant discharge are practiced: 1) direct estimate based on field indicators of bankfull stage, 2) indirect estimate based on a regional downstream hydraulic geometry statistical relation created from reference reaches, or scaled directly from a nearby reference reach, 3) indirect estimate based on a hydrologic metric (generally the 1.5 to 2 year flood: $Q_{1.5}$ and Q_2), and 4) indirect process-based estimate based on effective discharge analysis (herein referred to as magnitude-frequency analysis, MFA) to calculate the discharge that transports the most sediment over time or some other related sediment yield metric. In the present study, I compare indirect methods 3 (hydrologic) and 4 (process-based) to method 1: direct estimation of Q_{bf} with field measurements of bankfull stage indicators, which integrate channel processes.

As has been previously discussed in depth, all of these approaches have their limitations. Identifying Q_{bf} in the field is subject to error and interpretation [*Williams*, 1978; *Shields et al.*, 2003]. In some channels, a well-defined floodplain may not exist, or channel disturbance may create ambiguous indicators. Extrapolating information from a reference reach to a reach of interest [*Rosgen*, 1997, 2001] may not be appropriate in certain scenarios wherein the reach of interest is unstable or has different forcing and boundary conditions [*Simon et al.*, 2007].

Hydrologic predictors of the dominant discharge may suffice for "stable" channels lacking major anthropogenic influence such as river engineering or hydro-modification from land use change in the watershed or flow regulation [*Doyle et al.*, 2007]. Multiple studies have found a wide range of return intervals for Q_{bf}. The median value of the

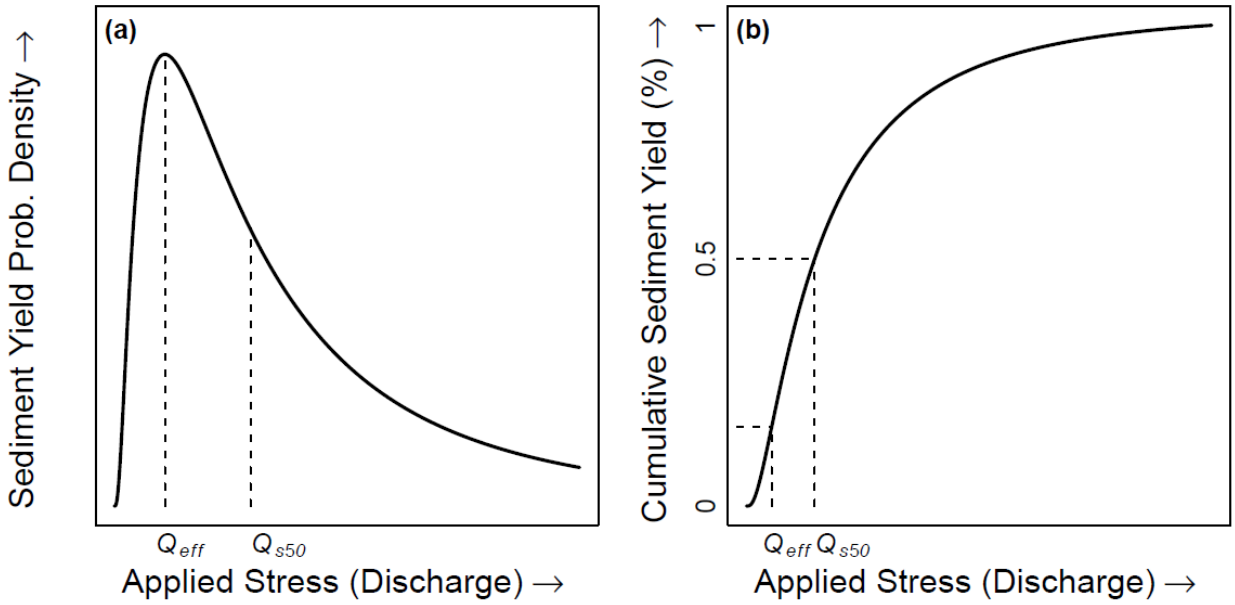

Figure 3.1 Conceptual diagram of process-based Q_{bf} predictors, Q_{eff} and Q_{s50}, based on (a) the sediment yield probability density curve, and (b) the cumulative sediment yield curve.

return interval of Q_{bf} often falls between 1 and 2 years on the maximum annual flood series, whereas the mean value is often greater than 2 years, indicating a positively skewed distribution in its return interval [*Wolman and Leopold*, 1957; *Williams*, 1978; *Castro and Jackson*, 2001]. The return interval of Q_{bf} for channels that have adjusted to disturbance by incising and/or widening will generally be greater than two years [*Doll et al.*, 2002].

Process-based predictors of Q_{bf} involve calculating discharge indices based on sediment yield curves, which are the product of a sediment transport relation with a representation of the flow frequency distribution. Though this calculation is more involved than other methods, it can provide more information to the channel designer or manager about sediment continuity, an important consideration in channel design and management [*Soar & Thorne*, 2001; *Shields et al.*, 2003; *Doyle et al.*, 2007]. The effective discharge, Q_{eff}, is the maximum value of the sediment yield frequency curve (product of flow frequency distribution and a sediment transport relation) [*Andrews*, 1980; *Wolman & Miller*, 1960] (Figure 3.1a). The half yield discharge, Q_{s50}, is the discharge associated with 50% of cumulative sediment yield [*Emmett and Wolman*, 2001; *Vogel et al.*, 2003]. It is calculated from a cumulative sediment yield curve plotted as a function of the sorted flow record [*Biedenharn and Thorne*, 1994] (Figure 3.1b). Methods for calculating these predictors of Q_{bf}, which rely on sediment transport magnitude-frequency analysis, are provided below in sections 2.3 and 4.3.

In general, Q_{eff} predicts Q_{bf} with mixed performance. In coarse bed rivers dominated by bed load sediment transport, Q_{eff} appears to predict Q_{bf} reasonably well [*Andrews*, 1980; *Emmett and Wolman*, 2001; *Hassan et al.*, 2014], or may be much greater than Q_{bf} [*Bunte et al.*, 2014]. In fine bed rivers dominated by suspended load sediment transport, Q_{eff} is often much smaller than Q_{bf} especially in flashy systems, depending in part on MFA methods used and channel type [*Pickup and Warner*, 1976; *Soar and Thorne*, 2001; *Hassan et al.*, 2014]. The half yield discharge tends to be larger than Q_{eff}. As such it may pose a better metric for summarizing the magnitude of transported load in rivers than Q_{eff}, especially in fine bed, suspended load-dominated rivers [*Vogel et al.*, 2003].

A small number of previous studies mention Q_{s50} [*Emmett and Wolman*, 2001; *Copeland et al.*, 2005; *Hassan et al.*, 2014]. To my knowledge, no work has directly evaluated the ability of Q_{s50} to predict Q_{bf}. Copeland et al. [2005] found that the discharge associated with 75% of cumulative sediment yield, Q_{s75}, predicts Q_{bf} well in fine bed rivers; however, they use total suspended load in their estimates, which includes wash load. Wash load comprises silt and clay-sized particles and generally does not form the channel bed of most sand bed streams [*Biedenharn and Thorne*, 1994; *Hey*, 1996]. Here I use bed material load data, defined for fine bed rivers in this study as the fraction of the suspended load ≥0.0625 mm, to calculate Q_{eff} and Q_{s50} and compare them with $Q_{1.5}$ and Q_2 in their ability to predict Q_{bf} as estimated in the field from bankfull

stage indicators. I calculate these metrics using a national database of fine and coarse bed sites and compare their predictive ability with hydrologic metrics.

I follow this introduction with a discussion of the sites, data, and methods used to estimate Q_{bf} and its predictors. I compare the Q_{bf} predictors using basic goodness-of-fit metrics and consider the sensitivity of prediction accuracy and bias. I conclude with a discussion of the findings in the context of previous work and consider the accuracy, bias, and ease of calculation of the predictors, making practical recommendations for their usage.

2 Data and Methods

This study involves three methods for estimating Q_{bf}: 1) direct estimation using measurements of field indicators of bankfull stage at a site with an established stage-discharge rating curve, 2) indirect estimation using an flood peak discharge with a specified return interval based on the annual maximum peak discharge series at a gaged site ($Q_{1.5}$ and Q_2), and 3) indirect estimation using process-based discharge indices based on MFA (Q_{eff} and Q_{s50}). I use basic goodness of fit calculations to compare direct estimates of Q_{bf} with predictors based on annual flood series and sediment yield MFA. I begin this section with a description of the sites used in for this study.

2.1 Site Data

Sites used in this study are located across the conterminous U.S. and Puerto Rico and include 60 fine bed sites and 36 coarse bed sites for which estimates of Q_{bf} were available near a gage with a long-term record and ≥15 paired bed material load-discharge measurements (Figure 3.2). In general, these sites were selected because the majority have been previously published in MFA studies or are located along the same river as previously-published sites. However, because the sand fraction of suspended load measurements, representing the bed material load at fine bed sites, is not often evaluated and sites with smaller drainage areas (e.g., <100 km^2) are under-represented in published MFA studies, other sites were brought in to this study to augment the data set. I included only alluvial rivers (mobile bed and banks) in dynamic equilibrium with the drivers of flow and sediment supply, meaning measured channel properties are likely to have a stable mean value over an engineering time frame (50-100 years). Fine bed sites are scattered geographically, whereas coarse bed sites are clustered in the U.S. Rocky Mountain and Northwest regions due to lack of concurrent bed load and stream gage data availability elsewhere. Anthropogenic impacts such as flow regulation, channelization, and land use change can result in transient influences on channel form and are therefore avoided in this study. I used aerial photograph reconnaissance as a rough method to verify that these sites are located on a river that was either regulated or channelized. Summary information for each site used in the present study can be found in Tables 3A.1 and 3A.2 in Appendix 3A.

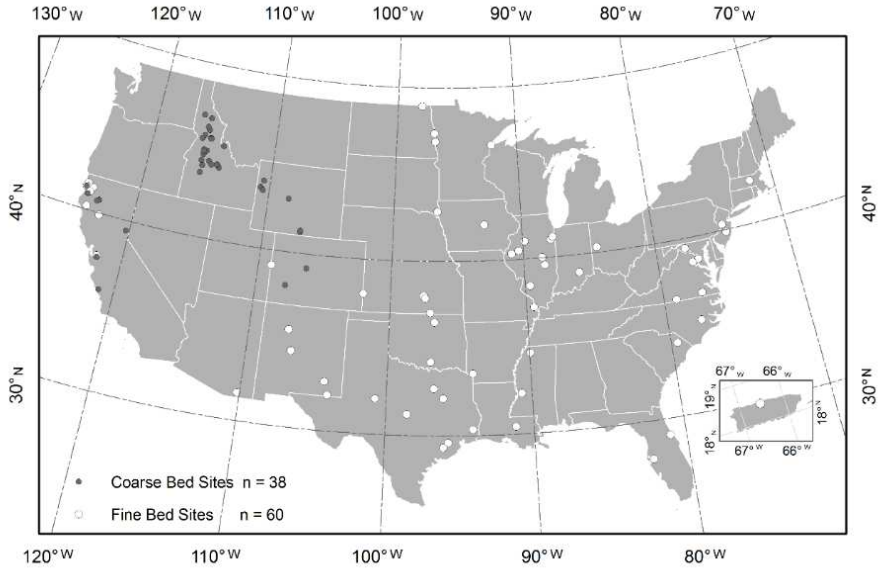

Figure 3.2 Site map of fine bed and coarse bed sites utilized in Chapter 3.

2.2 Bankfull Discharge Estimation

Estimates of Q_{bf} were primarily made directly in the field from surveyed elevations of the transition from bank to floodplain along a reach and then extrapolated to a nearby stream gage with an established stage--discharge rating curve [*King et al.*, 2004] or by using at-a-station hydraulic geometry relationships developed with USGS discharge field measurement data [*Williams*, 1978]. Regional downstream hydraulic geometry statistical relations were used to estimate Q_{bf} for four coarse bed sites [*Foster*, 2012].

Williams (1978) describes the following at-a-station hydraulic geometry relationships as useful for determining Q_{bf} based on identifying the discharge associated with: 1) the minimum value of the width-to-depth ratio (Figure 3.3a), 2) a break in slope from

steeper to less steep in the stage--discharge relationship (Figure 3.3b), 3) a discontinuity or vertical jump in the top width--discharge relationship (Figure 3.3c), and 4) a discontinuity or horizontal jump in the top width--cross sectional area relationship 3.3d). Not all of these relationships provided clear indicators of Q_{bf} for all sites. Method (4) proved least helpful, followed by method (1) and (2). Method (3) provided the clearest indication of Q_{bf} if such a break existed in the available data and at the cross section(s) where these measurements were collected.

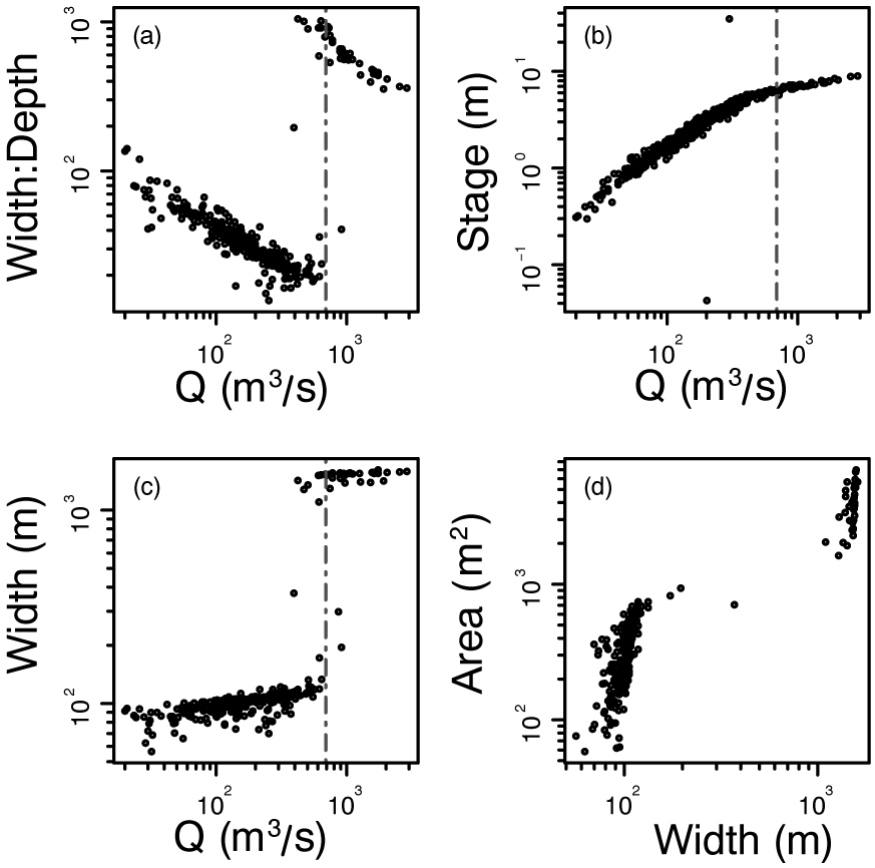

Figure 3.3 Example of Q_{bf} determination made from USGS field discharge measurements made on the Pee Dee River at Pee Dee, South Carolina (USGS Gage 02131000). Dashed vertical line indicates Q_{bf}. Note minimum value in the Q–W:D relationship (a), change in slope in stage--discharge relationship (b), as well as abrupt increase in width all at approximately the same discharge value (c). (d) indicates cross-sectional area and top width relationship.

In some cases, estimates based on the USGS field discharge measurements coincided with sites that had previously published, direct estimates of Q_{bf} ($n = 18$). Field-based estimates of bankfull stage and USGS field measurements were collected along the same reach of channel, though they may not coincide in time and space introducing some error. I used these concurrent estimates to evaluate the accuracy and bias of this approach to estimating Q_{bf}. A 1:1 plot of observed (published) and estimated (USGS field measurement methods) shows little bias in the estimation method and a reasonably good fit with observations (Figure 3.4a). The mean percent error is $+5\%$ and mean absolute percent error 50% (Figure 3.4b). Percent error is calculated as: $(Q_{bf,meas} - Q_{bf,est}) / Q_{bf,meas}$. This indicates that the at-a-station hydraulic geometry method for estimating Q_{bf} using USGS field measurements is only slightly positively biased and reasonably accurate.

2.3 Bankfull Discharge Prediction

I compare two different types of predictors of Q_{bf}: hydrology- and process-based. I calculate the hydrologic predictors using the annual maximum flood series available on the USGS National Water Inventory Service (NWIS) online database[7]. I estimate $Q_{1.5}$ and Q_2 floods using the Weibull plotting position, $p = m/(n+1)$, and linear

[7] http://nwis.waterdata.usgs.gov/usa/nwis/peak

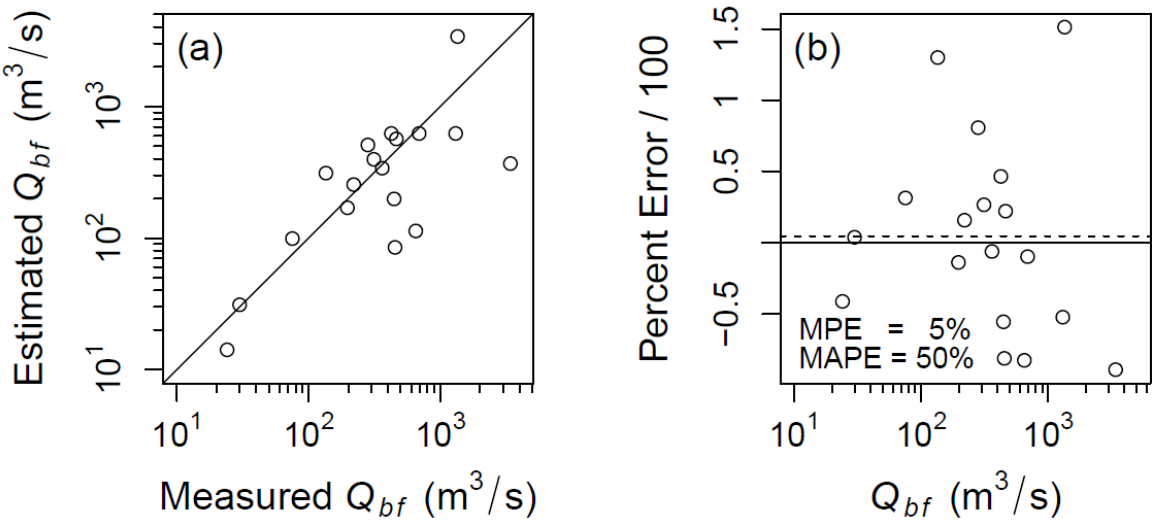

Figure 3.4 (a) Comparison between estimates of Qbf derived from at-a-station hydraulic geometry relationships made from USGS field measurements and estimates of Qbf directly determined in the field. (b) Values of the mean percent error (MPE), and mean absolute percent error (MAPE) are provided along with a dashed line indicating the value of the mean percent error (5%).

interpolation, where p is the probability of exceedance, m is the rank of the event with 1 being the largest, and n is the number of events on record.

Process-based predictors of Q_{bf}, such as sediment yield metrics Q_{eff} or Q_{s50}, rely on a frequency distribution (probability density function, PDF) or histogram of sediment yield or the cumulative distribution of sediment yield (sediment yield CDF). This can be thought of as the transformation of a flow duration curve into a sediment yield duration curve using a sediment rating curve (USACE, 1989). Biedenharn and Thorne [1994] demonstrate this with flow and sediment load data on the Mississippi River. Note that I use the terms PDF and CDF loosely here. This is because sediment yield PDFs and CDFs are not true PDFs and CDFs in the statistical sense. This is due to autocorrelation in flow records and the fact that they are derived distributions. I also

plot cumulative sediment yield and sediment yield density with discharge on the *x*-axis. I calculate Q_{eff} from the product of the empirical PDF of average daily flow, which is estimated by numerically-deriving the smoothed empirical CDF, with a sediment rating curve [*Orndorff and Whiting*, 1999]. The discharge value at which the peak of this sediment yield density curve occurs is Q_{eff} (Figure 3.1a). The half yield discharge, Q_{s50}, is the discharge associated with 50% of cumulative sediment yield as calculated from the sediment yield CDF. This is either calculated from the empirical CDF of the sediment yield record, or from the integral of the sediment yield PDF (Figure 3b).

The sediment rating curve is a log-linear regression equation of the form $Qs = \alpha Q^{\beta}$, between instantaneous discharge and bed material load. I used the `rlm()` function in the `MASS` package [*Venables and Ripley*, 2002] in `R` [*R Core Team*, 2014], which is a robust linear regression method that is less sensitive to outliers than ordinary least squares (OLS) regression. I corrected for transformation bias using the bias correction factor discussed by [*Ferguson*, 1986]. All log-linear slopes (β) were significant using an approximation of normality test calculated with the `lmRob()` function in the `robust` package [*Wang et al.*, 2014] (maximum $p = 0.014$). Multiple R^2 values from these robust linear models are calculated from the weighted residuals and ranged from 0.21 to 0.79 (median = 0.57); however, 70% of these values were greater than or equal to 0.5. These multiple R^2 values are lower than the conventional R^2 values derived from OLS regression. Values of R^2 from OLS regression ranged from 0.22 to 0.96 (median = 0.74) with $84\% \geq 0.5$.

Direct bed material load measurements are available for coarse bed rivers in units of (*mass/time*). I used Helley-Smith bed load sampler data only as this is the most widely available data. Bed material load for fine bed sites is calculated as the product of the sand fraction (≥0.0625 mm) of the measured suspended sediment concentration with the concurrent instantaneous discharge measurement to produce sediment load in units of (*mass/time*). Bed load data comes from a wide variety of sources listed in Table 3A.1 in the supplemental material. Suspended load data for all sites comes from the USGS Sediment Data Portal[8], an on-line database of suspended sediment measurements for sites across the U.S. and its territories.

I should also note that because my calculations of cumulative sediment yield for fine bed sites are solely based on suspended sand load and neglect the unmeasured bed load, these are likely underestimates of cumulative yield. Nash [1994] argues that the value of the rating curve exponent is not greatly impacted by inclusion of bed load in sand bed stream, and therefore sediment yield metrics such as Q_{eff} and Q_{s50} are not affected, as they are only sensitive to this parameter in the sediment rating curve. Unpublished work by Michels-Boyce [2014] supports this.

[8] http://cida.usgs.gov/sediment

3 Results

Here I compare the performance of hydrologic ($Q_{1.5}$ and Q_2) and process-based (Q_{eff} and Q_{s50}) predictors of Q_{bf} using basic goodness-of-fit metrics for coarse and fine bed sites (Table 3.1). The mean percent error (MPE) of the predicted values relative to the observed values gives a rough estimate of any bias in the predictors. If one type of predictor tends to over predict Q_{bf}, then MPE will be positive. The mean of the absolute values of percent error (MAPE), and the square root of mean squared error (RMSE) estimate the absolute error of the predictors. Finally, the slope and R^2 values of the ordinary least squares linear and log-linear regression lines fitted to the ($Q_{bf,obs}$, $Q_{bf,pred}$) data pairs aid in my characterization of the goodness-of-fit of each predictor (Table 3.1, Figure 3.5). I also consider the percent error of each predictor as a function of the sediment rating curve exponent β, the skewness of the daily flow record, and drainage area to determine if these factors influence the predictive error or create bias (Figure 3.6).

3.1 Performance of Bankfull Discharge Predictors

I begin by considering the log-linear regression lines fitted to the predicted and observed Q_{bf} values (Figure 3.5). This allows for rapid visual determination of bias and error. I calculate the median value and interquartile range (IQR) of cumulative sediment yields (Q_{s50}, Q_{s25}, and Q_{s75}, respectively) to compare their relationships with Q_{bf} as well (Figure 3.5, top row). The log-linear regression line for the Q_{s50}–Q_{bf} relationship falls

nearly on top of the 1:1 line for fine bed sites, and is bracketed by the Q_{s25}, and Q_{s75} (Figure 3.5, top row). The effective discharge tends to under predict Q_{bf} for both river types (Figure 3.5, middle row). Finally, the hydrologic predictors result in a fairly close fit with Q_{bf} for coarse bed sites, while tending to over predict Q_{bf} for fine bed sites (Figure 3.5, bottom row). For coarse bed sites, the log-linear regression line for the $Q_{1.5}$–Q_{bf} relationship nearly coincides with that of the Q_{s50}–Q_{bf} relationship, while Q_2 slightly over predicts Q_{bf} for these data.

The linear and log-linear slopes of the $Q_{1.5}$–Q_{bf} relationship are closest to unity (0.99 and 0.80, respectively) for coarse bed sites and tie with the Q_2–Q_{bf} relationships for the largest linear R^2 value (0.95), followed closely behind by Q_{s50} with an R^2 value of 0.94 (Table 3.1). In fact, all process-based and hydrologic metrics perform fairly similarly for coarse bed sites. The linear slope closest to unity for fine bed sites comes from the $Q_{1.5}$–Q_{bf} relationship. Both Q_{eff} and Q_{s50} relationships with Q_{bf} have slopes slightly larger than unity, though the intercept value for the Q_{eff} relationship is very large compared with that of the Q_{s50} relationship for these sites (172 vs. 16). The log-linear slope of the Q_{s50}–Q_{bf} relationship is closest to unity followed by $Q_{1.5}$, Q_2, and Q_{eff}. Finally, the greatest R^2 value for linear fits of fine bed Q_{bf} predictors results from the Q_{s50}–Q_{bf} relationship, which is much larger than the R^2 values of the other predictors (0.82 vs. 0.64 to 0.69).

When considering goodness-of-fit metrics, the MPE is lowest for $Q_{1.5}$ as are the MAPE and RMSE values for coarse bed sites, though the values of these metrics are not greatly

Table 3.1. Goodness of fit of various Q_{bf} predictors to the actual value of Q_{bf}

	MPE		MAPE		RMSE		Lin. Slope		Log Slope		Linear R^2	
	Fine	Crs.	Fine	Crs.	Fine	Crs.	Fine	Crs.	Fine	Crs.	Fine	Crs.
Q_{eff}	-52%	-18%	83%	41%	320	34	1.11	0.96	0.65	0.68	0.69	0.91
Q_h	27%	-6%	66%	38%	210	31	1.11	0.86	0.96	0.79	0.82	0.94
$Q_{1.5}$	96%	-3%	119%	31%	280	25	0.93	0.99	1.06	0.80	0.64	0.95
Q_2	164%	29%	176%	54%	320	36	0.75	0.81	1.09	0.79	0.66	0.95

different for Q_{s50} at these sites (Table 3.1). The effective discharge and then Q_2 follow in error magnitudes, respectively. All relative and absolute estimates of error are lowest for Q_{s50} for fine bed sites, followed by Q_{eff}, $Q_{1.5}$, and Q_2, though $Q_{1.5}$ has a lower RMSE value than Q_{eff}.

3.2 Predictor Bias and Sensitivity

I plot percent error for individual Q_{bf} predictors as a function of the sediment rating curve exponent, β, the skewness of the daily flow record, and the drainage area for all sites to evaluate if the prediction error is sensitive to these parameters (Figure 3.6). The hydrologic predictor $Q_{1.5}$ should not be influenced by β, because it is based solely on the peak flood record; however, β strongly influences the values of the process-based predictors [*Barry et al.*, 2008; *Bunte et al.*, 2014].

A positive trend between the percent error of Q_{eff} and Q_{s50} as a function of β is evident for coarse bed sites. They tend to over-predict Q_{bf} for larger values of β (greater than approximately 2.5). This same trend is also observed in fine bed sites, but it is not strong and the slope of the linear fit is not significant at $\alpha = 0.05$ ($p = 0.057$ and 0.068 for Q_{eff} and Q_{s50}, respectively). Because the value of β positively influences the absolute

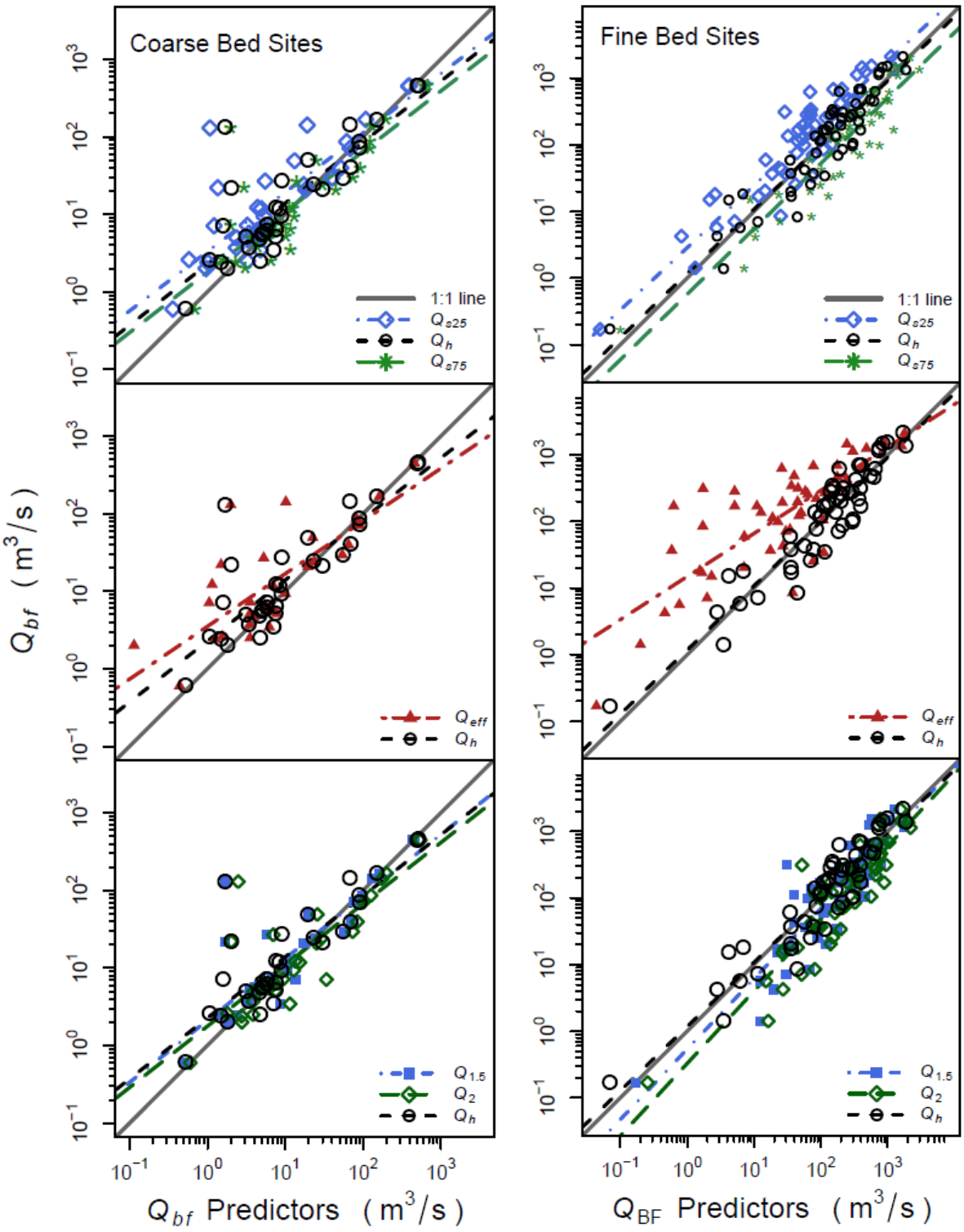

Figure 3.5 Log-log plots with log-linear regression lines between hydrology- and process-based predicted values and estimations of Qbf made from field measurements of bankfull indicators. Values of Q_{s25}, Q_{s50}, and Q_{s75} represent the discharges associated with 25%, 50% and 75% of cumulative sediment yield, respectively.

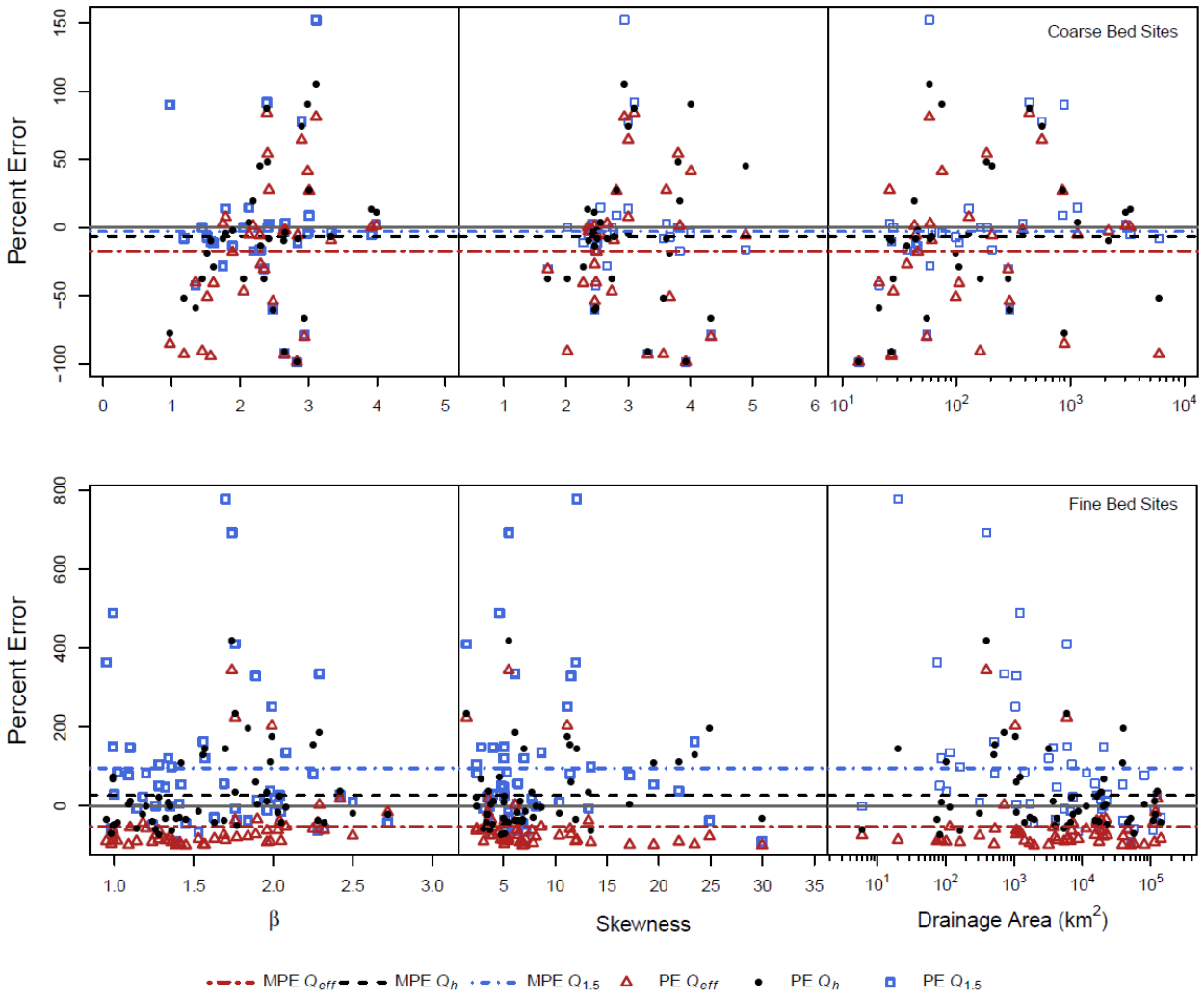

Figure 3.6 Percent error of various estimators of Q_{bf} as a function of the sediment rating curve exponent, β, the skewness of the daily flow record, and drainage area. Dashed lines indicate mean percent error values for each Q_{bf} estimator.

value of sediment yield, this is not surprising. Indeed, Bunte [2014] report values of Q_{eff} much larger than Q_{bf} in coarse bed streams with very large values of β.

Percent error also appears to increase slightly with skewness in fine bed sites, but this trend is also not significant ($\alpha = 0.05$). No trend or sensitivity is observed for any predictors as a function of skewness for coarse bed sites. As drainage area increases the

percent error of both Q_{s50} and $Q_{1.5}$ predictors decreases for fine bed sites only. This trend is significant for $Q_{1.5}$ but not for Q_{s50} ($p = 0.011$ and 0.218, respectively).

Mean values of percent error can indicate bias in these predictors (dashed lines, Figure 3.6 and Table 3.1). The MPE for Q_{eff} was negative for both types of sites indicating that it under-estimates Q_{bf} in most cases. The $Q_{1.5}$ and Q_{s50} estimators have small, negative MPE values for coarse bed sites. For fine bed sites, the $Q_{1.5}$ over-predicts Q_{bf} by a larger margin than Q_{s50}.

4 Discussion

4.1 Performance of Bankfull Discharge Predictors

Using a nationwide dataset of combined flow and sediment load data, I have found that Q_{s50} best predicts Q_{bf} for fine bed sites over Q_{eff}, $Q_{1.5}$, and Q_2. In coarse bed sites, $Q_{1.5}$, Q_{s50}, and Q_{eff} all predict Q_{bf} relatively well. However, $Q_{1.5}$ comes out slightly ahead when considering the goodness-of-fit metrics summarized in Table 3.1. The two-year return interval flood predicts Q_{bf} least well for both types of sites.

Hydrologic metrics based on annual maximum flow series such as $Q_{1.5}$ and Q_2 have been reported to approximate Q_{bf} fairly well, though considerable variability in the return interval of Q_{bf} exists [*Wolman and Leopold*, 1957; *Williams*, 1978; *Castro and Jackson*, 2001]. Estimating these hydrologic Q_{bf} predictors is much easier than process-based predictors because they require only an annual maximum flood peak series from a

nearby stream gage or readily available regional peak discharge regression equations. I do not evaluate the accuracy or bias of regional flood peak regression equations in this study; this is generally included in the USGS reports that publish these equations [*Jennings et al.*, 1994].

Comparisons of Q_{eff} with Q_{bf} have produced mixed results. Some workers have found a close 1:1 relationship between the two [*Andrews*, 1980; *Emmett and Wolman*, 2001; *Torizzo and Pitlick*, 2004], whereas others have found an inconsistent relationship, with Q_{eff} falling below the value of Q_{bf} [*Pickup and Warner*, 1976; *Soar and Thorne*, 2001; *Hassan et al.*, 2014] or well above [*Bunte et al.*, 2014]. Judging from the literature, it seems that Q_{eff} may approximate Q_{bf} for coarse bed, bedload dominated rivers, though Bunte et al. [2014] argue that this is an artifact of bed load sampling method. In their study of the most effective discharges in mountain streams in British Columbia, Canada, Hassan et al. [2014] modeled sand and gravel bed load transport using the Wilcock and Kenworthy [2002] relation. They found that in sites with more sand present in the bed, smaller discharges were relatively more effective, sand transport dominated the total sediment yield, and $Q_{eff} < Q_{bf}$. In sites with less sand present, Q_{eff} better approximated or even exceeded Q_{bf}. Infrequently mobile gravel and cobble dominated the beds in these sites. The effective discharge better approximated Q_{bf} for the coarse bed sites used in my study as well. In another study of the most effective flows for coarse bed material transport, Bunte et al. [2014] found that $Q_{eff} << Q_{bf}$. Sand was not included in the bed load measurements used in this study resulting in very large β values. Soar & Thorne

[2001] found that $Q_{eff} \approx Q_{bf}$ in fine bed rivers with low flow variability, but that Q_{eff} became increasingly smaller relative to Q_{bf} as flow variability increases.

This may indicate that there are two end members of effective flow frequencies. Either Q_{eff} is a very frequent flow that is less than bankfull in sand bed streams with more variable flow regimes and small β values. Or it is a vanishingly infrequent flow equal to or much greater than bankfull in infrequently-mobile, coarse bed streams with large β values and low flow variability. Low values of β (e.g., 1 to 2.5) are most often associated with fine bed, suspended load dominated rivers [*Nash*, 1994; *Syvitski et al.*, 2000].

The half yield discharge has not received much attention regarding its ability to predict Q_{bf} or its use as a design discharge. Emmett & Wolman [2001] calculate it in coarse bed streams and note that it tends to approximate Q_{eff} and Q_{bf}. Vogel et al [2003] derive closed-form solutions for Q_{s50} based on a power-law sediment rating curve and lognormal flow distribution. They compare it with Q_{eff} in suspended-load dominated rivers and argue that it may be a better discharge index for characterizing suspended and dissolved river loads because Q_{eff} tends to be a relatively frequent discharge in suspended and wash-load dominated rivers. Copeland et al. [2005] report that the discharge associated with the 75th percentile of cumulative sediment yield, Q_{s75}, best predicts Q_{bf}. However, like Vogel et al. [2003] they used total suspended load data, which includes wash load and not simply suspended sand load (suspended bed material). This resulted in them predicting a larger suspended sediment load for a given discharge,

especially at lower flow rates, likely reducing the value of β and upwardly biasing the cumulative sediment yield percentile most closely associated with bankfull discharge. My study extends and adds on previous work regarding Q_{s50} by considering its predictive ability over a wide range of river sites across both coarse and fine bed channels using bed material load data.

4.2 Cumulative Sediment Yield

To explore the relationship between cumulative sediment yield and various Q_{bf} predictors, I consider the cumulative sediment yield percentiles for Q_{bf} and Q_{eff} for the coarse and fine bed streams used in this study noting that this value is by definition 50% for Q_{s50}. The median value of cumulative sediment yield percentage at Q_{bf} is 50% for fine bed sites (35% to 70% IQR) and 53% for coarse bed sites (25% to 60% IQR) (Figure 3.7). The average value of cumulative sediment yield at Q_{bf} is also approximately 50% for fine bed sites, but is much lower for coarse bed sites indicating a distribution of cumulative sediment yield at Q_{bf} skewed to lower values. Median values of cumulative percent yield for Q_{eff} are much lower

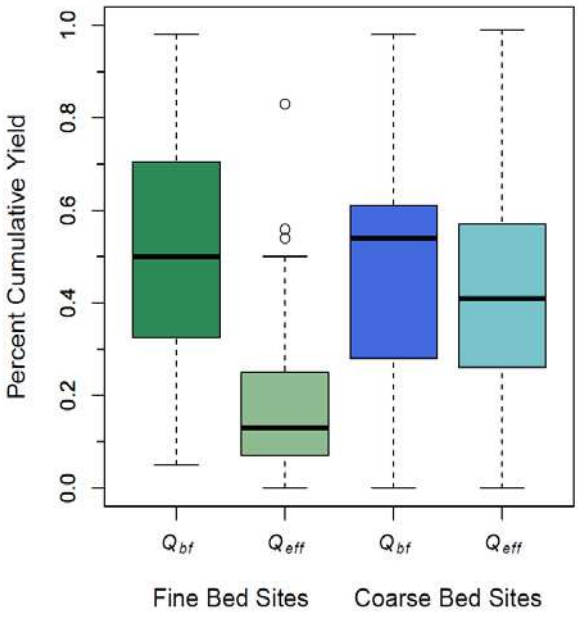

Figure 3.7 Box and whisker plots of the percentage of cumulative sediment yield evaluated at Q_{bf} and Q_{eff} for fine and coarse bed sites.

than those of Q_{bf} for fine bed sites, and slightly lower for coarse bed sites.

The question stands: Why does Q_{s50} predict Q_{bf} well? Choosing 50% as a value of cumulative sediment yield for Q_{bf} is arbitrary—rivers are not concerned with medians—though, as just discussed, this value matches the median value of cumulative sediment yield at Q_{bf} for fine bed sites, and is very close for coarse bed sites (Figure 3.7). Many theories exist regarding why Q_{eff} approximates Q_{bf} well [*Wolman and Miller*, 1960; *Carling*, 1988; *Hey*, 1996; *Soar and Thorne*, 2011]. The effective discharge maximizes the magnitude and frequency of sediment transport over all discharges. In bed load-dominated rivers, flow near bankfull tend to also be frequent and competent enough to meet this criterion [*Torizzo and Pitlick*, 2004]. Unlike Q_{eff}, little theoretical argument can be made for the discharge associated with 50% of cumulative sediment yield approximating Q_{bf}. The half yield discharge is nearly always larger than Q_{eff}, especially in fine bed rivers, making it a potentially more accurate predictor of Q_{bf} for these systems. It is a robust predictor of Q_{bf} in these rivers as it performs well across a wide range of physiographic regions (Figure 3.2). Additionally, calculating Q_{s50} does not suffer from the sensitivity Q_{eff} has to the flow frequency distribution estimation method such a histogram bin width selection [*Soar and Thorne*, 2001]. The ability of Q_{s50} to predict Q_{bf} for suspended sediment sites is a novel finding and an argument for process-based methods for channel design for these sites.

4.3 Using Bankfull Discharge Predictors

Calculating process-based Q_{bf} predictors is much more involved than calculating hydrologic predictors. However, because they incorporate physical representations of river hydrology, hydraulics, and morphology, they can provide more insight into the influence of process on channel form [*Soar and Thorne*, 2011] and even allow for prediction of channel response to hydrologic changes [*Tilleard*, 1999]. Based on previous work evaluating the utility of Q_{eff} in predicting Q_{bf} and on the findings of this study, I re-affirm that Q_{eff} is a good predictor of Q_{bf} in bed load-dominated, coarse bed streams. However, $Q_{1.5}$ appears to predict Q_{bf} fairly accurately as well in stable, quasi-equilibrium, coarse bed rivers. See Doyle et al. [2007] for criticisms and qualifications for the use of $Q_{1.5}$ or other hydrologic predictors of Q_{bf}, especially in unstable or urban channels. I submit that using Q_{s50} to predict Q_{bf} in suspended load-dominated rivers with fine beds is more accurate than Q_{eff} and the two hydrologic predictors evaluated in this study.

Barry et al. [2008] demonstrate that the Q_{eff} calculation based on calibrated sediment transport equations is not sensitive to the type of transport equation used in bed load-dominated, coarse bed rivers. This is because the location of peak of the sediment yield density curve (i.e., the discharge value or Q_{eff}) does not shift across different sediment transport relations (Figure 3.1a). The location of this peak is a function only of β or the slope of the empirical discharge-sediment load relation. The same is likely to be true for Q_{s50} because it is based on the relative position along the

cumulative sediment yield curve. Errors in absolute sediment yield estimates will not affect this. The value of β at a particular site is largely influence by channel geometry and bed material grain size [*Emmett and Wolman*, 2001; *Barry et al.*, 2004]. In the present study, I find that both Q_{eff} and Q_{s50} tend to over predict Q_{bf} for values of $\beta > 2.5$ in coarse bed streams. In forthcoming work, I am exploring the sensitivity of Q_{s50} to prediction from semi-empirical sediment transport relations used where sediment measurements are not available.

The Q_{s50} calculation requires the same data as the Q_{eff} calculation. See Biedenharn et al. [2000] and Soar & Thorne [2001] for thorough explanations of data sources and calculation procedures for Q_{eff}. Note that I use a method that diverges from conventional approaches in this study (see section 2.3). Below, I detail general approaches to calculating Q_{s50} given a variety of data sources and availability. Generic `R` code that can be used to perform some of these calculations is provided in Appendix 3C.

1. Flow Record
    a. *Ungaged Sites*: a scaled regional flow duration curve (FDC) or scaled flow record from a nearby river. Note that if using an FDC, it must first be converted to a CDF (CDF = 1 – FDC), and then converted to a PDF through numerical differentiation.
    b. *Gaged Sites*: a flow record with at least 10 years of daily flow data. Sub-daily flow data is preferred (e.g., hourly) due to the highly nonlinear relationship

between flow and sediment transport, but is often hard to find for longer periods of time.

2. Sediment Transport Relation

   a. *No Sediment Transport Data*: a calibrated sediment transport relation appropriate for the river of interested (e.g., total load equation for fine bed rivers and bed load equation for coarse bed rivers). See Hey [1996] and [*Torizzo and Pitlick*, 2004] for examples. I compare estimates of Q_{eff} and Q_{s50} generated from modeled sediment loads with those generated from the empirical models used herein in Chapter 4.

   b. *Measured Sediment Transport Data*: an empirical relation between discharge and sediment transport. For suspended bed material data (>0.0625 mm) data in fine bed sites as well as bed load data for coarse bed sites a bias-corrected linear regression between log-transformed variables can perform well [*Vogel et al.*, 2003; *Bunte et al.*, 2014]. `LOADEST` a USGS statistical package provides other options for multivariate linear regression between suspended bed material load and various flow metrics, which may improve the fit [*Runkle et al.*, 2004]. If using `LOADEST`, I recommend also using add-on software that formats data and outputs

for the USGS software such as LOADRUNNER[9], Purdue University's online sediment regression tool[10].

If using a flow record to calculate Q_{s50} (either scaled or from a nearby gage on the same river) one must simply calculate the sediment yield record using an appropriate sediment transport relation of the form: $Q_s = f(Q)$. The cumulative sediment yield curve can then be calculated by sorting the sediment yield record and creating a cumulative sediment yield curve (e.g., Figure 3.1b), which is essentially the cumulative sum of m/n plotted as a function of the sorted flow record, where m = rank, and n = the number of values in the flow record. The value of Q_{s50} can then be determined by finding the discharge at which the cumulative sediment yield is equal to 50% through linear interpolation.

If using a regional FDC scaled to a particular site, calculating Q_{s50} becomes much more cumbersome because one cannot directly calculate the cumulative sediment yield curve from the FDC. As previously discussed one must first convert the FDC to a CDF by taking its compliment, and then into a PDF through numerical differentiation [*Orndorff and Whiting*, 1999]. The sediment transport relation may then by multiplied by the flow PDF to create a sediment yield density curve. The cumulative sediment yield curve may then be calculated by numerically integrating the sediment yield

[9] http://environment.yale.edu/loadrunner/

[10] https://engineering.purdue.edu/~ldc/LOADEST/

density curve. Data acquisition as well as the hydrologic and sediment transport analysis necessary for this calculation have been automated within eRAMS, an online hydrologic database and analysis toolset with options for gages and ungaged basins[11].

5 Conclusion

I evaluate the accuracy and bias of two predominant methods used to predict Q_{bf}: (1) *Hydrologic predictors* based on a flood with a specified return interval as an analog to Q_{bf} based on the a flood series: the 1.5 to 2 year flood ($Q_{1.5}$ and Q_2, respectively), and (2) *Process-based predictors* based on the magnitude and frequency of sediment transport: the effective discharge, Q_{eff}, and the half yield discharge, Q_{s50}. I analyze bed material sediment transport data concurrent with long term flow records from 98 sites across the U.S. ranging from coarse bed, bed load-dominated channels and fine bed, suspended load-dominated channels with drainage areas ranging from 1 km^2 to $3x10^6$ km^2.

I find that:

1. The half yield discharge—the discharge associated with 50% of cumulative sediment yield, Q_{s50}—predicts Q_{bf} better than most other methods, especially in fine bed rivers.

[11] http://www.erams.com/crosssection

2. When compared to Q_{eff}, $Q_{1.5}$, and Q_2, Q_{s50} is the least biased estimator of Q_{bf} for fine bed sites, is nearly as unbiased as $Q_{1.5}$ for coarse bed sites, and has the lowest mean absolute percent error and root mean square error for fine bed sites.
3. $Q_{1.5}$ predicts Q_{bf} approximately as well as Q_{eff} and Q_{s50} for coarse bed sites.

I characterize the behavior of this process-based predictor of Q_{bf} to highlight circumstances where sediment yield analysis may be important in estimating the bankfull discharge. I also provide guidance for calculating and using process-based predictors of Q_{bf}. The ability of Q_{s50} to predict Q_{bf} in fine bed sites represents a novel finding not previously discussed in this context.

CHAPTER 4

Quantifying the uncertainty of sediment yield and sediment yield metrics

Summary

Uncertainty is endemic in any activity involving sediment yield estimation in rivers, which generally relies on statistical or physically-based models of sediment transport and hydrologic records. Uncertainty in estimates of sediment transport and sediment yield have been studied extensively; however, uncertainty in metrics that describe the magnitude and frequency of sediment yield has received little attention. In this chapter I consider the uncertainty of two sediment yield metrics: the most effective and half-yield discharges, Q_{eff} and Q_{s50}, from the perspectives of statistical uncertainty, environmental variability and non-stationarity, as well as physical model error.

To explore statistical uncertainty in estimating sediment yield metrics, I develop methods to propagate uncertainty in the sediment load-discharge relationship and in the

---

Not yet published. Joel Sholtes collected the data, conducted all of the research, analysis, and writing on this chapter with input and feedback from his advisor. Mazdak Arabi provided guidance on statistical uncertainty analysis. Specific information on the sites used in the urbanization study, such as population growth, was provided by Tyler Rosburg. Brian Bledsoe, Peter Nelson, and Daniel Baker co-authored the research proposal that funded a portion of this work. The basic framework for quantifying the uncertainty of sediment yield metrics was outlined in that proposal.

flow frequency distribution to create confidence intervals for Q_{eff} and Q_{s50}. I explore the relationship between the relative width of the uncertainty intervals and the uncertainty in the flow and sediment data. I find that as the number of sediment load observations, and the value of the sediment rating curve exponent increase, the relative width of the confidence interval for the half-yield discharge decreases. This uncertainty spread increases with the coefficient of variation of the flow record. In urbanizing watersheds, with increasing trends in flow variance, decadal estimates of Q_{eff} and Q_{s50} increase dramatically compared to estimates based on the entire flow period of record. Finally, I estimate Q_{eff} and Q_{s50} using empirical models of sediment load and one-dimensional, physically-based models. Physically-based models that match the slope of the sediment load-discharge relationship performed well. This is the case in estimating Q_{s50} using total load models for fine bed sites, but generally not the case for bed load models used on coarse bed sites. Estimates of Q_{eff} are not sensitive to modeled sediment load except in cases of multimodal sediment yield curves. By exploring the nature of uncertainty in sediment yield from these perspectives, I provide tools and guidance for calculating and utilizing sediment yield metrics for river design and management.

1 Introduction

The most effective discharge, Q_{eff}, and the half-yield discharge, Q_{s50}: that which half of cumulative sediment yield over a sorted flow record occurs are sediment yield

metrics that have been touted as important and useful discharge indices for predicting bankfull discharge as well as predicting river response to environmental change [*Andrews*, 1980; *Tilleard*, 1999; *Soar and Thorne*, 2001; *Doyle et al.*, 2007; *Simon et al.*, 2011, *Chapters* 2 and *3 of this Dissertation*]. Many studies have estimated Q_{eff} across a wide variety of rivers and estimated its frequency relative to the bankfull discharge as well as other peak flow indices [*Andrews*, 1980; *Biedenharn and Thorne*, 1994; *Nash*, 1994; *Emmett and Wolman*, 2001; *Hassan et al.*, 2014]. However, little work has been done to characterize the uncertainty associated with these metrics, focusing on Q_{eff} only, and considering error associated with calculation methodology [*Nash*, 1994; *Vogel and Fennessey*, 1994; *Orndorff and Whiting*, 1999; *Sichingabula*, 1999; *Soar and Thorne*, 2001; *Goodwin*, 2004; *Klonsky and Vogel*, 2011], rather than explicit quantification of uncertainty. To my knowledge, no studies consider uncertainty associated with Q_{s50}, a relatively unexplored sediment yield metric. Previous work on this these topics is discussed in more depth in relevant subsections in the Background and Methods section of this chapter.

Quantifying uncertainty for sediment yield metrics based on magnitude-frequency analysis must incorporate uncertainty associated with the sediment load-discharge relationship as well as the flow record. A multitude of factors contribute to uncertainty in sediment yield estimation on rivers. These include measurement error, model specification and parameter error, hysteresis in the sediment load-discharge relationship, as well as the cumulative error associated with integrating sediment load predictions

over an extended time series to name a few [*Wilcock*, 2001; *Bunte et al.*, 2004; *Grams and Schmidt*, 2005; *Schmelter et al.*, 2012; *Grams et al.*, 2013]. In the case of sediment yield metrics, I consider uncertainty from the perspectives of statistical uncertainty, environmental variability, as well as model error, and explore the sensitivity of sediment yield metric uncertainty these sources.

This chapter focusses on three main topics: 1) quantifying and propagating uncertainty associated with the sediment load-discharge relationship and the flow frequency distribution in calculating sediment yield metrics, 2) characterizing the influence of non-stationarity in the flow regime due to environmental change on sediment yield metrics, and 3) quantifying the error associated with calculating sediment yield metrics using measured vs. modeled sediment load.

Part 1 considers the uncertainty inherent in statistical representations of the sediment load-discharge relationship as well as statistical representations of the flow frequency distribution. In general, gaged flow records are considered absolute and their uncertainty is not considered [*Clarke*, 1999]; however, as with any natural system, inferences and predictions made on a sample (even a large sample) are subject to uncertainty because the sample—in this case the daily or instantaneous flow record—only captures a limited amount of variability from the underlying population. In this focus area, I explore methods to quantify uncertainty in the sediment load rating curve with confidence and prediction bands for log-linear regression models. I then consider methods for uncertainty analysis of the flow record, focusing on developing confidence

bands for representations of the flow probability density function (PDF). Using these representations of uncertainty in the sediment rating curve and flow PDF, I then propagate the uncertainty in calculating sediment yield metrics and consider its sensitivity to various sediment yield input and hydrologic variables.

Part 2 considers uncertainty from the standpoint of stationarity of the flow record used in calculating sediment yield metrics. Stationarity assumes that the mean, variance, and other statistical moments of the underlying population of flows at a point on a river do not change with time. Put another way, stationary natural systems "...fluctuate within an unchanging envelope of variability" [*Milly et al.*, 2008, p. 573]. This may not be the case in watersheds undergoing land use change due to urbanization or those acutely affected by climate change, for example.

As discussed in Chapter 3, Q_{eff} and Q_{s50} are in some cases useful in predicting the bankfull discharge for channel design and management. Part 3 of this chapter explores the question that practitioners may face when using sediment yield metrics: given the lack of site-specific sediment load data and the need to model this, how accurate are estimates of sediment yield metrics calculated from modeled sediment load? I compare estimates of sediment yield metrics calculated from empirical and physically-based sediment load models.

2 Background and Methods

2.1 Uncertainty in the Sediment Load Rating Curve

Continuous records of sediment load are limited and tend to exist only on larger rivers [*Turcios and Gray*, 2001; *USGS,* 2014]; therefore, regression methods are often necessary to develop continuous relationships between discharge—or other covariates such as turbidity—and sediment load. This is often referred to as double sampling [*Gilbert*, 1987] wherein simultaneous samples are collected of two variables and a statistical relationship is derived between the variable that is difficult or costly to measure (sediment load) and the variable that is easier to measure (discharge). Technically speaking, this is a triple sample problem because discharge is typically estimated as a statistical relationship between river stage (or some partial water column acoustic Doppler velocimeter measurement) and discrete discharge field measurements.

Quantifying sediment yield has many implications for environmental quality, watershed management, river and reservoir design and maintenance. Therefore, uncertainty analysis of sediment yield estimates based on sparse sediment load measurements and continuous flow records has been studied extensively [*Walling*, 1977b; *Moog and Whiting*, 1998; *Syvitski et al.*, 2000; *Simon et al.*, 2004; *Rustomji and Wilkinson*, 2008; *Vigiak and Bende-Michl*, 2013]. Not all methods involve bivariate regression analysis between flow and sediment load as in this study. Many forms of multivariate regression models which use various flow and season-related covariates

(some autoregressive) have been proposed [*Cohn et al.*, 1992; *Wang et al.*, 2011], as well as weighted averaging and random sampling methods for more dense and semi-continuous sampling designs [*Thomas*, 1985]. Incorporation of additional continuously-sampled covariates such as turbidity and "backscatter" signals from acoustic Doppler devices has been shown to improve predictions of suspended sediment load [*Topping et al.*, 2007; *Landers and Sturm*, 2013]. Finally, indirect methods that utilize geomorphic change over time from either topographic surveys or LiDAR differencing techniques are also used to estimate sediment yield and create sediment budgets [*Grams and Schmidt*, 2005; *Wheaton et al.*, 2009].

The present study focuses on bivariate models fitted to measurements of sediment load and discharge. Fitted non-linear models (e.g., $Q_s = \alpha(Q - Q_c)^{\beta}$, where Q_c is a critical discharge below which $Q_s = 0$) have been recommended, especially for bed load transport [*Wilcock et al.*, 1996]. However, Gaeuman et al. [2015] found that non-linear least squares fitting produces large error and bias when zero transport data exist. They recommend a maximum likelihood fitting procedure for the critical discharge nonlinear model for Q_s which requires specifying the log-likelihood function for sediment transport rate and finding model parameter combinations that maximize this function. While the method appears to perform better than log-linear and non-linear least squares regression mode, the data requirements for this approach extend beyond the data available for most coarse bed sites included in this study. Bayesian methods for

estimating nonlinear model parameters may also yield good model fits [*Reitan and Petersen-Øverleir*, 2007].

Due to the large number of sites in this study and limited data beyond sediment load and discharge measurements, I have chosen the generic log-linear model to fit to these data. As discussed in Chapter 2, I have culled sites where a poor log-linear fit exists between sediment load and discharge. I use three bivariate, log-linear regression methods that vary in their complexity based on assumptions about the data as well as methods for quantifying uncertainty. Bivariate sediment load–discharge data are often log-linear as sediment load is nearly always a non-linear function of discharge (e.g., $Q_s = \alpha Q^{\beta}$, where $\beta > 1$ for sediment). I have used this type of transformation for my sediment rating curves because it works well in most cases (see results from Chapter 2 in Appendix 2A) and because I require a parsimonious model that can be applied on 153 sites with limited data as discussed in Chapter 2.

A drawback of this model choice is that it cannot accommodate zero sediment load data. This may be significant in coarse bed rivers where a threshold for sediment entrainment exists [*Gaeuman et al.*, 2015]. However, the data needed to quantify Q_c is not available for all coarse bed sites and I therefore neglect zero transport data in fitting my models. If zero transport data exists for a site, I incorporate this information into the sediment yield analysis as discussed in Chapter 2. Finally, mean response calculated from un-transformed regression models based on log-transformed data are biased downward because negative residuals near the mean are given similar weight as more

distant positive residual, necessitating a log transformation bias-correction factor [*Ferguson*, 1986; *Cohn et al.*, 1989]. This is discussed in more depth in Chapter 2, though it does not apply to the present question of quantifying the uncertainty of the sediment yield metrics Q_{eff} and Q_{s50} because these metrics are not sensitive to the value of the coefficient in the sediment rating curve, only the exponent [e.g., *Barry et al.*, 2004].

I compare the following log-linear regression models: 1) an ordinary least squares model, 2) a robust linear regression model, and 3) a robust Bayesian linear regression model. With data from selected coarse and fine bed sites, I calculate the mean response or fitted regression line, a 95% confidence band for the mean response, as well as a 95% prediction band for a future predicted response using each method. Methods for each regression approach are outlined in Appendix 4A.

2.2 Uncertainty in the Flow Record

Uncertainty in a gaged flow record has not received much attention to date. Much work on flow uncertainty analysis has been focused on ungaged basins and continuous hydrologic model output [*Beven and Freer*, 2001; *Castellarin et al.*, 2004; *Pappenberger and Beven*, 2006]. Insofar as a flow record is a sample from an underlying population, it is uncertain in a statistical sense. Vogel and Fennessey [1994] introduced the annual flow duration curve (AFDC), which they argue can be treated as a random sample itself for which statistics may be calculated, such as the median AFDC as well as

the 2.5^{th} and 97.5^{th} percentile AFDCs. In this manner, a confidence interval may be constructed for an annual flow duration curve. Though this may be of interest for water resources planning and environmental flows questions, it is unfortunately not useful for sediment yield analysis. Average annual sediment yield, a non-linear function of discharge, is grossly under-estimated by the median AFDC because, by definition, it does not represent larger flow events well. Less frequent, larger flow events tend to drive the majority of sediment yield, especially in coarse bed systems.

Outside of this statistical uncertainty question, other forms of flow uncertainty exist. Some have considered the uncertainty inherent in the creation of discharge rating curves and quantified how this propagates to the flow record [*Moyeed and Clarke*, 2005; *Reitan and Petersen-Øverleir*, 2007]; but this is a measurement error question and I do not consider it here. Non-stationarity in precipitation due to climate change as well as in the runoff response due to both climate and land use change may create non-stationarity in the flow record. [*Christensen and Lettenmaier*, 2007; *Milly et al.*, 2008; *Vogel et al.*, 2011]. If the mean flow rate or the flow variance changes with time, then a flow record may not be sampling a stable underlying population distribution.

Here I consider the uncertainty in the flow record from a statistical standpoint as well as from an environmental non-stationarity standpoint. I first quantify uncertainty in the flow record by creating non-parametric confidence bands for the flow PDF. I also consider the influence of non-stationarity on the values of Q_{eff} and Q_{s50}. To do this, I compare estimates of these sediment yield metrics based on sequential decadal flow

records in several urbanizing watersheds previously studied by Konrad et al. [2005] to demonstrate their sensitivity to changing flow regimes.

2.2.1 Flow Frequency Distribution

Magnitude-frequency analysis of sediment transport involves representing the flow record probabilistically. When referring to the probability distribution of a flow record, I use the term PDF loosely. Representing a flow record as a probability distribution of independent samples, such as the lognormal distribution, has a long, inaccurate history of use in geomorphology and engineering [*Wolman and Miller*, 1960; *Andrews*, 1980; *Vogel et al.*, 2003; *Goodwin*, 2004]. Flow records are by definition autocorrelated, violating the independence assumption inherent in representing them as PDFs [*Salas*, 1993]. Perhaps using histograms to represent the relative frequency of binned flows in MFA avoids the independence assumption by not claiming to represent the probability density distribution, rather the frequency distribution. However, that may simply be an argument of semantics. Representing flow records as or fitting continuous PDFs to flow records may be sufficient for the purposes of MFA; however, deriving uncertainty estimates of flow records based on fitted PDFs (empirical or parametric) may cross into more dangerous territory, statistically-speaking. Nevertheless, I explore methods for representing uncertainty in PDFs fitted to flow records with the aim of propagating all forms of uncertainty into sediment yield metrics.

To represent the frequency of flows, a histogram approach is most often used [*Biedenharn et al.*, 2000] whereby flows are sorted into bins and the relative frequency of flows within each bin is calculated. Soar and Thorne [2001] have explored the sensitivity of the Q_{eff} estimate to the binning method extensively, recommending on the order of 25 arithmetically-spaced bins to be used in the calculation, finding that logarithmically-space bins result in overestimating Q_{eff}. Several studies have explored the sensitivity and error of estimates of Q_{eff} generated from different PDFs [*Nash*, 1994; *Vogel et al.*, 2003; *Goodwin*, 2004; *Sholtes et al.*, 2014], finding mixed results in their ability to represent the flow regime well.

In Chapter two, I compare several methods for representing the flow frequency distribution, including kernel density functions as proposed by Klonsky and Vogel [2011], and conclude that a modified method described by Orndorf and Whiting [1999] and also used by Emmett and Wolman [2001] performed the best over all data sets. This method involves numerical differentiation of the empirical CDF of the flow record to create a flow PDF, which can then be multiplied by a sediment transport function to generate the sediment yield curve.

This method works well when estimating a single PDF of a flow record, but does not work well when also calculating confidence bands of a PDF. Numerical differentiation is an approximate method and can result in unsmooth, and improper upper and lower-bound confidence band PDFs. Direct estimation of a statistic is preferred over indirect estimation. This means directly estimating confidence bands of a

PDF, rather than generating them by differentiating confidence bands for a CDF. I proceed with a method for calculating pointwise confidence bands for an empirical PDF, namely a kernel density function, using an asymptotic normality assumption [*Härdle*, 1991, p.62].

To my knowledge, no method exists for calculating confidence bands for parametric PDFs such as the lognormal distribution other than with bootstrap re-sampling. Bootstrapping a flow record and creating a bootstrap sample of the fitted PDFs results in very narrow confidence bands. This is because a flow record is generally composed of 1000's of highly auto-correlated samples. Any re-sample will be largely the same as the original. Confidence intervals for the parameters of a PDF can be calculated using Bayesian or maximum likelihood methods, but a confidence interval for model parameters does not translate to a pointwise confidence band of a density function. Therefore, I proceed with only one method for creating confidence bands for the flow frequency distribution based on an empirical PDF or ePDF.

Kernel density functions (KDFs) estimate the empirical PDF, $\hat{f}_h(x)$, by fitting a series of continuous kernel functions to the sorted data over a moving window with a specified bandwidth, h. While the kernel function is parametric, the resulting ePDF is non-parametric in that it takes on whatever shape the data distribution has as a function of the bandwidth value and choice of kernel function. As discussed in Chapter 2, KDFs did not perform well in MFA. This is due to the spiky and highly variable

nature of the sediment yield curve they generate upon transformation. While this behavior can be remedied by over-smoothing (large bandwidth value), over-smoothing results in increase bias in the estimate of density (generally reducing estimated density at a given discharge value), potentially leading to erroneous results. Nevertheless, KDFs represent the most direct method for calculating the uncertainty in the flow PDF.

While more accurate and complex methods exist [e.g., *Hall and Horowitz*, 2013], a basic approach to pointwise confidence bands for a KDF rely on the fact that under certain specifications of the bandwidth, the sampling distribution of the density estimate, $\hat{f}_h(x)$, is asymptotically-normal [*Härdle*, 1991]. The equation for the pointwise confidence band is:

$$\hat{f}_h(x) \in \left[\hat{f}_h(x) \pm z_{1-\alpha/2} \sqrt{\frac{\hat{f}_h(x) \mathrm{K}^2}{nh}} \right] \tag{4.1}$$

where K^2 is the square of the integral of the kernel function evaluated from (-∞, ∞). I used a Gaussian kernel resulting in $\mathrm{K}^2 = 1 / (2\sqrt{\pi})$. The width of this confidence band increases with the values of the estimated density, $\hat{f}_h(x)$, and decreases with the sample size (length of flow record). Note that I used the value of the effective sample size for n in (4.1). This adjusts the sample size by accounting for autocorrelation in the flow record and is an estimate of the number of independent samples. To calculate this, I used the `effectiveSize()` function in the `coda` package in `R` [*Plummer et al.*, 2006].

2.2.2 Flow Cumulative Probability Function

I derive the cumulative sediment yield curve $F_{Qs}(Q)$ from the following equation:

$$F_{Qs}(Q) = \frac{\int_0^Q f_{Qs}(Q)dQ}{\int_0^\infty f_{Qs}(Q)dQ} \approx \frac{\sum_{i=1}^{k} Q_s}{\sum_{i=1}^{n} Q_s}, k \in (1,...,n) \tag{4.2}$$

where $f_{Qs}(Q)$ is the sediment yield curve, a continuous function of Q, estimated by the cumulative summation of sorted sediment yield normalized by the total summation of sediment yield with k equal to the ith sorted Q_s value and n equal to the total number of values in the flow record. Note that this is not a CDF. For this study, I estimate F_{Qs} by taking the cumulative numerical integral of the sediment yield curve normalized by the total area under the sediment yield curve. Deriving the cumulative sediment yield curve from the sediment yield curve rather than directly from the flow record is required to incorporate the uncertainty bands estimated for the PDF. This cumulative integral estimate compares well with the direct estimate from the cumulative sediment yield record.

I cannot estimate the uncertainty of the cumulative sediment yield curve directly because it is *not* a cumulative probability function, which is defined as follows for a positive, random variable $X = \{x_1, x_2, \ldots, x_n\}$:

$$F_X(x) = \int_0^x f_X(x)dx \approx \frac{1}{n}\sum_{i=1}^{n} 1\{x_i \le x\} \tag{4.3}$$

where the right most equality defines the empirical CDF with {} equaling unity if the argument inside is true and zero if not. To estimate F_X for sediment yield, one could

calculate the eCDF of the sediment yield record or numerically-integrate the PDF of the sediment yield record. The distinction between 4.3 and 4.2 lies in the fact that equation 4.2 is generated from the product of a sediment rating curve and a PDF of flow, both a function of discharge, or from the cumulative, normalized sum of sediment yield. Whereas equation 4.3 would simply be calculated from a PDF of sediment yield or directly from an eCDF of the sediment yield record. Equation 4.2 is plotted with the fraction of cumulative sediment yield as ordinates and discharge as abscissa, whereas equation 4.3 is plotted with ordinate units of cumulative probability of sediment yield and abscissa units of sediment yield. While the cumulative probability of sediment yield is an interesting function to explore, the discharge values associated with its quantiles are not as physically-meaningful as those from the cumulative sediment curve.

2.2.3 Non-stationary Flow Record

Up to this point, I have calculated sediment yield metrics using all of the daily flow data within the period of record. This approach allows one to use more data (a larger sample), but it also assumes that the mean and variance in the flow record are constant or stationary over time. In other words, it assumes that the statistical moments of the population of flows, of which the gaged record is a sample, are temporally invariant. Because of environmental change (e.g., climate and land use change), precipitation patterns and intensity, evapotranspiration, the runoff response, and ultimately the flow regime may be changing with time [*Christensen and*

Lettenmaier, 2007; *Milly et al.*, 2008; *Vogel et al.*, 2011]. Discerning trends in the historical flow record due to climate change can be difficult given the variability in flow in most rivers resulting in many different interpretations of flow trends due to climate change [*Easterling et al.*, 2000; *Cayan et al.*, 2001; *Barnett et al.*, 2008; *Ray et al.*, 2008; *Rajagopalan et al.*, 2009]. However, discerning trends in the runoff response due to urbanization is often hard to miss from a statistical as well as geomorphic point of view [*Booth*, 1990; *Konrad et al.*, 2005; *Vogel et al.*, 2011].

To this end, I consider how a temporally variant mean and/or variance in a flow record might influence estimates of sediment yield metrics. I evaluate this in several urbanizing watersheds in which Konrad et al. [2005] studied how urbanization influences the values of certain flow percentiles. These streams are located in the greater metropolitan area of Seattle and have coarse beds. The watersheds of these streams began urbanizing in the 1970s with subsequent increases in flashiness and the magnitude of peak discharges over time. Konrad et al. [2005] provide additional background information on these sites. Rosburg [2015] did not find significant trends in annual precipitation depths near these watershed over the study period indicating that the change in flow mean and variance resulted primarily from land use change.

To study the influence of a non-stationary flow record, I divide the flow records from each stream by decade and calculate MFA metrics based on flows within each decade as well as for the entire period of record. As demonstrated in Chapter 1, MFA conducted using short flow records (e.g., ≤ 10 years) is sensitive to large values of β,

often resulting in Q_{eff} becoming the largest discharge on record (Figure 1.4). Using decadal flow records to directly calculate Q_{eff}, for example, results in highly-scattered values of Q_{eff} that are likely inaccurate. To explore how trends in mean and variance in the flow record due to urbanization influence sediment yield metrics, I fit continuous lognormal distributions to these data using the method of moments as discussed in Chapter 1. Because no sediment load data are available for these sites, I calculate sediment yield metrics using β values ranging from 1.5 to 4 (reasonable for coarse bed rivers such as these). I then explore sediment yield metric sensitivity to non-stationary flow records as a function of β. Note that the value of α does not influence these calculations and is therefore set to an arbitrary value of 0.01. As a control, I also conduct this same procedure on two rural watersheds from the same area that have not urbanized [*Konrad et al.,* 2005, *Rosburg* 2015].

2.3 Sediment Yield Metric Uncertainty

By combining uncertainty bands from the log-linear regression sediment load model with those of the flow PDF, I can generate confidence and prediction bands for the sediment yield curve as well as the cumulative sediment yield curve. Finding the discharge values associated with the upper and lower confidence and prediction bands for the sediment yield curve will then produce confidence and prediction intervals for Q_{eff}. Evaluating the confidence and prediction bands of the cumulative sediment yield

curve at values of 50% of cumulative yield will produce confidence and prediction intervals for Q_{s50}. The generic equation for sediment yield uncertainty bands is:

$$f_{Qs}(Q)_{low} = \hat{f}_h(Q)_{low} \times Q_s(Q)_{low}$$
$$f_{Qs}(Q)_{upp} = \hat{f}_h(Q)_{upp} \times Q_s(Q)_{upp} \quad (4.4)$$

where $f_{Qs}(Q)$ is the sediment yield curve, $Q_s(Q)$ is the sediment rating curve—both a function of Q—and the subscript *low* and *upp* indicate the lower and upper 95% confidence or prediction band value of these functions evaluated at Q.

The generic equation for cumulative sediment yield uncertainty bands is:

$$F_{Qs}(Q)_{low} = \int_0^Q \hat{f}_h(Q)_{low} Q_s(Q)_{low} dQ$$
$$F_{Qs}(Q)_{upp} = \int_0^Q \hat{f}_h(Q)_{upp} Q_s(Q)_{upp} dQ \quad (4.5)$$

I calculate confidence intervals for Q_{eff} and Q_{s50} using this methodology for all fine and coarse bed sites. I also calculate the normalized width of these intervals, $(Q_{eff,upp} - Q_{eff,low})/Q_{eff}$, and search for aspects of the flow and sediment load data that might influence the value of this normalized width.

As discussed in the Results below in Section 3.2, uncertainty intervals for Q_{eff} calculated from the product of upper and lower uncertainty bands for the sediment rating curve with upper and lower bands for the flow frequency distribution do not result in much uncertainty in the value of Q_{eff}, that is, the peak of the upper and lower sediment yield curve confidence and prediction bands tend to line up or fall very close to

one another. Therefore, I also use a different method to propagate uncertainty in sediment yield metrics: I bootstrap them.

To do this, I use bootstrap samples of the rating curve coefficients (see bootstrap confidence band description in Section 4A.2) to create bootstrap samples of the upper, middle, and lower sediment yield curves. These are calculated from the product of the bootstrapped sediment rating curves with the upper and lower confidence bands for the kernel density function of flow (red bounds, Figure 4.3b) as well as the originally-estimated (middle) kernel density function (black line, Figure 4.3b). I then calculate the cumulative integral of these bootstrapped curves to create bootstrap samples of the upper, middle, and lower cumulative sediment yield curves. This results in bootstrapped samples of upper, middle, and lower values of Q_{eff} and Q_{s50}. I calculate the outer confidence interval values for each metric using the 97.5^{th} and 2.5^{th} percentile values from the upper and lower bootstrapped samples, respectively. I also calculate these percentile values from the bootstrapped sediment curves themselves at gridded discharge values to create pointwise confidence bands for the sediment yield and cumulative sediment yield curves (Figure 4.5). However, confidence intervals for Q_{eff} and Q_{s50} are not based on these confidence bands, rather the bootstrapped values of these metrics themselves.

2.4 Modeled vs. Measured Sediment Yield Calculation

Here I compare estimates of Q_{eff} and Q_{s50} generated from empirical, statistical models of log-transformed sediment load and instantaneous discharge data (empirical models) with those generated from calibrated, physically-based, sediment transport capacity models (physical models). Note that I use the phrase "physical models" here to refer to physically-based equations and not in the literal sense of a physical model. In general, sediment load data are not available for a particular stream or river of interest as they are time consuming and expensive to collect. Therefore, I evaluate how robust estimates of sediment yield metrics are to the additional uncertainty associated with the lack of such data and the need to model sediment transport. In a comprehensive study of effective discharge calculation using bed load sediment transport relations, Barry et al. [2008] found that the choice of equation largely did not influence the value of Q_{eff} for a particular site. This is because the steepness of the sediment transport-discharge relationship in log-space is what influences the position of the peak of the sediment yield curve. The absolute value of sediment yield (area under the sediment yield curve) is not important in this particular calculation, hence the absolute accuracy of estimating sediment yield does not come into play. Like Q_{eff}, the Q_{s50} yield metric is also only sensitive to the rate of increase in sediment transport with discharge (e.g., the value of β). This is because the cumulative sediment yield curve is normalized by the total yield value removing the influence of uncertainty in the absolute value of yield and hence the values of the coefficient, α.

I compare estimates of Q_{eff} and Q_{s50} using various physically-based models with those calculated from the empirical models used in Chapters 2 and 3. I conduct this analysis on two coarse and two fine bed sites to explore the strengths and weaknesses of various sediment transport models as well as representations of the modeled stage-discharge relationship (Table 4.1). In an effort to include a variety of flow regimes and channel geometries, I selected sites with relatively small and large drainage areas in each bed material category.

For this comparison on coarse bed sites, I use three physical models and three representations of the stage-discharge relationship to model sediment transport. The two coarse bed sites studied are: Trapper Creek, Idaho (TC); and the South Fork of the Salmon River, Idaho (SR) (site numbers: 1333850F and 13310700). I use the following bed load models: Parker [1979], a single grain size, surface-based model; Wilcock and Kenworthy [2002], a two-fraction surface- or sub-surface based model; and Barry et al. [2004], a semi-empirical power-law model that is a direct function of discharge rather than bed shear stress (referred to as Parker, WK, and Barry hereafter).

Using the Parker model, I also explore different representations of the stage-discharge relationship, an important aspect and additional source of uncertainty in sediment transport modeling. Using Manning's flow resistance equation, cross-section geometry, and channel slope, I calculate cross-section averaged depth, bed shear stress, width, velocity, and discharge as a function of water surface elevation (averaged depths). However, due to the spatially-variable nature of sediment transport across a

Table 4.1. Modeled vs. Measured Sediment Yield Site Characteristics

Site No.	Site Name	Type	Q-D Relation	DA (km^2)	Slope (m/m)	FS (%)	D16 (mm)	D50 (mm)	D84 (mm)
1333850F	Trapper Ck, ID	Coarse	XS, HG	21	0.0414	5.2		79	210
13310700	SF Salmon River, ID	Coarse	XS, HG	855	0.0025	46		14	75
09260050	Yampa R. at Deerlodge, CO	Fine	XS, HG	20,541	0.0030	100	0.27	0.41	0.68
05568800	Indian Ck near Wyoming, IL	Fine	HG	162	0.0010	84	0.27	1.00	5.60

NOTE: "XS" refers to cross-section derived depth-discharge relationship using Manning's equation, and HG refers to at-a-station hydraulic geometry relation based on field measurements of channel and flow geometry at a range of discharges.

cross-section and the high degree of nonlinearity of sediment transport with discharge, using cross-section averaged values of hydraulic parameters to estimate sediment transport introduces additional error and may over- or under estimate sediment transport rate. Therefore, using the same flow resistance equation, I also calculate these hydraulic variables for vertical sections over the entire cross-section and sum sediment transport estimates across these intervals to calculate sediment load for a given discharge and water surface elevation (discrete depths). Finally, because a considerable number of stage, width, and flow area measurements were available for these two sites [BAT, 2013, describe by King et al. 2004] and are generally available at all USGS gages, I also used at-a-station hydraulic geometry relations derived from these data to calculate cross-section averaged shear stress and width as a function of discharge (hydraulic geometry depths). I provide graphs comparing the hydraulic geometry measurements, fitted at-a-station power law functions, and modeled results produced from the cross-section geometry and Manning's flow-resistance equation in Appendix 4C. There I also include the R code used to model the depth-discharge relationship at a cross section, create the at-a-station hydraulic geometry relations, and model sediment transport, and calculate the sediment yield metrics.

The fine bed sites included in this portion of the study are the Yampa River at Deerlodge, CO (YR) and Indian Creek near Wyoming, IL (IC) (gage numbers: 09260050 and 05568800, respectively). Considerably less channel geometry data are available for the fine bed sites used in Chapters 2 and 3. For these two sites, I relied on either a

cross-section derived from LiDAR and bathymetry surveys (YR), or hydraulic geometry data collected by the USGS at or near the stream gage as part of their regular field discharge measurements (YR and IC). I used the latter channel geometry data to create at-a-station hydraulic geometry relations for width, cross-sectional area, and average flow depth as a function of discharge. Channel slope was estimated from bed profile LiDAR data (YR) and from the topographic slope along the channel length as measured with a USGS topographic map in Google Earth (IC). I compare empirical models of sediment transport for these two sites with the following total load physical models: Yang's [1979] d50 sand model, and Brownlie's [1981] total load and depth predictor model, both of which model suspended bed material load (sand) (referred to as Brownlie and Yang hereafter). These models are driven by depth-, area- and velocity-discharge relationships derived from cross-sectional geometry and the Manning's flow resistance equation (YR) as well as at-a-station hydraulic geometry relations generated from USGS field measurements (YR and IC).

3 Results and Discussion

3.1 Uncertainty in the Sediment Load Rating Curve

Here I consider how the three different regression methods—ordinary least squares, robust, and Bayesian—compare in their representation of the mean response of sediment yield as well as their representation of confidence and prediction intervals for

coarse and fine sediment loads. At first glance over selected sites they all produce similar results (Figures 4.1 and 4.2, additional plots for three bed load sites are included in Appendix 4A). These sites were chosen to represent examples of regression with data having a small sample size, a large sample size, and heteroscedastic residuals. As discussed in Chapter 2 and Appendix 4A, OLS regression is sensitive to outliers. I have removed some outliers after an initial comparison between OLS and RLM models. These outliers were generally either incorrectly input data or very large or very small sediment loads at very small or very large discharge values and did not follow the general trend of the data. Having removed outliers from the sediment load data, OLS regression generated mean response lines that matched well with RLM and Bayesian lines.

Bayesian mean response lines as well as confidence and prediction bands matched those of OLS fairly closely (Figure 4.2). This is likely due to the similar model structure of the two. OLS regression assumes normally-distributed residuals and this Bayesian model assumes a Student's t-distribution with variable degrees of freedom based on the residual distribution for each site. Robust mean response lines tended to match Bayesian and OLS lines as well. However, the bootstrapped confidence and prediction bands tend to differ depending on the data variance structure. For example, with sparse data and a smaller log-linear correlation, case-resampling to construct a confidence band can lead to wildly varying model fits (mostly due to slope variation), and unrealistically-wide confidence bands. In one case, the variability was so large that the confidence bands crossed outside of the prediction band (Figure 4.2, top right). This is unrealistic and an

artifact of sparse and highly variable data as models fit with greater amounts of data—heteroscedastic or not—do not exhibit this behavior. In another example, case resampling to create a bootstrapped confidence band seems to capture heteroscedasticity in the residuals well resulting in a broader confidence interval on one side (Figure 4.2, bottom middle).

Bootstrapped prediction intervals tend to have the same width as those from the OLS and Bayesian models, though are often slightly out of phase. This may be associated with bootstrap bias—a result of slightly more positive vs. negative residuals, for example—for which I do not account. In all, prediction intervals from the three methods are approximately equal because all methods assume equal variance and sample from either the residuals themselves (bootstrap) or from symmetric distributions fitted to the residuals (OLS and Bayesian). Exploring unequal residual variance models is outside of the scope of this research, though Gaueman et al. [2015] propose such a model for bed load transport data with many zero transport observations.

Moving forward, I would recommend using the robust Bayesian linear regression model because it can account for heavy-tailed residual distributions, unlike OLS, and is not sensitive to outliers. However, it is much more computationally-intensive, taking one to 15 minutes to run on a consumer grade 2011 desktop computer (3.1 GHz dual core processor with 4GB of RAM)—depending on the amount of data being modeled—and is best suited for site-by-site analysis rather than processing scores of datasets as a batch.

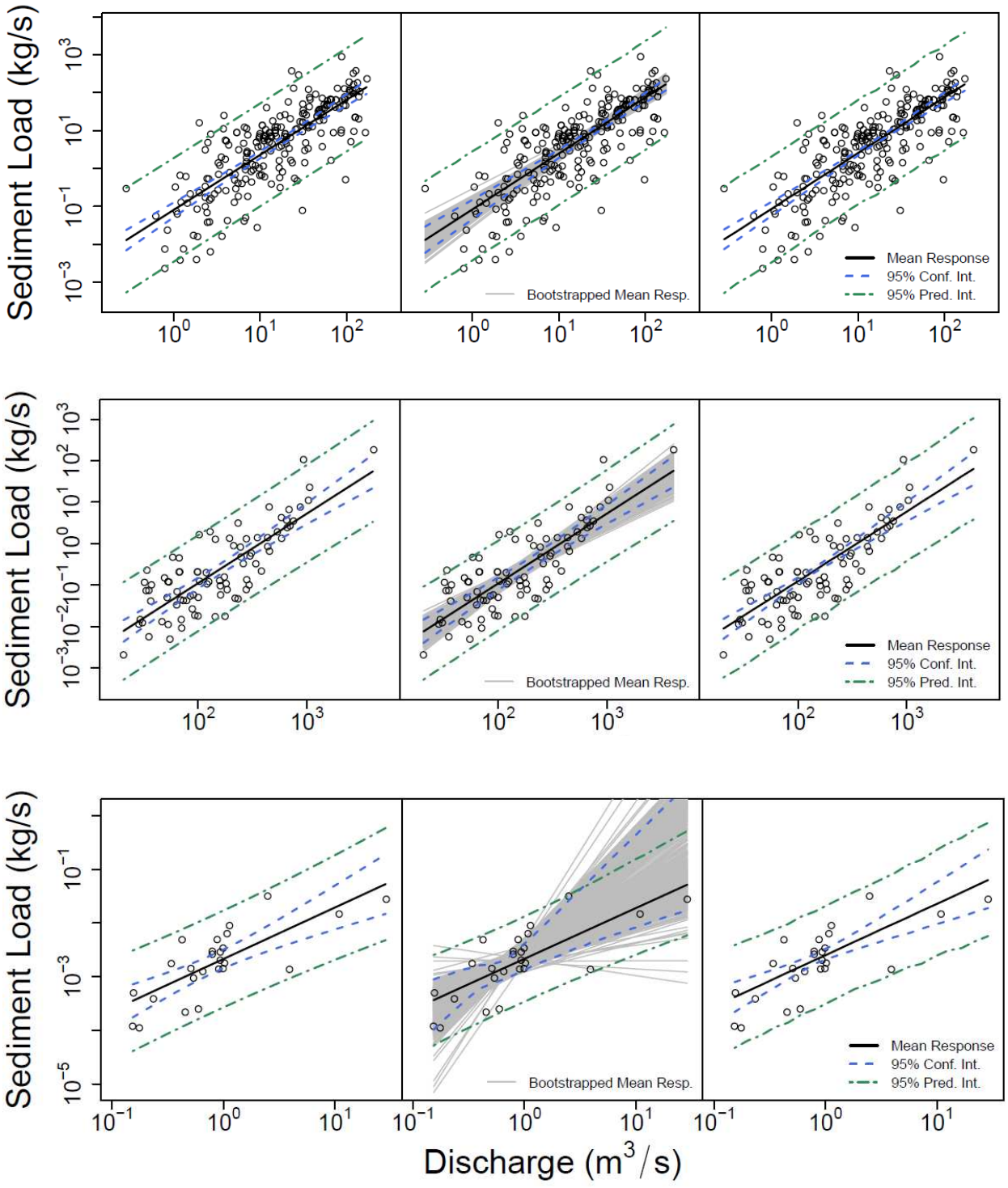

Figure 4.1 Side-by-side comparisons of OLS, RLM, and Bayesian regression models (left to right) for suspended sediment load at the Little Snake River near Lily, CO; the Potomac River at Shepardston, WV; and Bullfrog Creek near Wimauma, FL, respectively (top to bottom). Gray lines in middle column are bootstrapped mean response lines.

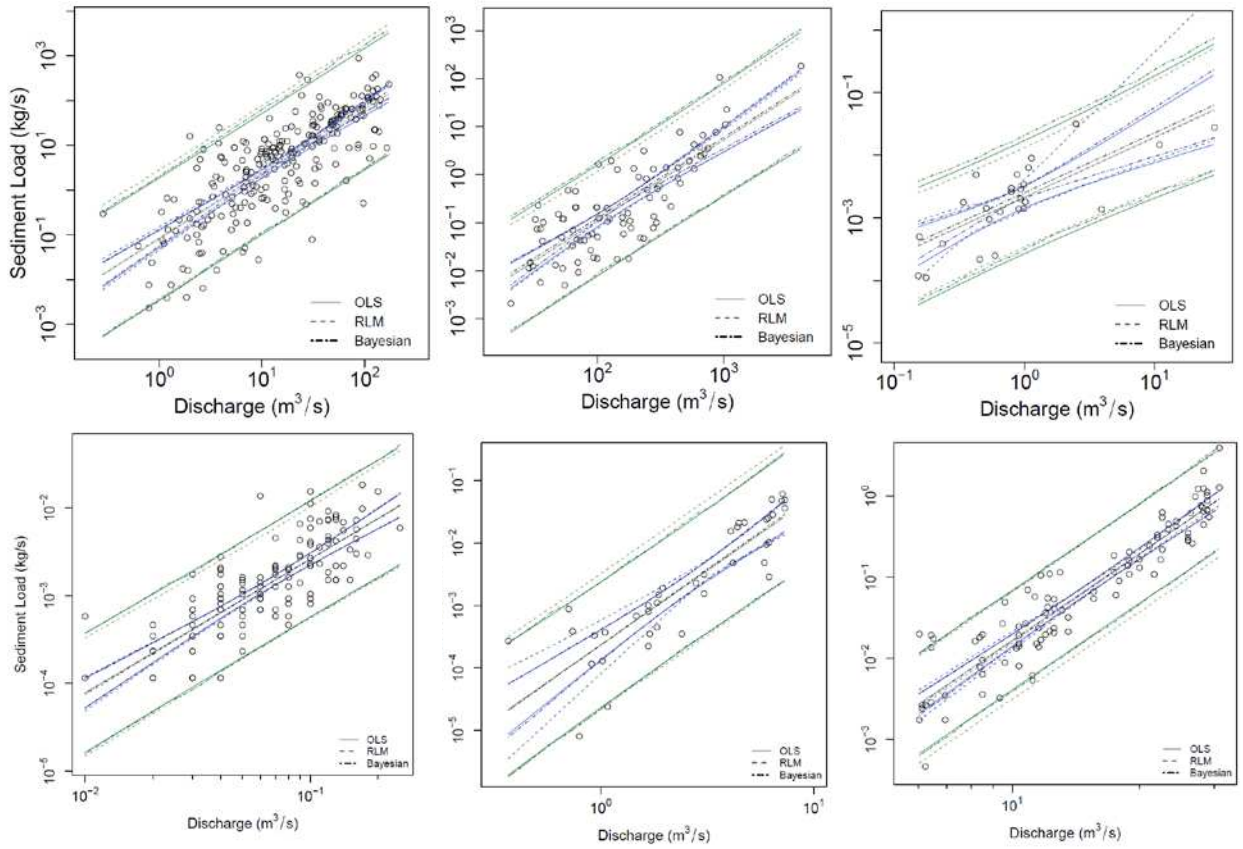

Figure 4.2 Overlapping mean response lines, confidence, and prediction bands using OLS (solid), RLM (dashed), and Bayesian (dot-dashed) models for suspended sediment load at the Little Snake River near Lily, CO; the Potomac River at Shepardston, WV; and Bullfrog Creek near Wimauma, FL (top row) and Eggers Creek, ID; Big Sandstone Creek near Savery, WY; and the Big Wood River near Ketchum, ID (bottom row).

All Bayesian models should be checked individually to ensure that the sampling scheme has converged on a stable posterior distribution for model parameters and predictions.

The bootstrapped method for prediction bands is also computationally intensive as it requires on the order to 50,000+ re-samples to create smooth bands. The bootstrapped confidence band requires much fewer re-samples (on the order 1,000), but can be unstable (producing different results over different bootstraps) and artificially

wide under conditions of sparse, highly variable data. Therefore, to conduct uncertainty analysis on sediment yield metrics across all sites in this study, I use the OLS methods to generate confidence and prediction bands because they perform nominally as well as the Bayesian method in most cases. Also, because they have closed form solutions, they are orders of magnitude faster to calculate.

3.2 Propagating Uncertainty in Sediment Yield Metrics

The majority of emphasis in this section is on method development; however, I also explore what aspects of uncertainty in the data most influence the magnitude of the uncertainty in sediment yield metrics.

3.2.2 Understanding Uncertainty of Sediment Yield Metrics

Here, I demonstrate how one may quantify the statistical uncertainty associated with the sediment load-discharge relationship and the flow frequency distribution, and propagate this to create confidence bands for the sediment yield and the cumulative sediment yield curves (Figure 4.3). Results from this analysis for all sites are given in Tables 4A.1 and 4A.2 in Appendix 4A. Here I use a parametric technique to estimate confidence bands for the sediment rating curve (OLS regression) and a non-parametric kernel density function to estimate the confidence bands for the flow frequency distribution.

One could also use a parametric technique for the flow frequency distribution uncertainty analysis and create a purely parametric confidence band for the sediment

yield curve. This would involve fitting a parametric PDF to the flow frequency distribution using the method of maximum likelihood, which generates confidence intervals for the parameters of a particular distribution. Confidence intervals for the regression coefficients of the sediment rating curve are also produced and depend on the linear model type such as OLS and RLM. In the case of the parametric sediment yield curve, the uncertain parameters are the sediment rating curve coefficients, α and β, and the parameters of the fitted PDF. In the case of the lognormal PDF, this would be μ_y and σ_y, or the mean and standard deviation of the logs of flow. Assuming normal

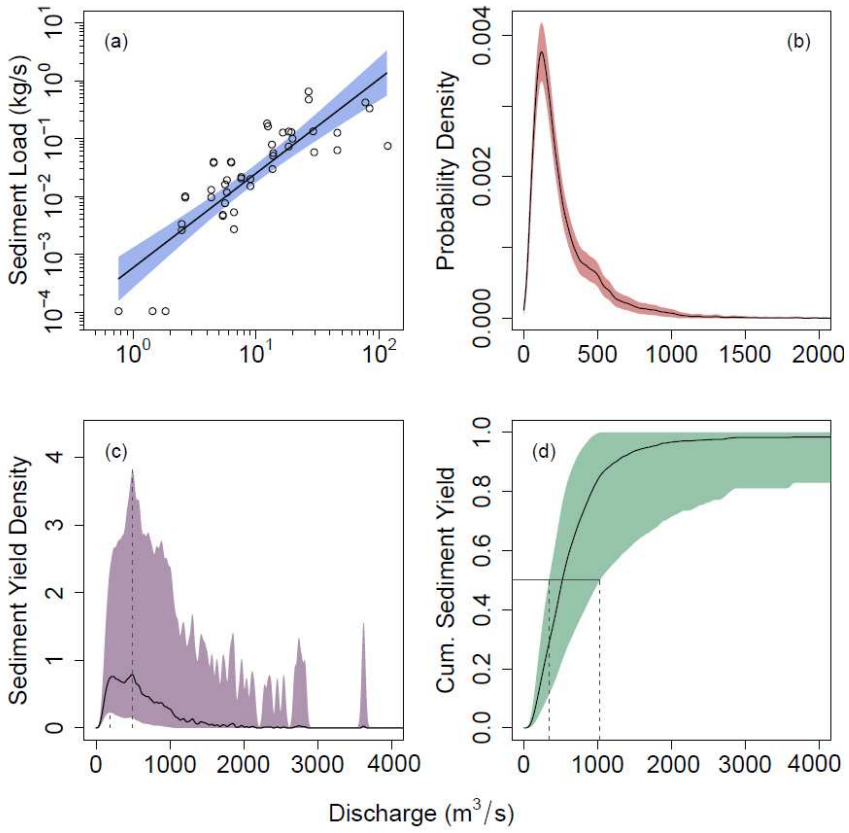

Figure 4.3 Example of combining uncertainty in sediment rating curve in the form of confidence bands (a), with uncertainty in flow PDF in the form of a confidence band for the kernel density function (b), to generate uncertainty bands for sediment yield curves (c), as well as cumulative sediment yield curves (d). Plots are based on sediment load and flow record data from the Dee Pee River at Pee Dee, SC.

distributions for all parameters and using the confidence intervals to define the distributions of each parameter, one can then use a Monte Carlo sampling scheme to generate a large sample of sediment yield and cumulative sediment yield curves.

A brief discussion on the use of prediction vs. confidence bands in calculating uncertainty intervals for sediment yield metrics is merited here. From both a frequentist and Bayesian perspective, prediction bands or intervals are the bounds within which future observations (a point rather than a mean) have a $(1 - \alpha)*100\%$ probability of falling. In a regression setting, this is a function of the variance of the residuals as well as the value of the covariates, in this case discharge. Whereas confidence intervals or bands bound the mean response as opposed to some future observation. In calculating Q_{eff}, one is simply interested in the mean frequency (or probability density) of sediment yield over time as well as the peak of that mean yield frequency. Therefore, using confidence bounds in the sediment yield curve as well as intervals for Q_{eff} is reasonable. However, in estimating the uncertainty of Q_{s50}, which is based cumulative sediment yield from individual observations, one could argue that using the prediction interval from the sediment rating curve is more appropriate.

If one were to only incorporate uncertainty from the sediment rating curve and not the flow frequency distribution, I recommend using the prediction bands of the sediment rating curve to create a prediction interval for Q_{s50} based on the sorted, cumulative sediment yield record. If incorporating statistical uncertainty from the sediment rating curve as well as the flow frequency distribution, then I recommend

using the confidence bands from the sediment rating curve as well as the flow frequency distribution. For the remainder of this section, I chose the confidence interval to calculate the relative width of uncertainty intervals for these metrics because they are based on long-term average sediment yields.

3.2.2 Propagating Uncertainty in Sediment Yield Metrics

I now turn to the results from propagating uncertainty in sediment yield metric estimates. As can be seen in Figure 4.3c, the above-reference method for propagating uncertainty into sediment yield metrics does not result in much variability in the estimate of Q_{eff}—the prediction interval appears as a single line in the figure. The confidence and prediction intervals for the effective discharge values were generally very narrow in absolute terms because the position of the peak of the sediment yield curve is influenced largely by the slope (in log space) of the sediment rating curve (β value). Upper and lower confidence and prediction bands for the sediment rating curve are essentially parallel (though curvilinear) to the mean response regression line. In addition, the confidence bands for the kernel density function are vertically symmetric. This means that while great uncertainty exists within the absolute value of sediment yield as well as the probability density of a particular discharge, very little uncertainty exists in the location (discharge value) of the peak of the sediment yield curve.

To further investigate the sensitivity of the relative width of the uncertainty interval for Q_{eff} to the variability in the sediment load data about the mean response

line, I explore an additional method to propagate uncertainty in sediment yield metrics: I bootstrap the sediment yield and cumulative sediment yield curves (Figure 4.5). This creates a bootstrapped sample of Q_{eff} and Q_{s50} values for which I calculate a confidence interval based on quantiles of the samples. Because these confidence bands are calculated from a bootstrap sample, they must be directly compared to the median estimate of the bootstrapped sediment yield and cumulative sediment yield curves and not the original, mean response estimate of these curves, the former are depicted as black lines in Figure 4.5. Confidence bands for Q_{eff} and Q_{s50} tend to be wider than those calculated using the first approach discussed. This is because uncertainty in the slope of the sediment rating curve is propagated through the bootstrap re-sampling methodology. The site-specific results presented in Tables 4A.1 and 4A.2 in Appendix

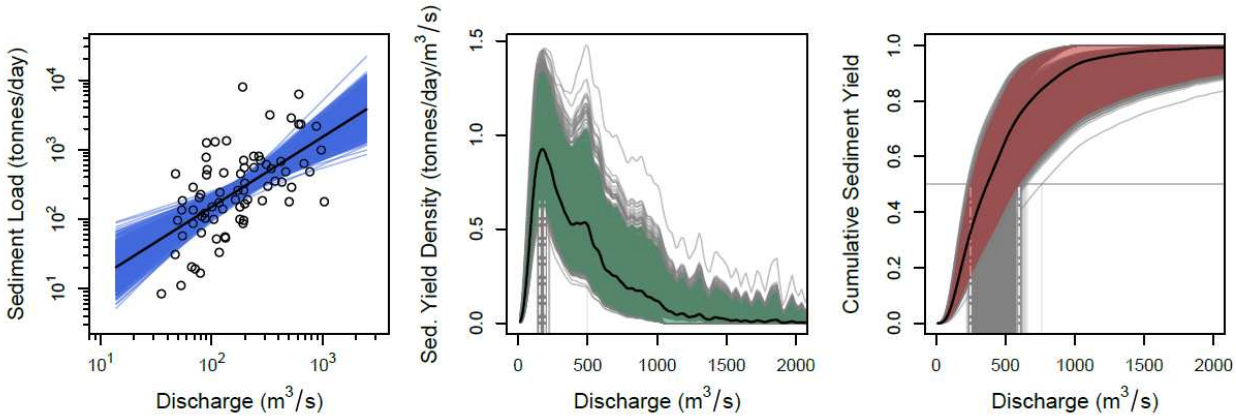

Figure 4.5 Uncertainty propagated using bootstrapped samples of the sediment rating curves (left) to generate bootstrap samples of the sediment yield curve (middle) and cumulative sediment yield curve (right) using sediment load and flow record data from the Dee Pee River at Pee Dee, SC. Upper and lower 95% confidence intervals for Q_{eff} and Q_{s50} are displayed based on the bootstrap sample of these values (vertical white dashed lines). Pointwise confidence bands for the curves themselves (shaded green and red areas) are also plotted.

4A, are from this latter uncertainty analysis.

Much greater absolute uncertainty is found in the estimation of Q_{s50} over Q_{eff} (Figure 4.3 and 4.5). However, when comparing the relative width of uncertainty for Q_{s50}, the "uncertainty spread" or $(Q_{s50.upp} - Q_{s50.low}) \ / \ Q_{s50}$, the uncertainty in Q_{s50} actually compares well with that of Q_{eff} for coarse bed sites and is overall much lower than that of Q_{eff} in fine bed sites under both uncertainty propagation methods (Figure 4.6). Results from the bootstrap method (Figure 4.6, right) produces median Q_{eff} uncertainty spread values of approximately one for coarse sites and just above one for fine bed sites. This means that the width of the uncertainty interval has approximately the same value as the value of the metric itself. However, the distribution of uncertainty spread values for Q_{eff} at fine bed sites is positively skewed with an upper interquartile range extending approximately six. Median values of uncertainty spread for Q_{s50} range

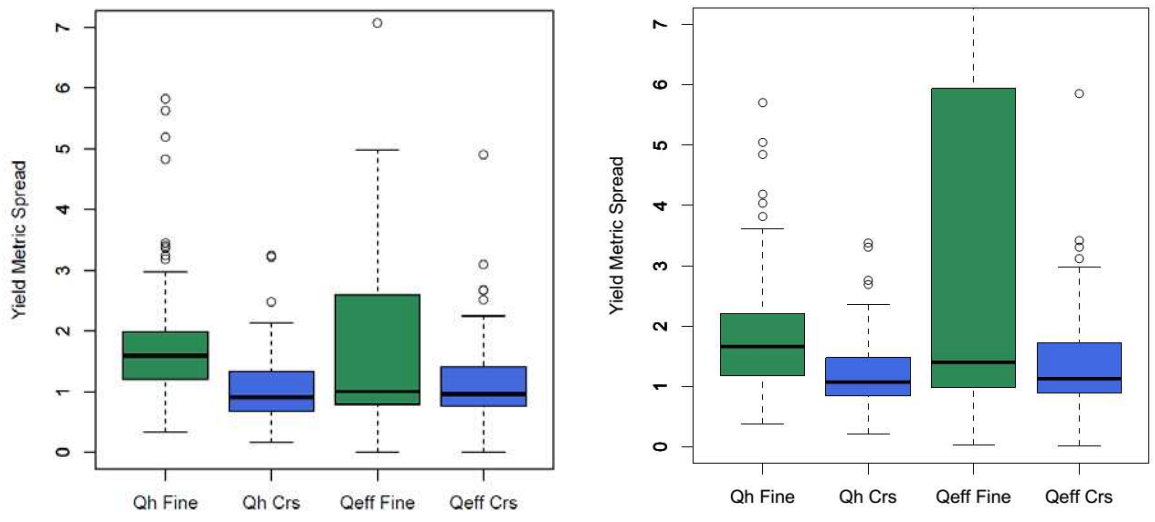

Figure 4.6 Boxplots of the calculated values of the spread or normalized difference between upper and lower uncertainty intervals for sediment yields metrics using OLS methods (left), and bootstrap methods (right). The upper whisker for bootstrapped Q_{eff} uncertainty spread at fine bed sites is approximately 13.

from just above one for coarse bed sites to about 1.5 for fine bed sites.

In Chapter 3, I found that both Q_{eff} and Q_{s50} approximated Q_{bf} well in coarse bed streams whereas Q_{s50} performed well in fine bed stream. This uncertainty analysis demonstrates that channel designs based on these metrics will have 95% confidence intervals that span approximately ± 50% to 75% of the estimated value in coarse bed streams and ± 75% to 100% in fine bed streams assuming a flow gage record and sediment load data are available.

3.2.3 Sensitivity of Sediment Yield Metric Uncertainty to Data Uncertainty

Here I examine the how the uncertainty spread for Q_{eff} and Q_{s50} is influenced by aspects of the flow and sediment load data that may lend themselves to increased uncertainty. Variability in the sediment load-discharge relationship, represented by the standard error of the residuals, as well as the strength of the correlation, represented by the R^2 value, influence the width of the confidence and prediction bands about the regression line. However, they do not largely influence the slope of this line, resulting in little influence on the spread of uncertainty in Q_{eff} and Q_{s50}. I also considered relationships between the variance term for the KDF (equation 4.1), the flow record length, the value of β, the number of sediment load measurements, n_{sed}, and the coefficient of variation of the flow regime, C_v.

With the exception of n_{sed}, C_v, and β, no clear relationships are observed between the uncertainty spread values and these metrics of hydrologic and sediment load

variability (Figure 4.7). A general increase in the uncertainty spread of Q_{s50} with C_v is observed for both site types, though the increase appears to flatten out for $C_v > 3$. For large values of n_{sed}, found mostly in the fine bed data set, Q_{s50} uncertainty spread decreases. Finally, the variability in the estimates of Q_{s50} uncertainty spread decrease with increasing β for coarse bed sites. This relationship was also found for the uncertainty spread of Q_{eff}, however, no other strong relationships were observed for this particular metric.

As discussed in Chapter 1, and below in the flow non-stationary analysis section, flow variability tends to be very influential on the value of Q_{eff} and Q_{s50}. Increases in flow variability, or C_v, result in increases in the absolute value of these metrics as well as the spread in sediment yield about them. Therefore, it is not surprising that an increasing relationship between C_v and Q_{s50} spread is evident. As the number of sediment load measurements increases, the width of the prediction and confidence bands for the regression line tends to decrease, unless the additional data add variability to the relationship. This may explain the reduction in Q_{s50} spread for the fine bed sites for which more measurements (> 200) where available. Finally, as the value of β increases, the variability and value of the uncertainty spread for of Q_{s50} and Q_{eff} decrease. This is similar to the relationship between the spread in sediment yield and β discussed in Chapter 2. It may be that because larger values of β lead to large estimates of Q_{s50} and Q_{eff}, the uncertainty about these larger values is narrower in a relative sense.

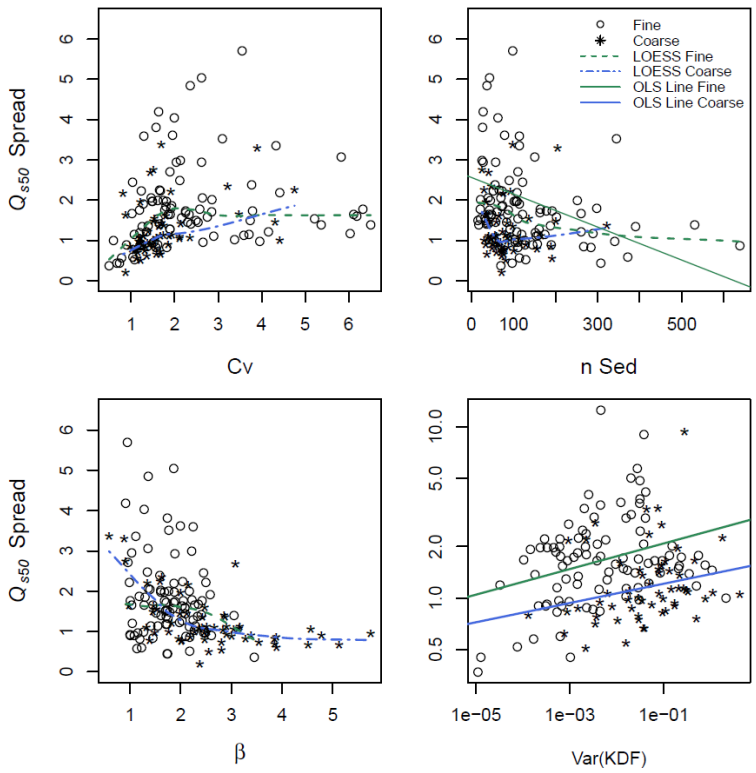

Figure 4.7 Relationships between the uncertainty spread in Q_{s50} and the flow coefficient of variation, C_v, the number of sediment load measurements, n_{sed}, the value of the sediment rating curve exponent, β, and the maximum value of the variance of the kernel density function of flows, Var(KDF). LOESS smoothing lines as well as log-linear OLS lines are included to show trends where appropriate.

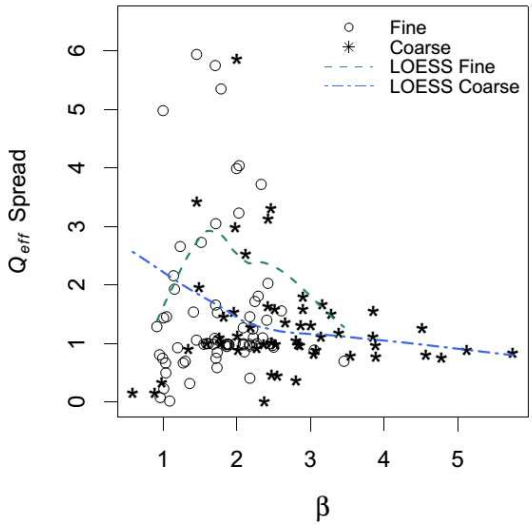

Figure 4.8 Relationship between the uncertainty spread in Q_{eff} as a function of the sediment rating curve exponent, β for coarse and fine bed sites.

3.3 Non-stationary Flow Record

To illustrate how a non-stationary flow record might influence sediment yield metric values, I compare sediment yield and cumulative sediment yield curves calculated from sequential, decadal flow records from a streams whose watersheds have urbanized over time and from those whose watersheds remained rural. I begin with Mercer Creek near Bellevue, WA, whose decadal flow duration curves (FDCs) demonstrate that both low ($< 10\%$) and high ($>90\%$) exceedance flows increased with time (Figure 4.9, top) as population density in the watershed increased nearly 600% from approximately 250 people/km^2 to 1,500 people/km^2 from 1960 to 2010 [*Rosburg*, 2015]. Temporal plots of the mean and variance of decadal discharge records demonstrate that while there is no trend in mean discharge, the variance increases significantly with time (0.07/decade, $p = 0.04$) (Figure 4.9, bottom). This follows the common trend of streams becoming flashier with urbanization [*Walsh et al.*, 2005].

Sediment yield and cumulative sediment yield curves calculated for each decade over a range of hypothetical β values demonstrate that for low values of β (≤ 2) the increase in flow variability does not have a large impact on Q_{eff} or Q_{s50}. However, as β increases beyond a value of 2, the influence of larger variance values increases dramatically resulting in much larger values of Q_{eff} and Q_{s50} (Figures 4.10). In general, as flow variability increases, the values of Q_{eff} and Q_{s50} also increase for larger values of β (Figure 4.11, top two plots of upper figure). As discussed in Chapter 2, the value of β

increases with increasing bed coarseness [*Emmett and Wolman*, 2001] as well as bed armor ratio [*Barry et al.*, 2004].

The population density in the watershed of Newakum Creek near Black Diamond, WA has not changed significantly from the 1950s when flows were first gaged on this creek, holding steady around 50 people/km^2 up through 2010 [*Rosburg*, 2015]. Decadal FDCs show some deviance around the period of record FDC; however, no secular trends are evident (Figure 4.11, top). Though variability exists, no significant trend in decadal mean flow or variance are evident either (Figure 4.11, bottom). This results in values of Q_{eff} and Q_{s50} that largely cluster around the values calculated from the period of record with the exception of the 1990s. Two exceptionally large, regional flood events during this decade result in a large discharge variance value, which influence the values of Q_{eff} and Q_{s50} calculated for this decade for values of $\beta > 2$ (Figure 4.12). Additional urban and rural examples demonstrating the relationships discussed herein are provided in Appendix 4B.

As urbanization progresses, and flow variability increases, these metrics increase from values smaller than the period of record value to values larger than the period record values (grey curves in Figures 4.10 and 4.12). This means that sediment yield metrics calculated from entire period of flow records in urbanizing watersheds may be underestimates, because period of record flow variability will likely be less than contemporary flow variability. Channel response to changes in flow variability or flashiness may occur over the course of years to decades [*Booth*, 1990; *Trimble*, 1997].

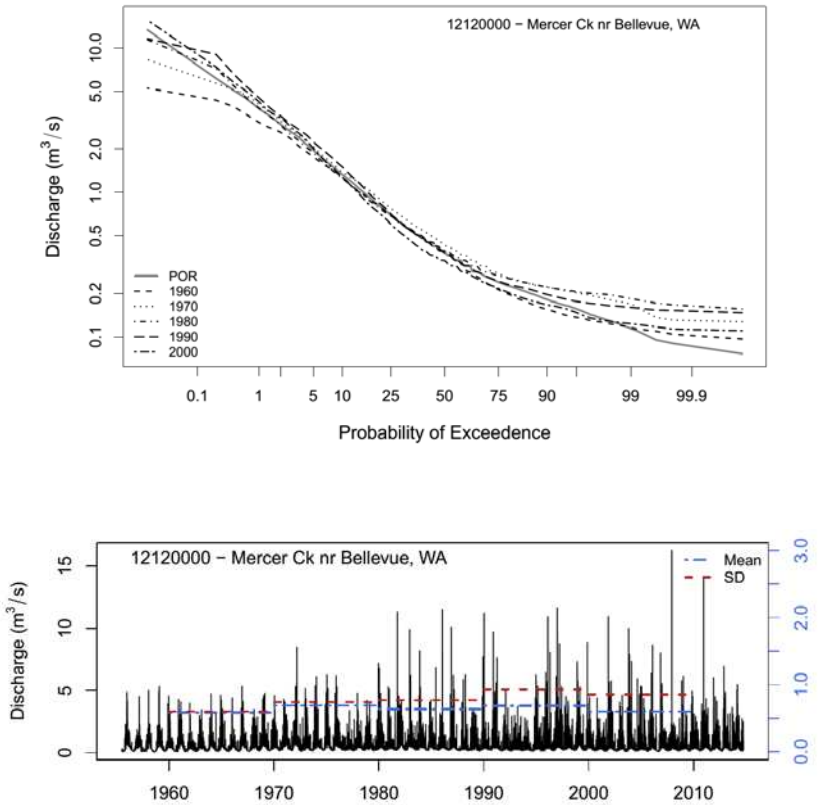

Figure 4.9 Flow duration curves by period of record and by decade for Mercer Creek near Bellevue, WA, an urban watershed (top), and daily flow record (left axis) plotted with decadal mean and standard deviation values (right axis) (bottom). Note that the mean and standard deviation are referenced to the right, vertical axis.

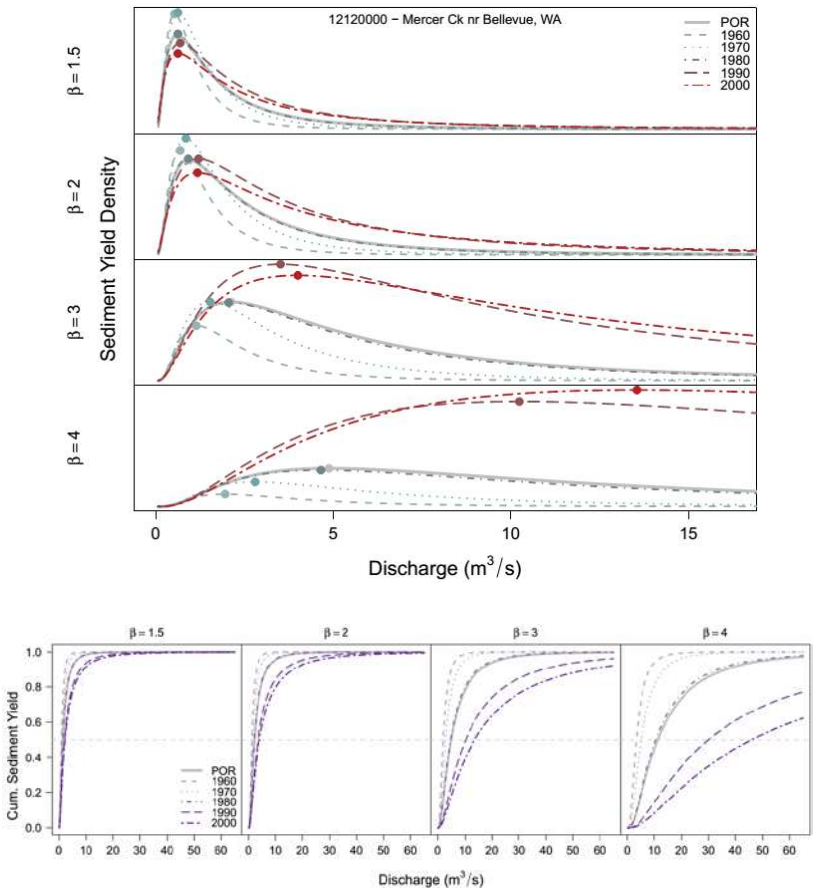

Figure 4.10 Sediment yield (effectiveness) curves for period of record as well as decade for a range of hypothetical β values for Mercer Creek near Bellevue, WA, an urban watershed (top). Cumulative sediment yield curves for period of record and by decade for various hypothetical values of β (bottom).

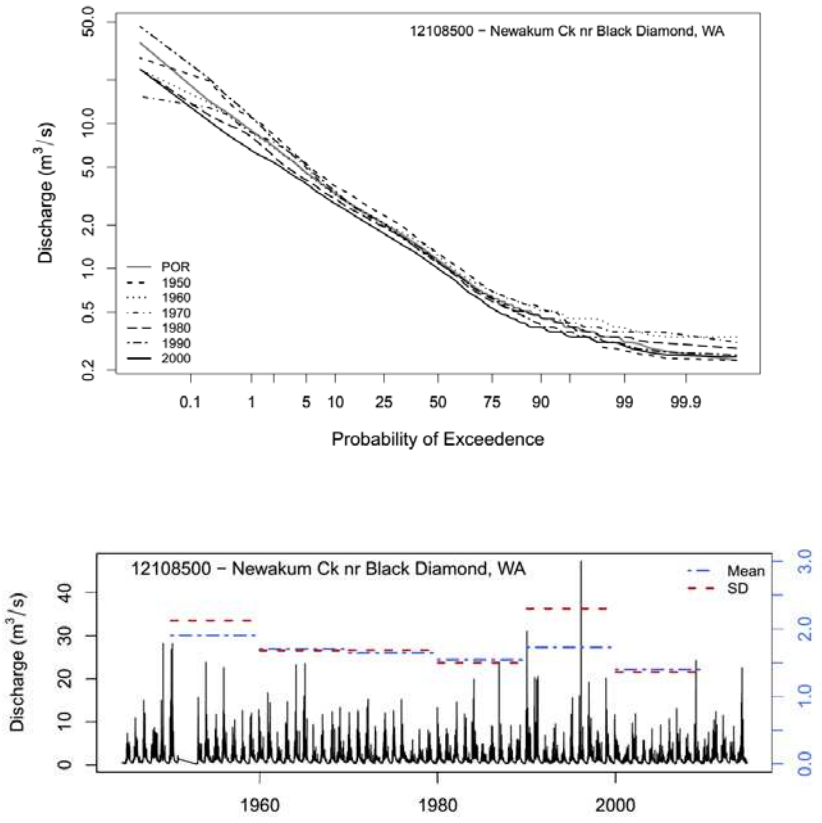

Figure 4.11 Flow duration curves by period of record and by decade for Newakum Creek near Black Diamond, WA, a rural watershed (top), and daily flow record (left axis) plotted with decadal mean and standard deviation values (right axis) (bottom). Note that the mean and standard deviation are referenced to the right, vertical axis.

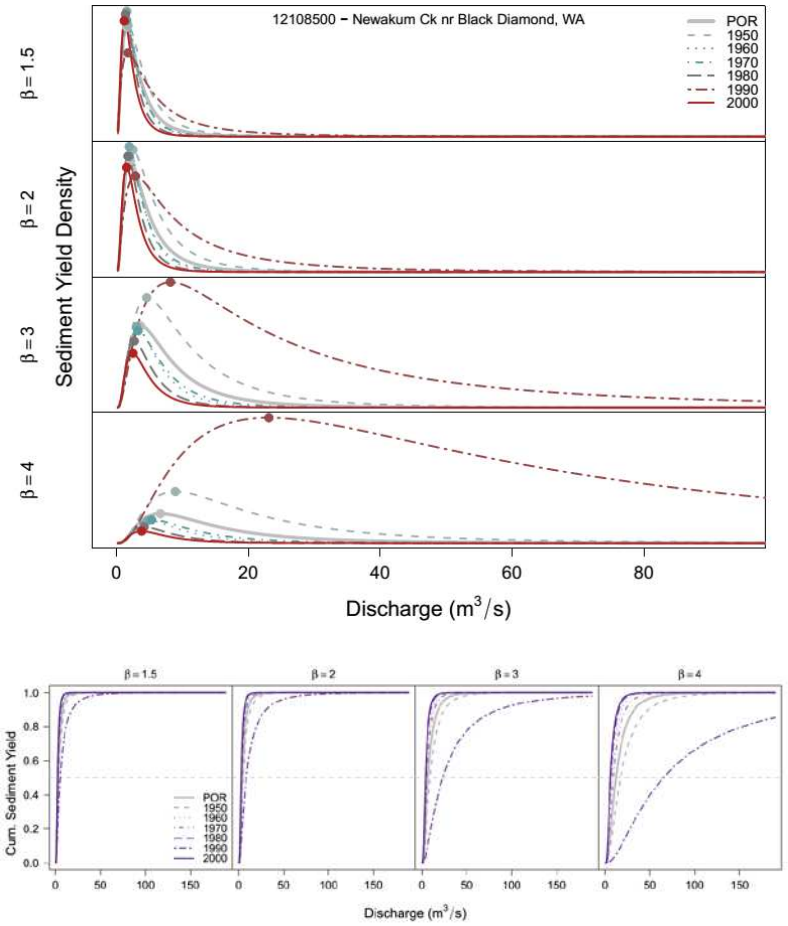

Figure 4.12 Sediment yield (effectiveness) curves for period of record as well as decade for a range of hypothetical β values for Newakum Creek near Black Diamond, WA, a rural watershed (top). Cumulative sediment yield curves for period of record and by decade for various hypothetical values of β (bottom).

Though a channel may be actively adjusting to hydro-modification due to urbanization, contemporary geomorphology will likely reflect contemporary hydrology. These trends in sediment yield metrics are also apparent for other urbanizing watersheds analyzed. Similar figures for additional urban and rural sites are included in Appendix 4B.

3.3 Modeled vs. Measured Sediment Yield

3.3.1 Coarse Bed Sites

Though sediment yield metrics are insensitive to absolute values of predicted sediment yield, quite a range of values result when comparing empirical and physical models to calculate Q_{eff} and Q_{s50} (Figure 4.13, Table 4.2). The peak of the various sediment yield curves tend to match well for Trapper Creek (TC) and South Fork Salmon River (SR); however, in some cases an additional peak at smaller discharges associated with sand transport dominates over the central peak associated with gravel transport. In some models, including the empirical model for TC, this results in a very low predicted value of Q_{eff}. This "sand peak" becomes the most effective for sediment transport-discharge (Q_s–Q) relationships that have a milder slope in logarithmic space. The Parker equation becomes very steep in log space as the value of the dimensionless shear stress, τ^*, approaches the critical dimensionless shear stress τ_c^*, at smaller discharge values. This means that it under-estimates sand bed load transport for TC. Indeed, it was derived for coarse gravel ($>$ 16 mm) bed load transport [*Parker*, 1979], suggesting it is not appropriate for TC, which is a steep, armored channel whose

bedload is dominated by sand and fine gravel transport over cobbles [*Whiting et al.*, 1999; *King et al.*, 2004].

The Barry model emulates a power law equation whose coefficient is a function drainage area and whose exponent is a function of the ratio of critical shear stress for the surface and subsurface median sediment size: essentially a bed armoring ratio [*Barry et al.*, 2004], and was calibrated using sediment load data that included these two coarse bed sites. The Q_s–Q relationship it predicts matches that of the empirical model fairly well and tends to produce sediment yield metric estimates closest to those estimated from the empirical model.

To accommodate the transport of sand at smaller discharges evident in the TC sediment load data, I also implement the Wilcock and Kenworthy [2002] two-fraction bed load model (WK), which accounts for the sand-gravel interaction. The WK model over-estimates sediment load at both sites. However, it does capture the general slope of the Q_s–Q relationship resulting in the same peak location in the sediment yield curve as predicted with the empirical model for TC (Figure 4.13, top middle graph).

The slope of the Q_s–Q relationship from the sediment load data for SR is steeper than that of TC, indicating more gravel transport. This results in a peak in the empirical sediment yield curves which occurs in the middle of the range of flows. The Q_s–Q relationship predicted by the WK model for SR is too mild relative to the empirical relationship resulting in a sediment yield curve peak that occurs at a much smaller discharge value relative to the position of the peaks predicted by the empirical

and other physical models (Figure 4.13, bottom row). Again, the Barry model best predicts the location of Q_{eff}.

All physical models perform relatively poorly in predicting Q_{s50} (Figure 4.13, right column). Differences in the slope of the Q_s–Q relationship between the empirical and physical models results in cumulative error in predicting relative sediment yield as a function of the sorted flow regime. For TC, the Parker and Barry curves under-predicts the rate of cumulative sediment transport for low flows resulting in large predicted values of Q_{s50}. The WK curve over-predicts cumulative transport of sand at low flows resulting in an underestimation of Q_{s50}. For SR, all physical models have milder Q_s–Q slopes resulting in them over-predicting the rate of cumulative sediment transport at low discharges and underestimating Q_{s50}.

Some influence of the different methods for representing the one-dimensional stage-discharge relationship used to drive the physical models can be seen in the Q_s–Q relationship for both sites; however, this influence does not translate to influencing estimates of Q_{eff}. The cross section-averaged and discrete width relationships also do not produce meaningful differences in the estimate of Q_{s50} with the Parker model. The at-a-station hydraulic geometry relation perform better than both cross section methods in the case of TC and poorer in the case of SR. This could be due to how well the cross section geometry and slope—single, one-dimensional estimates of channel geometry—reflect the three dimensional hydraulics at these sites.

Table 4.2 Sediment yield metric values calculated from various transport equations.

Site	Metric	RLM	Parker Avg.	Parker Disc.	Parker HG	Barry	WK	Brownlie	Brownlie HG	Yang	Yang HG
Trapper Ck.	Q_{s50}	0.97	1.63	1.56	1.47	1.44	0.54				
	Q_{eff}	0.09	1.68	1.68	1.52	1.52	0.09				
	τ_c*		0.030	0.030	0.042	0.030					
S.F. Salmon	Q_{s50}	90.3	67.4	65.4	53.8	75.0	49.3				
	Q_{eff}	90.1	50.8	50.8	50.8	81.9	4.3				
	τ_c*		0.030	0.030	0.030	0.030					
Yampa	Q_{s50}	291						274	261	254	245
	Q_{eff}	278						228	11.6	11.6	11.6
Indian Ck.	Q_{s50}	6.8							11.3		8.9
	Q_{eff}	1.55							1.98		1.98

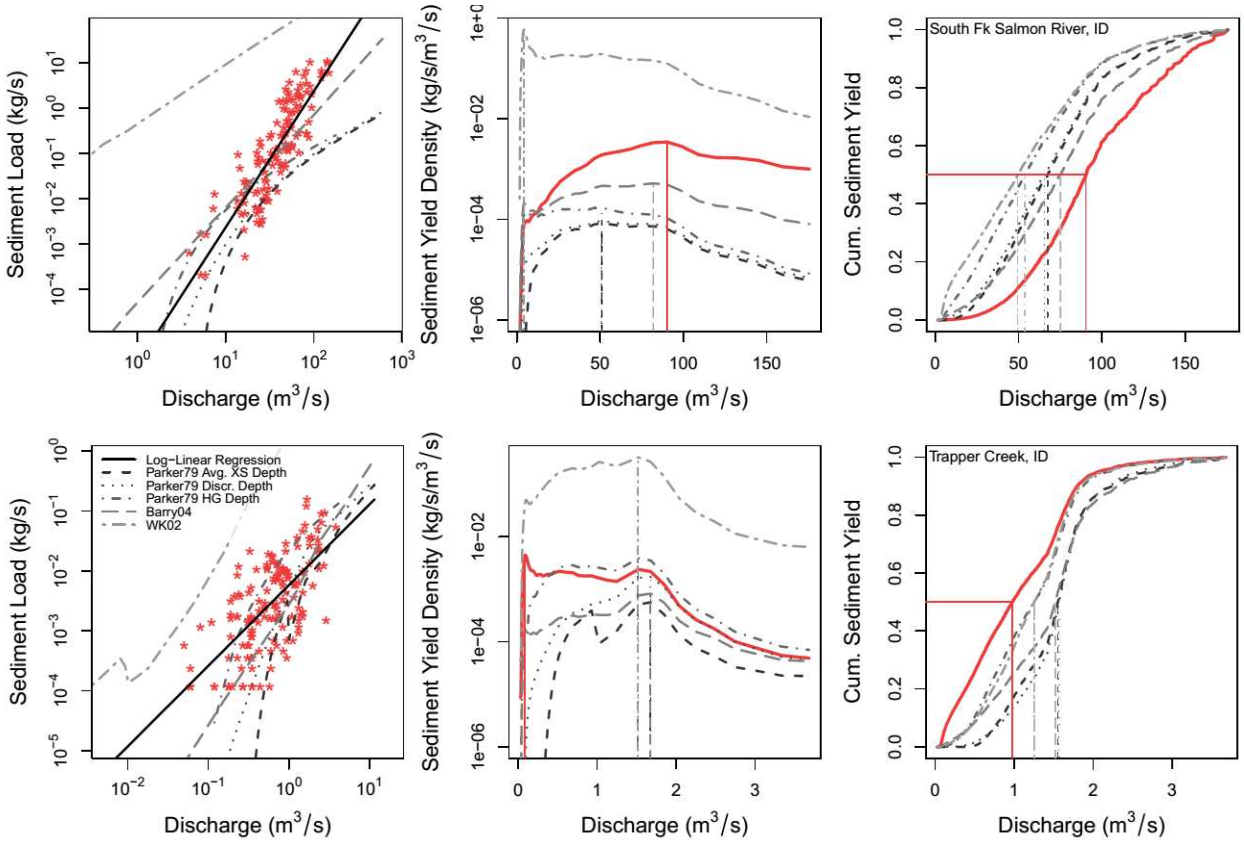

Figure 4.13 Comparison of sediment yield estimates and metric values calculated from empirical relations (log-linear regression), as well as calibrated sediment transport relations for bed load transport using various representations of the stage-discharge relationship for Trapper Creek (top) and the S.F. of the Salmon River (bottom).

3.3.2 Fine Bed Sites

Total sediment load physical models for fine bed streams estimate sediment yield metrics better than bed load physical models do in coarse bed sites (Figure 4.14, Table 4.2). For these sites, I used the Brownlie and Yang total load models as well as at-a-station hydraulic geometry and a cross section-averaged flow-resistance (Manning's) model for the relationship between flow, depth, area, and velocity.

Though these physical models tend to over-estimate absolute sediment load at YR, the slopes of both the Brownlie and Yang predicted Q_s–Q relationships match those of the empirical models well at both sites. This results in the sediment yield curve peaks produced from the physical models lining up well with those from the empirical model for both sites. However, at YR a peak for very fine material results in very low values of Q_{eff} for all but the Brownlie–Manning and empirical models. Judging from the shape of the sediment yield curves for YR as well as the location of Q_{eff} from the empirical

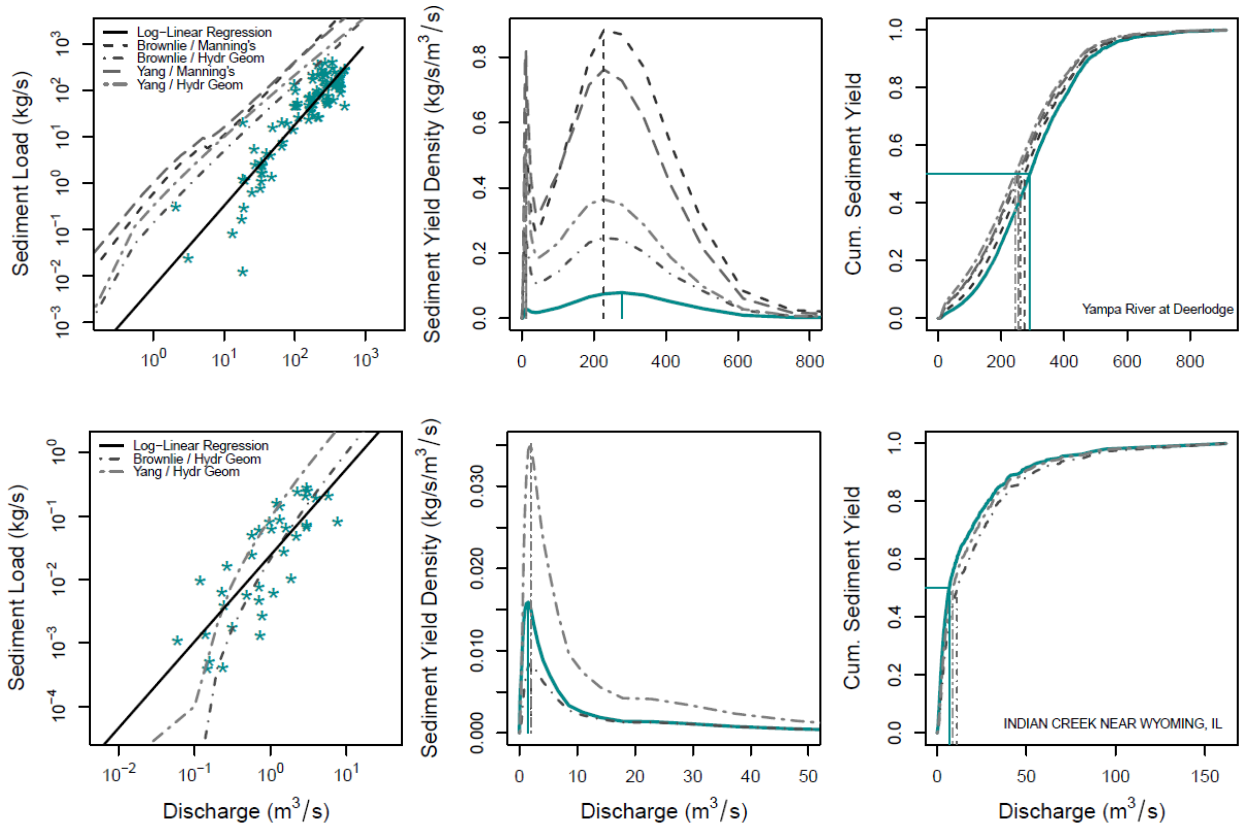

Figure 4.14. Comparison of sediment yield estimates and metric values calculated from empirical relations (log-linear regression), as well as calibrated sediment transport relations for total bed material load (sand) transport using various representations of the stage-discharge relationship for the Yampa River (top) and Indian Creek (bottom).

model, this small value of Q_{eff} is likely not the most effective discharge. Rather, the central peaks appear to be more effective and these line up well among all models. The sediment yield curves for IC are all unimodal and match well at relatively small discharge values.

All models and depth-discharge representations predict values of Q_{s50} relatively close to the empirical value for both sites. Because the physical models over-predict sediment load compared to the empirical model for YR, especially for smaller flows, they also over-predict the rate of cumulative sediment transport for small flows resulting in slight under-predictions Q_{s50}. The physical models for IC fit the data better, though slightly under-predict Q_s for lower discharges resulting in slightly greater predicted values of Q_{s50}. The hydraulic geometry relations result in Q_s–Q relationships that are slightly closer to the empirical relationship for YR. A cross section survey was not available for IC, therefore only hydraulic geometry relations are used to drive the physical models.

On whole, using physical bed load and total load models to calculate sediment yield metrics produces similar results to empirical models for Q_{eff} for both coarse and fine bed sites, respectively. This finding parallels that of Barry et al. [2008], who studied this in coarse bed streams. However, in cases of multimodal sediment yield curves, one must use their judgment in choosing a particular peak to represent Q_{eff}. This is especially true in modeled bed load scenarios where peaks for sand and fine gravel as well as coarse gravel may exist depending on the flow regime. The value of Q_{s50} is much

more sensitive to model error for both types of sites due to cumulative error. Given the wide range of results produced from bed load equations, estimates of Q_{s50} in coarse bed streams are likely to have large error in general. Because this portion of the study was not comprehensive and only includes two of each types of sites and physical models, I cannot make quantitative estimates of error or uncertainty associated with modeling bed material load in calculating these sediment yield metrics. I recommend calculating Q_{s50} using multiple models and using the median or average value from these results in coarse bed sites. These results indicate that estimating Q_{s50} in fine bed streams using physical models produces much more accurate results. This is a welcomed finding because Q_{s50} performs most well in predicting bankfull discharge (Chapter 3).

4 Conclusion

In this chapter, I examine the sensitivity of sediment yield metrics to uncertainty from the perspectives of statistical uncertainty, environmental variability and non-stationarity, as well as sediment transport model error. By exploring the nature of uncertainty in sediment yield metrics from multiple new perspectives, I provide tools and guidance for calculating and utilizing sediment yield metrics for river design and management.

Using established statistical uncertainty methods for log-linear regression and kernel density function models I develop confidence and prediction bands for sediment

yield and cumulative sediment yield curves as well as confidence and prediction intervals for the most effective discharge, Q_{eff}, and the half yield discharge, Q_{s50} (Figures 4.3 and 4.5). I find that the relative width of the confidence interval for Q_{s50}—the uncertainty spread—decreases as the number of sediment load observations, the value of the sediment rating curve exponent, and the kernel density function maximum variance value all increase (Figure 4.6). Half yield discharge uncertainty spread increases with flow record coefficient of variation. This uncertainty analysis demonstrates that coarse bed channel designs based on Q_{eff} or Q_{s50} will have 95% confidence intervals that span approximately ± 50% to 75% of the estimated value and ± 75% to 100% of estimated Q_{s50} in fine bed streams assuming a flow gage record and sediment load data are available.

In urbanizing watersheds, with increasing trends in flow variance, decadal estimates of Q_{eff} and Q_{s50} increase dramatically relative to estimates based on the entire period of flow record (Figures 4.9 to 4.12). Therefore, using an entire flow period of record to calculate sediment yield metrics in an urbanizing watershed will likely underestimate their value. This means that channels design to match Q_{eff} or Q_{s50} calculated from an entire flow period of record will likely be undersized in this setting.

Physically-based models must be used to estimate values of sediment yield metrics where no sediment load data are available. Physical models that match the slope of the sediment load-discharge relationship in log-space—the rate of increase of sediment transport with discharge in arithmetic space—performed reasonably well. This

was the case with total load models for fine bed sites, but generally not true for bed load models for coarse bed sites. As found previously for bed load sites, the value of Q_{eff} is not sensitive to modeled results, except in cases where the sediment yield curve is multimodal. The value of Q_{s50} was more sensitive to model error than Q_{eff} because error accumulates over the calculated sediment yield record used to estimate this metric. Modeled total load in fine bed sites produced fairly accurate estimates of Q_{s50}, but modeled bed load in coarse bed sites did not.

The preceding three chapters develop relationships between the physical drivers of sediment yield in rivers and sediment yield metrics that integrate aspects of the magnitude and frequency of sediment yield relationship. In Chapter 3, I also evaluate how well some of these metrics perform as estimates of the dominant discharge by their ability to predict bankfull discharge. To date, little work has been done to quantify the uncertainty associated with Q_{eff} and no work for Q_{s50}. Additionally, no previous work explicitly creates confidence intervals for these metrics. In the present chapter, I quantify uncertainty in these metrics from multiple aspects, including explicit calculation of confidence intervals for Q_{eff} and Q_{s50}. I also quantify the range of relative uncertainty interval widths across a large number of sites in coarse and fine bed rivers. Others have used Q_{eff} to examine how changes in flow regime and sediment properties might influence channel form over time [e.g., *Tilleard*, 1999; *Dodov and Foufoula-Georgiou*, 2005]. With the methods and findings presented in this chapter, managers

and channel designers may now also quantify the uncertainty associated with designs or predicted changes based on these sediment yield metrics.

REFERENCES

Ackers, P. (1993), Stage-Discharge Functions for Two-Stage Channels: The Impact of New Research, *Water Environ. J.*, *7*(1), 52–59.

Andrews, E. D. (1980), Effective and bankfull discharges of streams in the Yampa River basin, Colorado and Wyoming, *J. Hydrol.*, *46*(3-4), 311–330.

Andrews, E. D. (1984), Bed-material entrainment and hydraulic geometry of gravel-bed rivers in Colorado, *Geol. Soc. Am. Bull.*, *95*(3), 371–378.

Andrews, E. D. (1994), Marginal bed load transport in a gravel bed stream, Sagehen Creek, California, *Water Resour. Res.*, *30*(7), 2241–2250.

Andrews, E. D. (2000), Bed material transport in the Virgin River, Utah, *Water Resour. Res.*, *36*(2), 585–596.

Andrews, E. D., and J. M. Nankervis (1995), Effective Discharge and the Design of Channel Maintenance Flows for Gravel-Bed Rivers, in *Natural and Anthropogenic Influences in Fluvial Geomorphology*, vol. 89, edited by J. E. Costa, A. J. Miller, K. W. Potter, and P. R. Wilcock, pp. 151–164, American Geophysical Union, Washington, D. C.

Ashmore, P. E., and T. J. Day (1988), Effective discharge for suspended sediment transport in streams of the Saskatchewan River Basin, *Water Resour. Res.*, *24*(6), 864–870.

Baker, D. B., R. P. Richards, T. T. Loftus, and J. W. Kramer (2004), A new flashiness index: characteristics and applications to Midwestern rivers and streams, *J. Am. Water Resour. Assoc.*, *40*(2), 503–522.

Barabási, A.-L. (2005), The origin of bursts and heavy tails in human dynamics., *Nature*, *435*(7039), 207–11.

Barnett, T. P. et al. (2008), Human-induced changes in the hydrology of the western United States., *Science*, *319*(5866), 1080–3.

Barry, J. J., J. M. Buffington, and J. G. King (2004), A general power equation for predicting bed load transport rates in gravel bed rivers, *Water Resour. Res.*, *40*(10).

Barry, J. J., J. M. Buffington, P. Goodwin, J. G. King, and W. W. Emmett (2008), Performance of Bed-Load Transport Equations Relative to Geomorphic Significance: Predicting Effective Discharge and Its Transport Rate, *J. Hydraul. Eng.*, *134*(5), 601–615.

Benson, M. A., and D. M. Thomas (1966), A definition of dominant discharge, *Int. Assoc. Sci. Hydrol. Bull.*, *11*(2), 76–80.

Beven, K., and J. Freer (2001), Equifinality, data assimilation, and uncertainty estimation in mechanistic modelling of complex environmental systems using the GLUE methodology, *J. Hydrol.*, *249*(1-4), 11–29.

Biedenharn, D. S., and C. R. Thorne (1994), Magnitude-frequency analysis of sediment transport in the lower Mississippi river, *Regul. Rivers Res. Manag.*, *9*(4), 237–251.

Biedenharn, D. S., R. R. Copeland, C. R. Thorne, P. J. Soar, and R. D. Hey (2000), *Effective Discharge Calculation : A Practical Guide*, Vicksburg, MS.

Bledsoe, B. P., S. K. Carney, and R. J. Anderson (2011), Scale-Dependent Effects of Bank Vegetation on Channel Processes: Field Data, Computational Fluid Dynamics Modeling, and Restoration Design, in *Stream Restoration in Dynamic Fluvial Systems*, edited by A. Simon, S. J. Bennett, and J. M. Castro, American Geophysical Union, Washington, D. C.

Booth, D. B. (1990), Stream-channel incision following drainage-basin urbanization, *J. Am. Water Resour. Assoc.*, *26*(3), 407–417.

Brown, C. B. (1950), Sediment transportation, in *Engineering Hydraulics*, edited by H. Rouse, pp. 769–857, Wiley & Sons, Inc., New York.

Brownlie, W. R. (1981), *Prediction of flow depth and sediment discharge in open channels*, W. M. Keck Laboratory of Hydraulics and Water Resources Div. of Engr. and Applied Sci., California Institute of Technology, Pasadena, CA.

Buffington, J. M., and D. R. Montgomery (1997), A systematic analysis of eight decades of incipient motion studies, with special reference to gravel-bedded rivers, *Water Resour. Res.*, *33*(8), 1993–2029.

Bunte, K., and S. R. Abt (2009), *Transport relationships between bedload traps and a 3-inch Helley-Smith sampler in coarse gravel-bed streams and development of adjustment functions*, Vicksburg, MS.

Bunte, K., S. R. Abt, J. P. Potyondy, and S. E. Ryan (2004), Measurement of Coarse Gravel and Cobble Transport Using Portable Bedload Traps, *J. Hydraul. Eng.*, *130*(9), 879–893.

Bunte, K., S. R. Abt, K. W. Swingle, and D. A. Cenderelli (2014), Effective discharge in Rocky Mountain headwater streams, *J. Hydrol.*, *519*, 2136–2147.

Carling, P. (1988), The concept of dominant discharge applied to two gravel-bed streams in relation to channel stability thresholds, *Earth Surf. Process. Landforms*, *13*(4), 355–367.

Carling, P. A. (1983), Threshold of coarse sediment transport in broad and narrow natural streams, *Earth Surf. Process. Landforms*, *8*(1), 1–18.

Castellarin, A., R. M. Vogel, and A. Brath (2004), A stochastic index flow model of flow duration curves, *Water Resour. Res.*, *40*(3), n/a–n/a.

Castro, J. M., and P. L. Jackson (2001), Bankfull discharge recurrence intervals and regional hydraulic geometry relationships: patterns in the Pacific Northwest, USA, *J. Am. Water Resour. Assoc.*, *37*(5), 1249–1262.

Cayan, D. R., M. D. Dettinger, S. A. Kammerdiener, J. M. Caprio, and D. H. Peterson (2001), Changes in the Onset of Spring in the Western United States, *Bull. Am. Meteorol. Soc.*, *82*(3), 399–415.

Chow, V. T. (1964), *Handbook of Applied Hydrology: A Compendium of Water-resources Technology*, McGraw-Hill Company.

Christensen, N. S., and D. P. Lettenmaier (2007), A multimodel ensemble approach to assessment of climate change impacts on the hydrology and water resources of the Colorado River Basin, *Hydrol. Earth Syst. Sci.*, *11*(4), 1417–1434.

Clarke, R. (1999), Uncertainty in the estimation of mean annual flood due to rating-curve indefinition, *J. Hydrol.*, *222*(1-4), 185–190.

Cohn, T. A., L. L. Delong, E. J. Gilroy, R. M. Hirsch, and D. K. Wells (1989), Estimating constituent loads, *Water Resour. Res.*, *25*(5), 937–942.

Cohn, T. A., D. L. Caulder, E. J. Gilroy, L. D. Zynjuk, and R. M. Summers (1992), The validity of a simple statistical model for estimating fluvial constituent loads: An Empirical study involving nutrient loads entering Chesapeake Bay, *Water Resour. Res.*, *28*(9), 2353–2363.

Copeland, R. R., P. J. Soar, and C. R. Thorne (2005), Channel-Forming Discharge and Hydraulic Geometry Width Predictors in Meandering Sand-Bed Rivers (ASCE), *EWRI Conf. Impacts Glob. Clim. Chang.*

Crowder, D. W., and H. V. Knapp (2005), Effective discharge recurrence intervals of Illinois streams, *Geomorphology*, *64*(3-4), 167–184.

Dade, W. B., and P. F. Friend (1998), Grain-Size, Sediment-Transport Regime, and Channel Slope in Alluvial Rivers, *J. Geol.*, *106*(6), 661–676.

Darby, S. E., and C. R. Thorne (1996), Predicting Stage-Discharge Curves in Channels with Bank Vegetation, *J. Hydraul. Eng.*, *122*(10), 583–586.

Dietrich, W. E., J. W. Kirchner, H. Ikeda, and F. Iseya (1989), Sediment supply and the development of the coarse surface layer in gravel-bedded rivers, *Nature*, *340*(6230), 215–217.

Dodov, B., and E. Foufoula-Georgiou (2005), Fluvial processes and streamflow variability: Interplay in the scale-frequency continuum and implications for scaling, *Water Resour. Res.*, *41*(5), n/a–n/a.

Doll, B. A., D. E. Wise-Frederick, C. M. Buckner, S. D. Wilkerson, W. A. Harman, R. E. Smith, and J. Spooner (2002), Hydraulic geometry relationships for urban streams throughout the piedmont of North Carolina, *J. Am. Water Resour. Assoc.*, *38*(3), 641–651.

Doyle, M. W., D. Shields, K. F. Boyd, P. B. Skidmore, and D. Dominick (2007), Channel-Forming Discharge Selection in River Restoration Design, *J. Hydraul. Eng.*, *133*(7), 831–837.

Easterling, D. R., J. L. Evans, P. Y. Groisman, T. R. Karl, K. E. Kunkel, and P. Ambenje (2000), Observed Variability and Trends in Extreme Climate Events: A Brief Review, *Bull. Am. Meteorol. Soc.*, *81*(3), 417–425.

Emmett, W. W. (1980), *A field calibration of the sediment-trapping characteristics of the Helley-Smith bed-load sampler*, USGS Professional Paper 1139. 44p.

Emmett, W. W., and M. G. Wolman (2001), Effective discharge and gravel-bed rivers, *Earth Surf. Process. Landforms*, *26*(13), 1369–1380.

Erwin, S. O., J. C. Schmidt, and N. C. Nelson (2011), Downstream effects of impounding a natural lake: the Snake River downstream from Jackson Lake Dam, Wyoming, USA, *Earth Surf. Process. Landforms*, *36*(11), 1421–1434.

Ferguson, R. I. (1986), River Loads Underestimated by Rating Curves, *Water Resour. Res.*, *22*(1), 74–76.

Foster, K. (2012), *Bankfull-channel geometry and discharge curves for the Rocky Mountains Hydrologic Region in Wyoming*. U.S. Geological Survey Scientific Investigations Report 2012–5178. 20p.

Gaeuman, D., C. R. Holt, and K. Bunte (2015), Maximum likelihood parameter estimation for fitting bedload rating curves, *Water Resour. Res.*, *51*(1), 281–301.

Gilbert, G. K. (1914), *The Transportation of Débris by Running Water*, USGS Professional Paper 86. 263p.

Goodwin, P. (2004), Analytical Solutions for Estimating Effective Discharge, *J. Hydraul. Eng.*, *130*(8), 729–738.

Graf, W. L. (1983), Flood-related channel change in an arid-region river, *Earth Surf. Process. Landforms*, *8*(2), 125–139.

Grams, P. E., and J. C. Schmidt (2005), Equilibrium or indeterminate? Where sediment budgets fail: Sediment mass balance and adjustment of channel form, Green River downstream from Flaming Gorge Dam, Utah and Colorado, *Geomorphology*, *71*(1-2), 156–181.

Grams, P. E., D. J. Topping, J. C. Schmidt, J. E. Hazel, and M. Kaplinski (2013), Linking morphodynamic response with sediment mass balance on the Colorado River in Marble Canyon: Issues of scale, geomorphic setting, and sampling design, *J. Geophys. Res. Earth Surf.*, *118*(2), 361–381.

Grimm, J., and W. Grimm (1884), *Grimm's Household Tales*, edited by M. Hunt, George Bell and Sons, London.

Hall, P., and J. Horowitz (2013), A simple bootstrap method for constructing nonparametric confidence bands for functions, *Ann. Stat.*, *41*(4), 1892–1921.

Härdle, W. (1991), *Smoothing Techniques With Implementation in S*, Springer S., Springer, New York.

Hassan, M. A., D. Brayshaw, Y. Alila, and E. Andrews (2014), Effective discharge in small formerly glaciated mountain streams of British Columbia: Limitations and implications, *Water Resour. Res.*, *50*(5), 4440–4458.

Hey, R. D. (1996), *Channel response and channel forming discharge*, Vicksburg, MS. U.S. Army Corps of Engineers, E.R.D.C. Report 6871-EN-01. 112p.

Hey, R. D., and C. R. Thorne (1986), Stable Channels with Mobile Gravel Beds, *J. Hydraul. Eng.*, *112*(8), 671–689.

Holmquist-Johnson, C. L. (2002), Computational methods for determining effective discharge in the Yazoo River Basin, Mississippi. MS Thesis, Colorado State University, Fort Collins, CO.

Huber, P. J., and E. M. Ronchetti (2009), *Robust Statistics*, 2nd ed., Wiley & Sons, Inc., Hoboken, NJ.

Inglis, C. C. (1949), *The behavior and control of rivers and canals, Part II*, Central Waterpower Irrigation and Navigation Research Station, Poona, India. 485p.

Jackson, W. L., and R. L. Beschta (1982), A model of two-phase bedload transport in an oregon coast range stream, *Earth Surf. Process. Landforms*, *7*(6), 517–527.

Jennings, M. E., W. O. T. Jr., and H. C. Riggs (1994), Nationwide summary of US Geological Survey regional regression equations for estimating magnitude and frequency of floods for ungaged sites, 1993, Water-Resources Investig. Rep. 94-4002.

Jones, M. L., and H. R. Seitz (1980), Sediment transport in the Snake and Clearwater rivers in the vicinity of Lewiston, Idaho. U.S. Geological Survey Open File Rep. 80-690.

Julien, P. Y. (2010), *Erosion and Sedimentation*, Cambridge University Press.

Kesseli, J. E. (1941), The Concept of the Graded River, *J. Geol.*, *49*(6), 561–588.

King, J. G., W. W. Emmett, P. J. Whiting, R. P. Kenworthy, and J. J. Barry (2004), *Sediment Transport Data and Related Information for Selected Coarse-Bed Streams and Rivers in Idaho*, U.S.D.A., Forest Service, Rocky Mountain Research Station, Boise, ID.

Kirby, W. (1969), On the Random Occurrence of Major Floods, *Water Resour. Res.*, *5*(4), 778–784.

Klonsky, L., and R. M. Vogel (2011), Effective Measures of "Effective" Discharge, *J. Geol.*, *119*(1), 1–14.

Knight, D. W., and J. D. Demetriou (1983), Flood Plain and Main Channel Flow Interaction, *J. Hydraul. Eng.*, *109*(8), 1073–1092.

Knighton, D. (1998), *Fluvial Forms and Processes: A New Perspective*, 2nd ed., Arnold.

Kondolf, G. M. et al. (2006), Process-based ecological river restoration: Visualizing three-dimensional connectivity and dynamic vectors to recover lost linkages, *Ecol. Soc.*, *11*(2), 1–16.

Konrad, C. P., D. B. Booth, and S. J. Burges (2005), Effects of urban development in the Puget Lowland, Washington, on interannual streamflow patterns: Consequences for channel form and streambed disturbance, *Water Resour. Res.*, *41*(7), n/a–n/a.

Landers, M. N., and T. W. Sturm (2013), Hysteresis in suspended sediment to turbidity relations due to changing particle size distributions, *Water Resour. Res.*, *49*(9), 5487–5500.

Lane, E. W. (1954), *The importance of fluvial morphology in hydraulic engineering*, US Department of the Interior, Bureau of Reclamation, Commissioner's Office.

Leopold, L., and T. Maddock (1953), *The Hydraulic Geometry of Stream Channels and Some Physiographic Implications*. USGS Professional Paper 252.

Limbrunner, J. F., R. M. Vogel, and L. C. Brown (2000), Estimation of Harmonic Mean of a Lognormal Variable, *J. Hydrol. Eng.*, *5*(1), 59–66.

Mackin, J. H. (1948a), Concept of the graded river, *Geol. Soc. Am. Bull.*, *59*(5), 463.

Mackin, J. H. (1948b), The concept of a graded river, *Geol. Soc. Am. Bull.*, *59*(5), 463.

Meyer-Peter, E., and R. Müller (1948), Formulas for bed-load transport, in *Proc., 2nd Meeting, IAHR*, pp. 39–64, Stockholm, Sweden.

Michels-Boyce, S. (2014), A comparison between rating curves generated from total bed material and suspended bed material loads, Dept. of Civil and Env. Engr., Colorado State University, Fort Collins, CO.

Millar, R. G. (2005), Theoretical regime equations for mobile gravel-bed rivers with stable banks, *Geomorphology*, *64*(3-4), 207–220.

Milly, P. C. D., J. Betancourt, M. Falkenmark, R. M. Hirsch, Z. W. Kundzewicz, D. P. Lettenmaier, and R. J. Stouffer (2008), Climate change. Stationarity is dead: whither water management?, *Science*, *319*(5863), 573–4.

Montgomery, D. R., and J. M. Buffington (1997), Channel-reach morphology in mountain drainage basins, *Geol. Soc. Am. Bull.*, *109*(5), 596–611.

Moog, D. B., and P. J. Whiting (1998), Annual hysteresis in bed load rating curves, *Water Resour. Res.*, *34*(9), 2393–2399.

Moog, D. B., P. J. Whiting, and R. B. Thomas (1999), Streamflow record extension using power transformations and application to sediment transport, *Water Resour. Res.*, *35*(1), 243–254.

Moyeed, R. A., and R. T. Clarke (2005), The use of Bayesian methods for fitting rating curves, with case studies, *Adv. Water Resour.*, *28*(8), 807–818.

Nash, D. B. (1994), Effective Sediment-Transporting Discharge from Magnitude-Frequency Analysis, *J. Geol.*, *102*(1), 79–95.

Nolan, K. M., T. M. Lisle, and H. M. Kelsey (1987), Bankfull discharge and sediment transport in northwestern California, in *Erosion and Sedimentation in the Pacific Rim*, edited by R. L. Beschta, pp. 439–450, IAHS Publications, Wallingford, Oxfordshire, UK.

Orndorff, R. L., and P. J. Whiting (1999), Computing effective discharge with S-PLUS, *Comput. Geosci.*, *25*(5), 559–565.

Ott, R. L., and M. Longnecker (2001), *An introduction to statistical methods and data analysis*, 5th ed., Duxbury, Pacific Grove, CA.

Pappenberger, F., and K. J. Beven (2006), Ignorance is bliss: Or seven reasons not to use uncertainty analysis, *Water Resour. Res.*, *42*(5).

Parker, G. (1979), Hydraulic Geometry of Active Gravel Rivers, *J. Hydraul. Div. ASCE*, *105*(9), 1185–1201.

Pickup, G., and R. F. Warner (1976), Effects of hydrologic regime on magnitude and frequency of dominant discharge, *J. Hydrol.*, *29*(1-2), 51–75.

Pizzuto, J. E. (1994), Channel adjustments to changing discharges, Powder River, Montana, *Geol. Soc. Am. Bull.*, *106*(11), 1494–1501.

Plummer, M., N. Best, K. Cowles, and K. Vines (2006), CODA: Convergence Diagnosis and Output Analysis for MCMC, *R News*, *6*(1), 7–11.

Poff, N. L. (1996), A hydrogeography of unregulated streams in the United States and an examination of scale-dependence in some hydrological descriptors, *Freshw. Biol.*, *36*(1), 71–79.

Quader, A., and Y. Guo (2009), Relative Importance of Hydrological and Sediment-Transport Characteristics Affecting Effective Discharge of Small Urban Streams in Southern Ontario, *J. Hydrol. Eng.*, *14*(7), 698–710.

R Core Team (2014), *R: A Language and Environment for Statistical Computing*. R Foundation for Statistical Computing. Vienna, Austria.

Rajagopalan, B., K. Nowak, J. Prairie, M. Hoerling, B. Harding, J. Barsugli, A. Ray, and B. Udall (2009), Water supply risk on the Colorado River: Can management mitigate?, *Water Resour. Res.*, *45*(8).

Rankl, J. G., and M. L. Smalley (1992), *Transport of sediment by streams in the Sierra Madre, Southern Wyoming*, Cheyenne, WY. U.S.G.S. WRIR 92-4091.

Ray, A., J. Barsugli, and K. Averyt (2008), *Climate Change in Colorado: A Synthesis to Support Water Resources Management and Adaptation*, Report for the Colorado Water Conservation Boar, Western Water Assessment, Boulder, CO.

Reitan, T., and A. Petersen-Øverleir (2007), Bayesian power-law regression with a location parameter, with applications for construction of discharge rating curves, *Stoch. Environ. Res. Risk Assess.*, *22*(3), 351–365.

Rosgen, D. L. (1997), A Geomorphological Approach to Restoration of Incised Rivers, in *Proceedings of the Conference on Management of Landscapes Disturbed by Channel Incision*, edited by S. S. Y. Wang, E. J. Langendoen, and F. D. J. Shields, pp. 1–11.

Rosgen, D. L. (2001), A hierarchical river stability/watershed-based sediment assessment methodology, in *Proc. of the Seventh Federal Interagency Sedimentation Conference*, pp. 91–106, Reno, NV.

Runkle, R. L., C. G. Crawford, and T. A. Cohn (2004), Load Estimator (LOADEST): A FORTRAN Program for Estimating Constituent Loads in Streams and Rivers, in *U.S.G.S. Techniques and Methods Book 4*, p. 69, U.S.G.S., Reston, VA.

Rustomji, P., and S. N. Wilkinson (2008), Applying bootstrap resampling to quantify uncertainty in fluvial suspended sediment loads estimated using rating curves, *Water Resour. Res.*, *44*(9).

Salas, J. (1993), Analysis and Modeling of Hydrologic Time Series, in *The Handbook of Hydrology*, edited by D. R. Maidment, p. 72, McGraw-Hill Company, United States.

Schmelter, M. L., S. O. Erwin, and P. R. Wilcock (2012), Accounting for uncertainty in cumulative sediment transport using Bayesian statistics, *Geomorphology*, *175*, 1–13.

Schumm, S. A., and R. W. Lichty (1965), Time, space, and causality in geomorphology, *Am. J. Sci.*, *263*(2), 110–119.

Segura, C., and J. Pitlick (2010), Scaling frequency of channel-forming flows in snowmelt-dominated streams, *Water Resour. Res.*, *46*(6).

Shields, F. D, J., R. R. Copeland, P. C. Klingeman, M. W. Doyle, and A. Simon (2003), Design for Stream Restoration, *J. Hydraul. Eng.*, *129*(8), 575–584.

Shiono, K., J. S. Al-Romaih, and D. W. Knight (1999), Stage-Discharge Assessment in Compound Meandering Channels, *J. Hydraul. Eng.*, *125*(1), 66–77.

Sholtes, J., K. Werbylo, and B. Bledsoe (2014), Physical context for theoretical approaches to sediment transport magnitude-frequency analysis in alluvial channels, *Water Resour. Res.*.

Sichingabula, H. M. (1999), Magnitude-frequency characteristics of effective discharge for suspended sediment transport, Fraser River, British Columbia, Canada, *Hydrol. Process.*, *13*(9), 1361–1380.

Simon, A., W. Dickerson, and A. Heins (2004), Suspended-sediment transport rates at the 1.5-year recurrence interval for ecoregions of the United States: transport conditions at the bankfull and effective discharge?, *Geomorphology*, *58*(1), 243–262.

Simon, A., M. Doyle, M. Kondolf, F. D. Shields, B. Rhoads, and M. McPhillips (2007), Critical Evaluation of How the Rosgen Classification and Associated "Natural Channel Design" Methods Fail to Integrate and Quantify Fluvial Processes and Channel Response, *J. Am. Water Resour. Assoc.*, *43*(5), 1117–1131.

Simon, A., S. J. Bennett, and J. M. Castro (Eds.) (2011), *Stream Restoration in Dynamic Fluvial Systems*, Geophysical Monograph Series, American Geophysical Union, Washington, D. C.

Smalley, M. L., W. W. Emmett, and A. M. Wacker (1994), Annual replenishment of bed material by sediment transport in the Wind River near Riverton, Wyoming. USGS Water Resources Inv. Rep. 94-4007.

Soar, P. J., and C. R. Thorne (2001), *Channel Design for Meandering Rivers*, US Army Corps of Engineers, ERDC, CHL, Vicksburg, MS.

Soar, P. J., and C. R. Thorne (2011), Design Discharge for River Restoration, in *Stream Restoration in Dynamic Fluvial Systems*, edited by A. Simon, S. J. Bennett, and J. M. Castro, American Geophysical Union, Washington, D. C.

Soar, P. J., C. C. Watson, and C. R. Thome (2005), Channel-Forming Flow : Representations and Variability, in *EWRI Conference: Impacts of Global Climate Change*, vol. 44, pp. 1–12.

Syvitski, J. P., M. D. Morehead, D. B. Bahr, and T. Mulder (2000), Estimating fluvial sediment transport: The rating parameters, *Water Resour. Res.*, *36*(9), 2747–2760.

Thomas, R. B. (1985), Estimating Total Suspended Sediment Yield With Probability Sampling, *Water Resour. Res.*, *21*(9), 1381–1388.

Tilleard, J. (1999), Effective discharge as an aid to river rehabilitation, in *Proc. of the 2nd Australian Stream Management Conf.*, pp. 629–635.

Topping, D. J., S. A. Wright, T. S. Melis, and D. M. Rubin (2007), High-resolution measurements of suspended sediment concentration and grain size in the Colorado River in Grand Canyon using a multi-frequency acoustic system, in *Proceedings of The Tenth International Symposium on River Sedimentation*, pp. 330–339, Moscow, Russia.

Torizzo, M., and J. Pitlick (2004), Magnitude-frequency of bed load transport in mountain streams in Colorado, *J. Hydrol.*, *290*(1), 137–151.

Trimble, S. W. (1997), Contribution of Stream Channel Erosion to Sediment Yield from an Urbanizing Watershed, *Science*, *278*(5342), 1442–1444.

Turcios, L. M., and J. R. Gray (2001), U.S. Geological Survey sediment and ancillary data on the world wide web, in *7th Federal Interagency Sedimentation Conference*, pp. 1–6, U.S.G.S., Reno, NV.

U.S.F.S. (2014), Sediment Transport in Colorado and Wyoming,

U.S.G.S. Center for Integrated Data Analytics (2014), USGS Sediment Data Portal,

U.S.A.C.E. (1989), *Sedimentation Investigations of Rivers and Reserviors. Engr. Manual 1110-2-4000*, Washington, DC.

USFS Boise Adjudication Team (2014), Sediment Transport in Idaho and Nevada, <http://www.fs.fed.us/rm/boise/AWAE/projects/sediment_transport/sediment_transport_BAT.shtml>. Accessed May 18, 2014.

USGS (2014), National Water Information System, <http://waterdata.usgs.gov/nwis/>

Venables, W. N., and B. D. Ripley (2002), *Modern Applied Statistics with S*, 4th ed., Springer, New York.

Vigiak, O., and U. Bende-Michl (2013), Estimating bootstrap and Bayesian prediction intervals for constituent load rating curves, *Water Resour. Res.*

Vogel, R. M., and N. M. Fennessey (1994), Flow-Duration Curves. I: New Interpretation and Confidence Intervals, *J. Water Resourses Planning and Mgmt. 120*(4), 458-504.

Vogel, R. M., J. R. Stedinger, and R. P. Hooper (2003), Discharge indices for water quality loads, *Water Resour. Res.*, *39*(10).

Vogel, R. M., C. Yaindl, and M. Walter (2011), Nonstationarity: Flood Magnification and Recurrence Reduction Factors in the United States1, *JAWRA J. Am. Water Resour. Assoc.*, *47*(3), 464–474.

Walling, D. E. (1977a), Assessing the accuracy of suspended sediment rating curves for a small basin, *Water Resour. Res.*, *13*(3), 531–538.

Walling, D. E. (1977b), Limitations of the rating curve technique for estimating suspended sediment loads, with particular reference to British rivers, in *Erosion and Solid Matter Transport in Inland Waters Symposium*, pp. 34–48, IAHS-AISH Publication No. 122, Paris, France.

Walsh, C. J., A. H. Roy, J. W. Feminella, P. D. Cottingham, P. M. Groffman, and R. P. Morgan (2005), The urban stream syndrome: current knowledge and the search for a cure, *J. North Am. Benthol. Soc.*, *24*(3), 706–723.

Wang, J., Zamar, R., Marazzi, A., Yohai, V., Salibian-Barrera, M., Maronna, R., Zivot, E., Rocke, D., Martin, D., Maechler, M., Konis., K. (2014), robust: Robust Library in R. <http://cran.r-project.org/package=robust>.

Wang, Y.-G., P. Kuhnert, and B. Henderson (2011), Load estimation with uncertainties from opportunistic sampling data – A semiparametric approach, *J. Hydrol.*, *396*(1-2), 148–157.

Watson, C. C., D. Dubler, and S. R. Abt (1997), *Demonstration erosion control project report: Design hydrology investigations*, Fort Collins, Colorado.

Wheaton, J. M., J. Brasington, S. E. Darby, and D. A. Sear (2009), Accounting for uncertainty in DEMs from repeat topographic surveys: improved sediment budgets, *Earth Surf. Process. Landforms*, n/a–n/a.

Whiting, P. J., J. F. Stamm, D. B. Moog, and R. L. Orndorff (1999), Sediment-transporting flows in headwater streams, *Geol. Soc. Am. Bull.*, *111*(3), 450–466.

Wilcock, P. R. (2001), Toward a practical method for estimating sediment-transport rates in gravel-bed rivers, *Earth Surf. Process. Landforms*, *26*(13), 1395–1408.

Wilcock, P. R., and S. T. Kenworthy (2002), A two-fraction model for the transport of sand/gravel mixtures, *Water Resour. Res.*, *38*(10), 12–1–12–12.

Wilcock, P. R., G. M. Kondolf, W. V. G. Matthews, and A. F. Barta (1996), Specification of Sediment Maintenance Flows for a Large Gravel-Bed River, *Water Resour. Res.*, *32*(9), 2911–2921.

Williams, G. P. (1978), Bank-full discharge of rivers, *Water Resour. Res.*, *14*(6), 1141–1154.

Wohl, E., B. P. Bledsoe, R. B. Jacobson, N. L. Poff, S. L. Rathburn, D. M. Walters, and A. C. Wilcox (2015), The Natural Sediment Regime in Rivers: Broadening the Foundation for Ecosystem Management, *Bioscience*, biv002.

Wolman, M. G., and R. Gerson (1978), Relative scales of time and effectiveness of climate in watershed geomorphology, *Earth Surf. Process.*, *3*(2), 189–208.

Wolman, M. G., and L. B. Leopold (1957), *River flood plains; some observations on their formation*. USGS Professional Paper: 282-C.

Wolman, M. G., and J. P. Miller (1960), Magnitude and Frequency of Forces in Geomorphic Processes, *J. Geol.*, *68*(1), 54–74.

Yang, C. T. (1979), Unit stream power equations for total load, *J. Hydrol.*, *40*(1), 123–138.

Yevjevich, V. V. (2010), *Probability and Statistics in Hydrology*, 2nd ed., Water Resources Publications, Highlands Ranch, CO.

APPENDICES

A – Empirical MFA Site Information and Results Tables

B – Sediment Load Regression Diagnostic Plots

C – Site Specific Sediment Yield and Cumulative Sediment Yield Plots

D – Flow Record Extension Methods and Site Specific Plots

E – Site Specific Bankfull Predictor Results Tables

F – Bankfull Discharge by At-A-Station Hydraulic Geometry Plots

G – Uncertainty Analysis Regression Methods, Results

H – Flow Non-stationarity Plots

I – At-A-Station Hydraulic Geometry Relations